A Study of Vibration-induced Fretting Corrosion in Electrical Connectors Based on Experimental Test and FEA Simulation

by

Fuxi Zhang

A thesis submitted to the Graduate Faculty of
Auburn University
in partial fulfillment of the
requirements for the Degree of
Master of Science

Auburn, Alabama
August 2, 2014

Key words: fretting corrosion, FEA simulation, electrical contact,

Approved by

George T. Flowers, Chair, Professor of Mechanical Engineering
Jeffrey Suhling, Professor of Mechanical Engineering
Robert N. Dean, Associate Professor of Electrical and Computer Engineering

Abstract

In the field of electrical contacts, vibration induced fretting corrosion is generally recognized as one of the major failure mechanisms. Many factors affect fretting corrosion, including the normal force and the surface friction coefficient. Previous literature has identified the basic mechanisms of fretting degradations. Nevertheless, due to the complex structure and the uncertainty of random noise excitations, vibration induced fretting corrosion of connector systems still needs more research and understanding. The random vibration and first mode natural frequency vibration along the axial direction were applied to investigate the fretting threshold for a sample connector. Variations in finish type, friction forces, normal forces and issues with wire length were studied. In addition, it is difficult to experimentally observe the motion inside a connector pair. Computer-based FEA is utilized to assist in analyzing the motion of contact parts inside the connector.

In the present study, the dynamic response and fretting characteristics of a series of connectors were investigated. Four different types of connectors, identified as 2C, 3A, 3B and 3C, with different finishes and spring forces, were considered. Each type was evaluated for wire lengths of 2cm, 4cm, 6cm and 8cm. For the experimental testing, each sample configuration considered five samples for the transfer function and fretting input threshold tests.

ABAQUS and ANSYS three dimensional FEA models were developed to gain further insight into the experimental results. The dynamic model was examined for both overall dynamic

response and for the specific transfer function of a given configuration. The results of the FEA simulation are compared to the experimental test results. The basic results are summarized below:

- The friction forces and spring forces for type 2C, 3A, 3B and 3C are obtained experimentally. From these results, the corresponding coefficients of friction are calculated.
- 3D ABAQUS Explicit FEA models are developed. Using the spring forces and coefficients of friction acquired in the experimental tests, the simulation friction forces are calculated and compared to the experimental friction force results.
- The transfer functions of all four types of connector with different wire lengths are determined experimentally and compared to results from the FEA simulations with good correlation.
- Using the transfer function results as a guide, fretting thresholds at the natural frequency for each sample are determined experimentally and compared to the results predicted by the corresponding simulation model, with good correlation.

Acknowledgments

I would like to express my sincere thanks and deep appreciation to my advisor Dr. George T. Flowers for his guidance in the completion of this research work. His wise suggestions, generous support and his encouragement contributed immensely to my study and lighted my path towards the science palace.

I also would like to thank my committee members, Dr. Jeffrey Suhling and Dr. Robert N. Dean for their academic instructions and assistance.

Special thanks is given to all my friends, especially Dr. W. Ge, Dr. M. Ma and Dr. S. Xing's couple, and my lab mates Dr. P. Soobramaney, Mr. H. Yang, and Mr. J. Jantz, which without their constant support and friendship this "journey" would have been much more difficult to accomplish.

Finally, I would like to express my gratefulness to my parents Mr. Zengke Zhang and Mrs. Aixiang Zhang, and my dear wife Mrs. Wei Xing, whose love, care and support have been invaluable for the completion of this degree (Master of Science).

Table of Contents

List of Tables

List of Illustrations

List of Nomenclature

μ	Coefficient of Friction
Fs	Friction Force (N)
Fn	Normal Force or Spring Force (N)
M	Magnitude of The Vibration Input (um)
ϕ	Phase Angle of the Vibration Input (°)
Z_F	Relative Motion between the Two-half Interfaces
g_{RMS}	Root Mean Square of g-level (g)
f	Input Frequency (Hz)
a	Periodic Motion (m)
ω	Circular Frequency (Hz/2)
A_0	Initial Amplitude of Periodic Motion (m)
A_n	Constant Parameters
B_n	Constant Parameters

Chapter 1 Introduction and Literature Review

In the electrical contact field, vibration induced fretting corrosion is generally acknowledged as one of the major failure mechanisms. Previous researchers recognized this phenomenon and focused on the causal agencies of this mechanism for a more complete understanding and increased prevention. The traditional means of research work on connector fretting requires exhaustive experiments, which are time consuming and expensive. In addition, attempting to observe the motion and degradation mechanism inside the connector pair is a difficult undertaking. Using computer-based modeling and simulation techniques to assist in analyzing various design factors on electrical connector vibration-induced fretting corrosion is potentially of great benefit.

1.1 Fretting Corrosion

Fretting corrosion is widely recognized as a major cause of failure between the interfaces of electrical contacts. It is a phenomenon caused by mechanical stresses and repeated relative motion among contact surfaces and eventually leads to contact failure. This small-scale repeated relative motion is called slip. Slip can be induced by many external excitations, such as mechanical vibration, thermal alternation caused material expansion, load alternation, and power junction heating. Frictional wear and oxidation are associated problems caused by fretting corrosion.

Fretting corrosion damage in metal is identified by the presence of discolored and pitted surfaces in the oscillatory motion case. The original oxidation layer is broken and metallic debris is produced, which causes mechanical wear and material transfer. The fresh metallic surfaces are exposed to the air and oxidizes rapidly, accelerating the fretting cycle. Eventually, the surface cracks and metallic and oxide debris cause mechanical malfunction by surface jerking, lost dimensional accuracy and contact clogging.

Fretting corrosion is a major reason of mechanical failure, including electrical connectors, king-pins in a cardan shaft, gears in a powertrain, jewel bearings, connecting rods, variable-pitch propellers, and other vibrating machinery parts. It also may accelerate discoloration and oxidation of metal during transport.

Fretting corrosion is not a new problem. The first description of this phenomenon was reported by Eden, Rose and Cunningham in 1911 in reference to their steel fatigue testing [1]. The terminology “fretting corrosion” was first used by Tomlinson, Thorpe, and Gough in 1939, in their report on experiments of different metal contact corrosion [2]. In 1968, this phenomenon was further defined by Bethune and Waterhouse. Waterhouse published a book describing the considerable details and potentially disastrous effects caused by fretting corrosion in an electric contact field [3]. The oxidizing effect, wear debris and the benefits of lubrication were also presented. In 1973, fretting corrosion aroused much more attention from engineers, scientists and the public, particularly with regard to electrical contacts. Many laboratory experiments were prevented to investigate fretting on a variety of contact materials. In E. M. Bock and J. H. Whitley’s work, they tested 36 different contact

material combinations under mechanical and electrical loads in order to study the effect of fretting corrosion on electrical contact resistance [4].

Later, a series of tests under different thermal conditions, moisture levels and air compositions were conducted. Results indicated oxygen is the main contributing factor of fretting corrosion damage in steel-on-steel, not moisture. Low temperature, increasing mechanical load, and slip magnitude also increase the damage. Frequency has much less influence on the damage, and in a nitrogen environment no effect is obtained.

1.2 Mechanism of Fretting Corrosion

Corrosion damage at the contacting points of surfaces is called fretting corrosion. On the small scale, there are only a few contact sites between touching surfaces, called asperities. To generate fretting corrosion, some basic conditions are required: the contact surfaces should be loaded; the interface should be under relative slip repeated motion, usually caused by vibration or thermal effects; the load and motion should have sufficient magnitude.

Wear-oxidation and oxidation-wear are recognized as two theories of the mechanisms of fretting corrosion. The first theory proposes that under load and relative motion, contacting asperities occur due to cold welding and metal debris will be removed from metal surfaces and will re-oxidize quickly. This whole process repeats and results in oxide residue. The oxidation-wear theory states the surfaces already have an oxide layer before they come in contact with each other. The oxide layer will be ruptured at asperities

when the contacting surfaces are subjected to slip motion under a load. This process produces oxide debris and causes the fresh metal to be oxidized repeatedly.

Some experiments investigated how oxygen plays a crucial part in the fretting corrosion process. Compared to dry air, the damage is much less in a moisture condition, and even negligible in a nitrogen atmosphere. A lack of oxidation will prevent or slow down the fretting corrosion damage. Temperature can also influence the fretting corrosion process. Previous research work has shown the fretting corrosion damage will be decreased in a high temperature environment in the case of iron and steel. Also, the fretting process will produce heat in the contact area. The local high-temperature oxidation phenomenon produces Fe_3O_4 instead of Fe_2O_3 under normal air temperature conditions. Compared to Fe_2O_3, Fe_3O_4 is much more stable and stiff. It provides a harder layer that is more difficult to wear, and prevents the exposure of the fresh metal to oxygen, slowing down the fretting corrosion process [5].

1.3 Finite Element Analysis

Finite Element Analysis (FEA) divides a complex problem into many smaller and simpler parts, which are called finite elements, with some physical and mathematical connection between the elements. All loads and boundary conditions are added on mesh grids and transferred to the nearby elements by a mathematical matrix on the shared grid points. Depending upon the particular dimensions and requirements, different finite elements are used to make a problem easier to formulate and analyze.

The first published literature of the matrix theory for the structural analysis problem appeared in the early 1940's. In the 1960's, the term "finite element" was first used by Clough to describe this technique in his plane-stress analysis paper [6]. In the 1970's and 1980's a group of organizations and companies started to develop finite element programs for large, general-purpose analysis situations. These organizations and companies, such as NASTRAN, ANSYS, ABAQUS, MARC, STARDYNE, and SAP, became the leaders in the FEA computing field. The graphical GUI for finite element pre and post processors appeared in the 1980's. Automatic meshing achieved another great step in the FEA field in the 1990's. It provided a more accurate and faster meshing method. Currently, FEA technology is used in many engineering fields, including static structural, dynamic structural, heat transfer, magnetic field, transient dynamic, fluid dynamic, and electronics.

In recent years, many studies on the fretting corrosion of electrical contacts have used FEA computer simulations. ABAQUS and ANSYS are the most popular FEA software in these studies. Researchers and technicians have used this technology to verify their experiments and assist their analysis. Some remarkable electrical contacts FEA simulation works have been published by researchers, such as Villeneuve [7], Monnier [8] and their co-workers.

1.4 Literature Review of Fretting Corrosion in Electrical Contacts

For most electrical and electronic equipment, fretting corrosion is a very common and significant kind of failure. It causes fatal damages or malfunctions of important equipment and leads to expensive inspection and replacement. Sometimes this fatal fretting

damage is difficult to detect in a complex system, causing the whole system to require replacement. Nevertheless, the detrimental effect of fretting corrosion was not considered a serious factor in electrical connector failure until its importance was demonstrated in Bock and Whitley's work in 1974 [4]. They revealed that the physical causes of fretting actions, such as vibration or thermal expansion, will increase the electrical resistance for non-noble contacts in experiments. Abrasion of the oxidation layer on the contacting materials is the main cause of the continual fretting corrosion. Since then, there has been considerable systematic research focused on the phenomenon of fretting corrosion in electronic connectors [9] [10] [11] [12] [13].

In 1984, a comprehensive fretting corrosion review was published by Antler [14]. His work contained a detailed discussion of fretting mechanisms referring to transfer, wear, and oxidation along with frictional polymerization that applies to the fretting of contacts; the effect of operational parameters such as force and cycle rate on contact resistance change; a survey of materials whose fretting behavior has been characterized; and an analysis of the different roles that lubricants play in controlling fretting according to the contact materials. Considering the expected lifetime and reliability of connectors, the structure design and material chosen should satisfy the condition for a given application. Furthermore, before engineers make a new structure design, a sequence of hardware tests, including shock and vibration, should be conducted. It was also concluded that the determination of contact resistance is given by the composition of the interface, and this composition may cause the transfer, wear, and film formation between different metals. Furthermore, unstable contact

resistance will be found in the longer wipe situations for fretting corrosion and friction polymerizing systems.

During this same time period, a number studies on automotive connector fretting corrosion were also conducted [15] [16] [17]. Lee and Mamrick reported their study on the fretting corrosion of tin-plated copper alloy excited by a stepper motor which caused relative motion between the contacts of the alloy. Their work focused on the physical phenomena of tin-plated contacts under fretting corrosion and the influence of electric load on the fretting corrosion process. The rise in contact resistance of tin-plated copper alloy was studied under minute cyclical motion. They found the electrical load did not affect the electrical conduction through slightly corroded contacts over the rage of circuit voltage and current. For the moderately corroded case, the resistance characteristic showed a sustained plateau near the melting voltage of Sn; and for severely corroded contacts, a plateau occurred in the resistance range corresponding to the voltage range of the melting, sublimation, and decomposition of the oxides and vaporization of tin. They found that when the current passed through the contact constriction, thermal effects were generated. The temperature increased, which melted the tin coating surface. The continuing corrosion produced more heat and a higher resistance. The temperature rose further, resulting in the melting, sublimation, and decomposition of the oxides and eventually producing the vaporization of tin, collectively forming a second contact resistance.

In IC devices and other application fields, researchers also studied fretting corrosion [18]. Mottine and Reagor [19] conducted an investigation on dissimilar metal interfaces and

fretting corrosion in socketed IC device applications. The research focused on a variety of socket devices with dissimilar metal interfaces under mild vibration conditions. After a ten-month test period, the samples were disassembled to study the static resistance behavior. All the contact surfaces were examined by Scanning Electron Microscope (SEM) and Scanning Auger Microprobe (SAM) equipment. Their also considered the effects of disk drives and cooling fans in minicomputer systems. The DIP/sockets suffered mild vibration, which caused the tin-plated or gold-plated interfaces to undergo fretting corrosion and contact resistance failure. Experimental test results confirmed the failure mechanism, which was the build-up deposits of tin-oxide particulate in the contact mating area. The results for DIP/socket systems showed that similar lubricated metal interfaces, such as Au-Au and SnPb-SnPb, had only low-level fretting and were reliable for such applications.

The development of comprehensive models for predicting contact resistance behavior under fretting corrosion is a difficult task. A comprehensive model for predicting the contact resistance under the n^{th} fretting cycle was proposed by Bryant [20] in 1994. He also gave a prediction of the ultimate usable lifetime of the contact. In his work, contact wipe, fretting vibration amplitude and frequency, contaminant chemistry, material properties, plating thickness, asperity deformations, normal load, electrical load, and surface topography were considered. This work was based upon two corrosive fretting failure mechanisms. One considered wear debris generated by fretting filling of surface valleys. The other one involved changes in surface asperities, which was caused by contamination of the corrosion products. A proper sequence of magnitude scales for fretting tests and failures was given for both mechanisms estimates. The model assumed that the exposed corroded asperities were pulled

back together by the fretting motions. The corrosion products were scraped off by the fretting motions and the debris deposited among the valleys of the surface. Finally, ultimate failure was caused by the separating a-spots and the valleys filled with debris. The corrosive debris deposited into the contact was estimated by a material balance between the amounts produced and scraped off. The corrosive product particles were mixed into the asperity metal by the shifting of molecules under plastic deforming motion. This model gave an approach for calculating the amount of corrosion product produced on the exposed surfaces during the separation phase of a cycle of fretting. The contaminated asperity conductivity could be estimated based on correlating mixing plastic flow and modern composite theory. The asperity resistance could be given by integration over the asperity volume. So, Greenwood's theory allowed an estimate of the total contact resistance.

Malucci [21] [22] provided a new single analytic model in the early 1990's. This model combined and refined the previous contact resistance model and the oxide build-up model under fretting conditions. The average effects of contact force and fretting amplitude on contact degradation can be predicted by using this model. The results of tin plated contacts were used to verify and explain this model within the framework. In his study, a phenomenon was discovered: decreasing contact force or increasing fretting amplitude producing increased degradation. An increase in oxide buildup due to either asperity deformation or an increase in the number of asperity deformations over cycle gave an explanation for the phenomenon. Thermal shock tests provided important data which was analyzed and used to determine the relationship between the temperature swing ΔT and acceleration factor. He also concluded that assuming the connection between the temperature swing and fretting amplitude was

consistent in both fretting and thermal shock tests. This work and related results became a base model for the degradation rate in terms of fretting cycles and the temperature. Malucci's work was used to estimate the acceleration factor for a given parameter to simulate field degradation in the lab.

However, few researchers have paid attention to vibration thresholds of fretting corrosion of electrical connectors. Flowers and his colleagues [23-34] started to investigate the relationship between applied excitation levels and fretting rates using single frequency vibration in 2002. Their work discovered a threshold level of input excitation, which could cause fretting corrosion. The fretting rates increased monotonically when excitation levels were above the threshold. Then they found that a function of the dynamic behavior of the connector, the tie-off conditions and its mass or stiffness properties, affected the threshold g-level. The experimental results of this study showed that, for the primary mode ofconnector rocking-type interface motion, the relative movement at the location served as a good indicator of the expected fretting rate. The simulation could also predict the relative motion for a given excitation level and frequency. Then, they proposed a transfer matrix model for analyzing the results. When damping was applied to the model, the results gave an empirical match to the correlative data. The analysis revealed the bending movement between contact surfaces played a crucial part as a result of excitation levels and tie-off configurations. Later, researchers showed that different g-levels and tie-off configurations impacted the dynamic response and performance of a connector system under vibration stresses.

In 2005, another method for measuring the relative motion of fretting excitation was proposed by Lam, et al [24]. A novel thick film sensor was used to measure the displacement at the connector interface to test for environmental influences on electrical contact fretting. The male component of the connector was replaced by a sensor incorporated into the female part. The linear change of resistance was measured when the interface experienced movement causing the relative displacement of the contact point. The sensors were validated in a series of experiments and subsequent field tests to detect the relationships between the fretting effects and temperature, humidity, and differential pressure. In their work, the temperature and humidity had negligible influences on the relative displacement compared to the variations of pressure loads.

In the past twenty years, computer based simulations have improved rapidly and been used in studies of fretting corrosion in electrical contacts. Many companies and their researchers used computer based FEA technology to perform simulations and analyses. ABAQUS and ANSYS are the two main tools in this field. As mentioned in Chapter 1.3, in 1996 Villeneuve et al [25] from the Ford Motor Company applied FEA techniques to simulate the terminal crimping process for vehicle connectors. In their work, the terminal grip cross section, the punch tooling and the wire strands were modeled. To imitate the real working situation, the grip was forced into the punch which was sitting on the anvil. The results showed the friction between the surfaces is crucial for the crimp's quality. In 2005, Monnier, et. al. [26] used Finite Element Analysis to simulate the behavior of a sphere-plane electrical contact under high current load. Several analyses were applied to simulations on mechanical, electrical and thermal coupling tasks. The results provided the contact terminal

voltage, the contact resistance of the system, and the solid temperature. In 2008, Jackson and colleagues [27] developed a finite element model of the bulk region of electrical connectors with multi-physics circumstances, such as structural, electrical and thermal. The model combined the MATLAB and the ANSYS together to solve the Multi-scale Sinusoidal Rough Surface (MSRS) contact. The results provided the temperature and voltage changes across the bulk regions of the connector parts, and also provided a highly accurate approach in a coupled multi-physics model for the prediction of contact forces, electrical contact resistance (ECR) and thermal contact resistance (TCR).

1.5 Overview of Current work

In this thesis, a series of research work was focused on experimental validation and FEA simulation of vibration-induced fretting corrosion and tribology properties of electrical contacts. The thesis is divided into four chapters.

Chapter One is the introduction and literature review. It describes the main work and introduces the concept and mechanism of fretting corrosion, as well as fundamental background material, research history, and the present status in an electrical contacts field and application of Finite Element Analysis in the electrical contact field.

In Chapter Two, normal spring force, friction force tests, and FEA simulation of the electrical connector pair are described. It provides a discussion of the use of this work, followed by experimental and simulation details, including test samples, equipment, test access, test setup, 3-D models, and simulation boundary condition setup. Both experimental

results and analysis data are compared. The results of these tests and simulations include a study of the physical characteristics of the connector pair, which influences the connector natural frequency and relevant vibration threshold and define the major fundamental parameters for FEA simulations in later chapters.

Chapter Three and Chapter Four describe the vibration-induced fretting of electrical connector experimental tests and corresponding FEA simulations under different oscillation directions, different cases of interface surface finishing, and various wire lengths.

In Chapter Three, experimental tests and FEA simulations of frequency responses are described which focus on axial vibration-induced fretting degradation of electrical connectors. In all, four different types of surface finishing and four different cable lengths of the receptacle side are used in experimental tests and FEA simulation, with the objective of determining the natural frequencies of each case and obtaining the corresponding transfer functions, which are critical parameters for the determining the fretting threshold.

Chapter Four focuses on the fretting corrosion input threshold for axial direction vibration and the relative motion between the blade and receptacle using the same samples as in Chapter Three. Experimental tests and 3-D FEA simulation are performed, and input threshold results and relative notions results are obtained for the various types of connector with different wire lengths.

Chapter Five summarizes the research work and conclusions in this thesis. It also provides recommendations and suggestions for further work on fretting corrosion in electrical connectors.

Chapter 2 Experimental Tests and FEA Simulation on Static Friction Force and Coefficient of Electrical Connectors

2.1 Introduction

In this chapter, the static friction forces and the coefficients of static friction for 5 types of commercial electrical connectors are studied. This is essential data for predicting the natural frequency and fretting corrosion characteristics of electrical connectors. An MT-200 tension/torsion experimental test system is employed to determine the static friction force and spring normal force experimental test. An ABAQUS^{TM} FEA 3-D simulation model is also developed using the coefficients of static friction and normal forces and validated using the measured the static friction forces.

Electrical connections are widely used in a wide variety of advanced equipment. One of the main failure mechanisms of electrical connectors is fretting corrosion which occurs on the contacting surfaces of receptacle and blade exposed to harsh vibration environments [4] (Figure 2-1). Fretting corrosion results in an increase in connector impedance and ultimate failure.

Figure 2-1. Fretting corrosion spot on sample connector blade

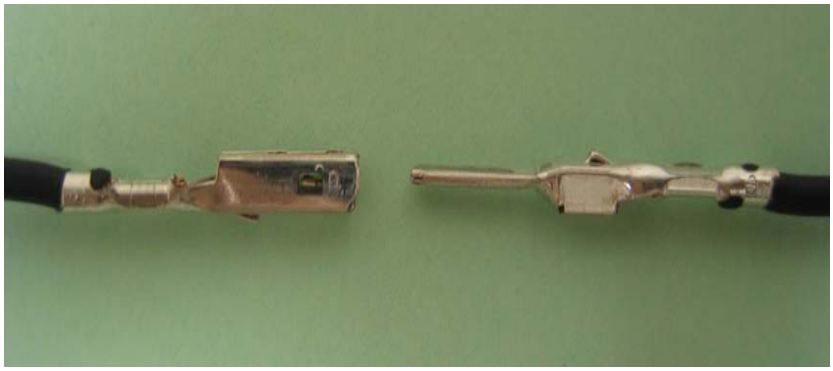

Figure 2-2. Connector pair with single wire

The interior of the connector receptacle contains a spring which serves to clamp the blade, providing both a normal spring force and friction force. From the perspective of corrosion technology and vibration theory, the normal force (the contact pressing force) and the friction force are the key factors affecting the fretting corrosion and natural frequency of connectors. Research on connector normal and friction forces is a critical element of the connector study.

2.2 Friction and Normal Force Experimental Tests

2.2.1 Connector Samples

For the purposes of this study, the sample set consists of five different types of receptacles and one type of blade. The receptacle types are identified as 2A, 2C, 3A, 3B, and 3C. The number represents the surface finish type. The letter identifies the receptacle spring deflection, which determines the level of the normal force.

Table 2-1. Spring deflection of different types

Type	A	B	C
Deflection /mm	0.27	0.32	0.37

For the friction and normal force tests, three connectors of each sample type were prepared for each test, with 15 pairs of connectors in total. (Figure 2-3, 2-4).

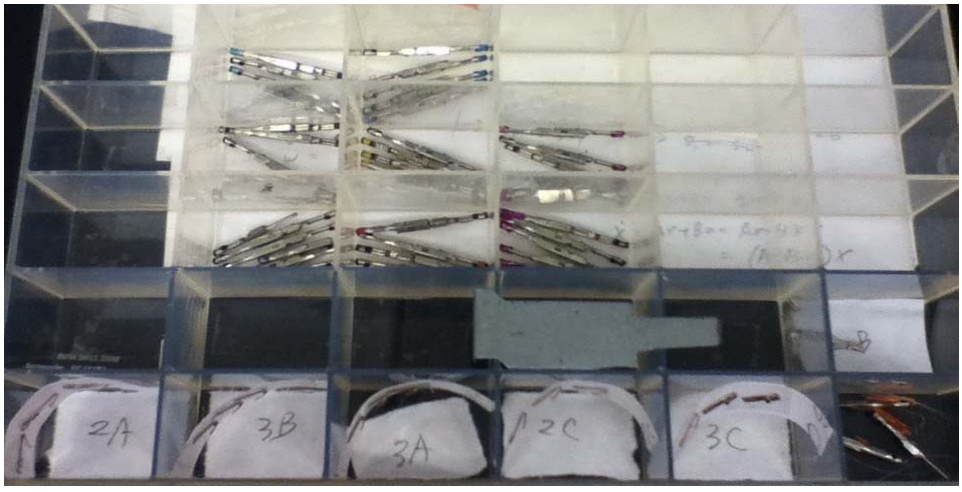

Figure 2-3. Photograph of all samples

Figure 2-4. Photograph of samples with cut-away to expose receptacle springs

2.2.2 Experimental Equipment

The equipment used in the friction (tensile) and normal force test is a Wisdom Technology MT-200 tension/torsion test system. It has a 0.1 microns axial resolution and a 0.0001° rotational resolution, with an adjustable operational speed.

2.2.3 Experimental Setup

In this study, the compression and tensile functions of the MT-200 tension/torsion system are used to measure the normal force and the friction force between the receptacle and the blade of the electrical connector. To protect the sensor head of MT-200, a steel sheet is mounted on one side. The steel sheet presses against the spring, but protects the sensor heads from damage (Figure 2-5 to 2-8).

In the tensile-friction force experimental tests, the MT-200 heads apply a tension force to both ends of the connector pair across a nylon line attached to each end to minimize axial misalignment, with an axial speed of 0.003mm/s.

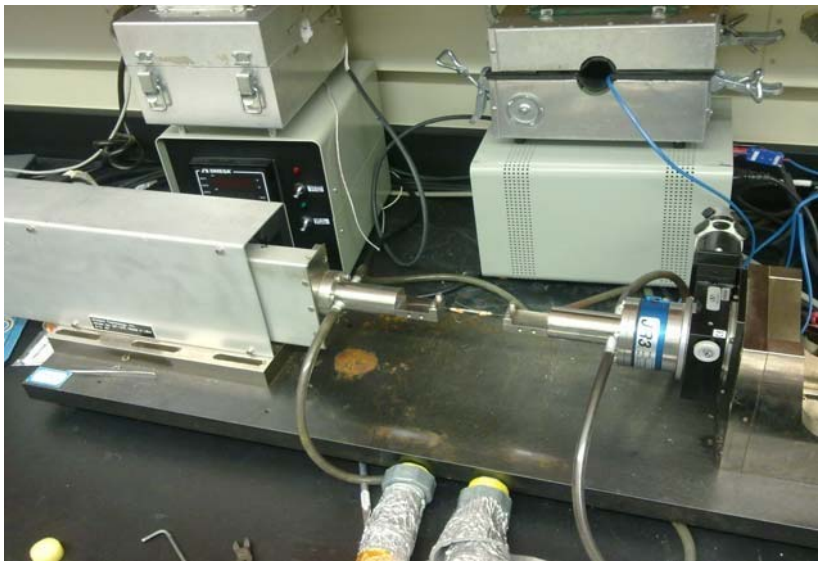

Figure 2-5. Photograph of tensile test setup

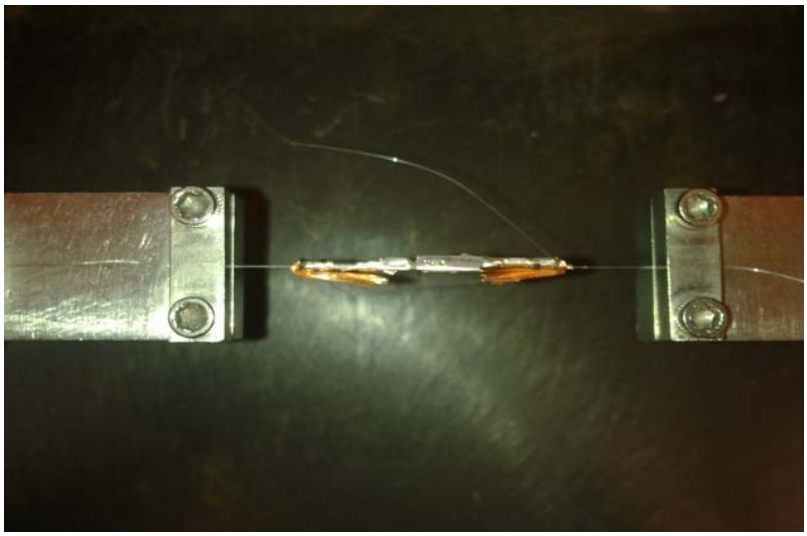

Figure 2-6. Detail photograph of tensile test setup

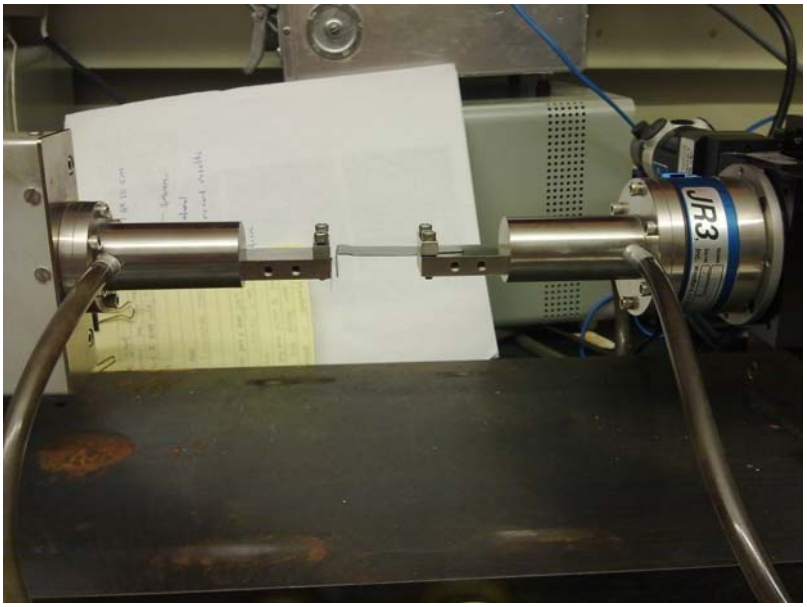

Figure 2-7. Photograph of compression test of receptacle spring

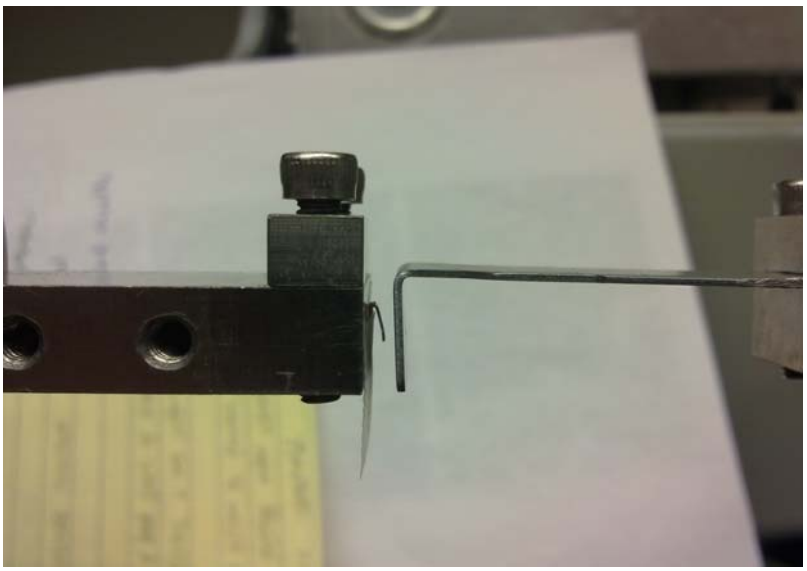

Figure 2-8. Detail photograph of compression test of receptacle spring

In the spring normal force tests, due to slightly differences in mounting conditions, the distance between fixed spring and MT-200 moving sensor head may have will vary. To ensure a more honest discernment of the results, all the original figures were not rescaled.

The spring normal force and deflection distances of type A, type B and type C all have a quite linear shape. The spring forces and the slope rates are quite close to each other for the dissimilar types of receptacles.

In the friction force test, the nylon line was attached between the MT-200 sensor heads and both ends of the connector pair. According to G. Flowers, Fei Xie, Chen Chen, and H. Yang's previous work [23] [30] [31] [32], the reason for using the nylon line instead of rigid connecting links is that it minimizes misalignment of both parts of the connector pair in the axial direction.

2.2.4 Experimental Results

The results of the experimental data curves show that friction force increases up to a certain point and then the force curve becomes relatively flat, with a somewhat erratic jerking motion, due to stick-slip. This can be treated as noise and does not affect the basic results. To identify the static friction force, the first peak of each curve was chosen and a mean value for all of the tests for a given sample type was used as the effective friction force for that type.

The normal force tests used the same basic method as the tensile-friction force test, only with the opposite moving direction to provide a compression force. The results of the data curves show that all the springs are quite linear. A mean value for all of the tests for a

given sample type are used as the effective spring force for that type. The final results and data curves are presented in Table 2. Figures 2-9, 2-10 and Appendix C show the test results for the spring forces and friction forces for each type of sample.

Table 2-2. Average values of friction force F_s and normal force F_n

	2A	2C	3A	3B	3C
Fs (N)	1.57	1.927	2.064	1.417	2.75
Fn (N)	3.187	5.215	4.335	5.072	5.965

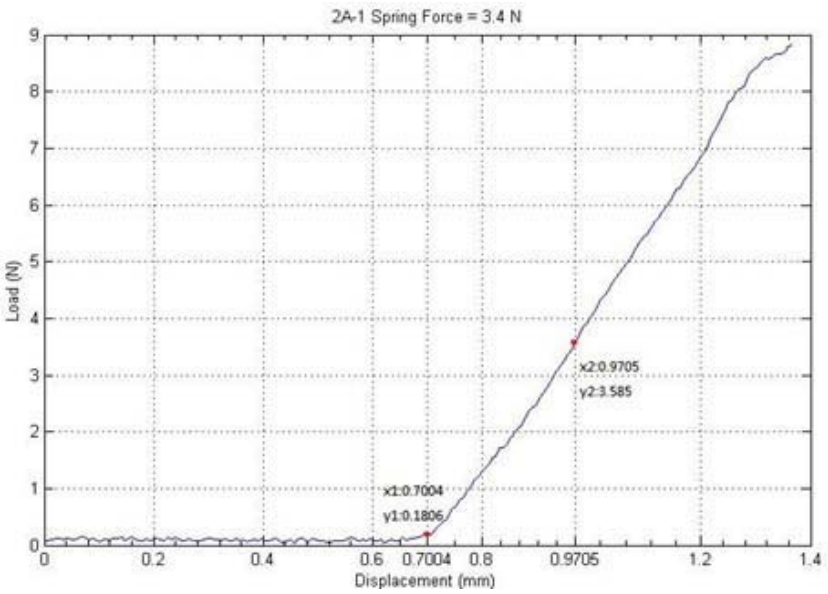

Figure 2-9. 2A-1 spring normal forces.

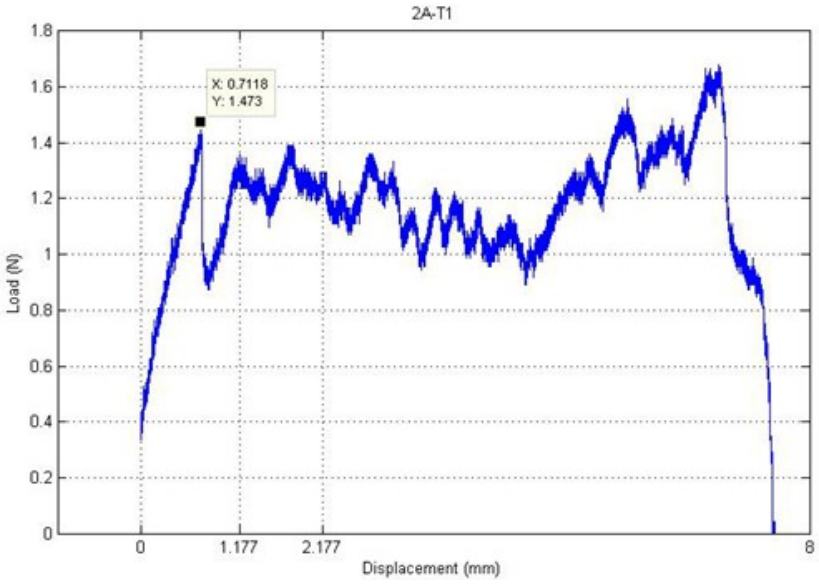

Figure 2-10. 2A-1 friction forces

The Coulomb friction equation is applied to obtain the coefficient of static friction, as shown in equation (2-1):

$$\mu = \frac{Fs}{Fn} \tag{2-1}$$

From the experimental test data, the coefficients of static friction of 5 types of connectors are shown in Table 2-3.

Table 2-3. The coefficients of static friction of 5 types of connectors

	2A	2C	3A	3B	3C
Fs (N)	1.57	1.927	2.064	1.417	2.75
Fn (N)	3.187	5.215	4.335	5.072	5.965
μ	0.493	0.369	0.476	0.279	0.431

2.3 FEA Simulation

2.3.1 Geometric Model Mesh and Material Property

The FEA simulation consists of a full 3-D model in the ABAQUSTM explicit dynamic package. Compared with a 2-D model or a reduced 3-D model, a full 3-D simulation requires a longer time to compute, but does not require modeling assumptions regarding boundary conditions and is much nearer to actual physical configuration. Based on the dimensions of the connectors used in the experimental tests, a rendering of the 3-D model is presented in Figure 2-11.

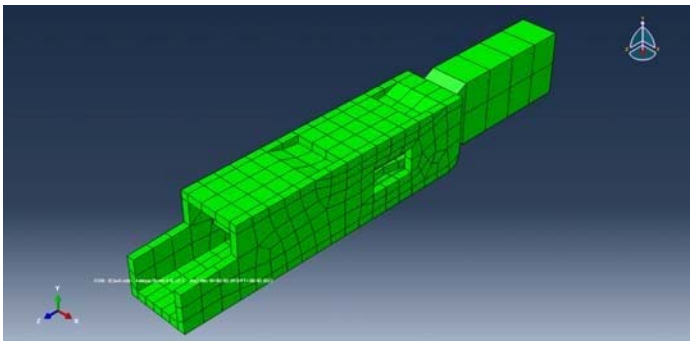

Figure 2-11. 3-D model in ABAQUS^{TM}

Mesh grids are an essential part in the simulation. They affect the result quality with their density and also influence computational speed. To balance quality and speed, meshing techniques, such as surface mapping and part dividing, are applied. The solid C3D8R elements have been utilized for the assembly model. The material properties are listed in Table 2-4.

Table 2-4. Material properties for connector model

Components	Density	Young's Modulus
Blade	8910 kg/m3	130,000MPa
Spring in receptacle	8910 kg/m3	130,000MPa
Receptacle	8794 kg/m3	130,000MPa

2.3.2 Boundary Conditions

In order to properly model the experimental conditions, boundary conditions should match the physical conditions in the experimental test as closely as possible. The contact pair is between to the blade surfaces and receptacle inside surface and spring surface. Coefficients of static friction and spring normal forces are equal to values derived from the experimental test. The receptacle is allowed six degrees of freedom (DOF). The blade is allowed one DOF along the single axis direction. Axial speed and distance are those used in the experimental tests. Figure 12 shows a section view of the contact pair of the 3-D model [33] [34] [35].

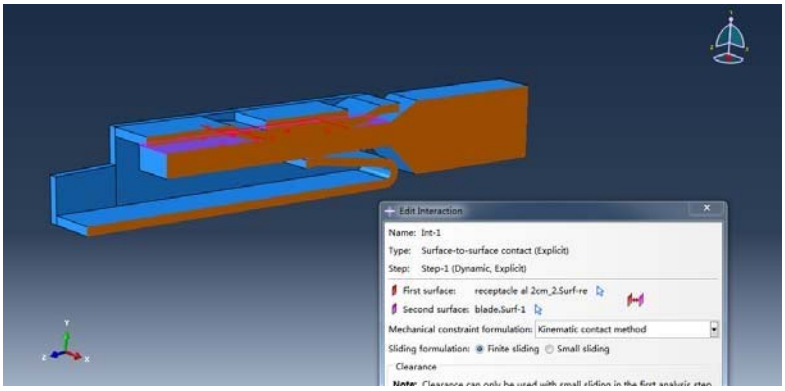

Figure 2-12 Section view of the contact pair of the 3-D model and contact pair sets

2.3.3 Simulation Results

Figure 2-13 to 2-17 show the FEA friction force simulation results. Unlike the experimental results, FEA results are quite smooth and have a steep slope.

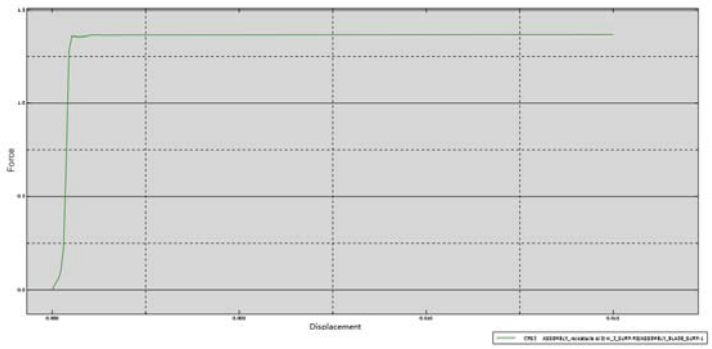

Figure 2-13. 2A ABAQUS friction force result

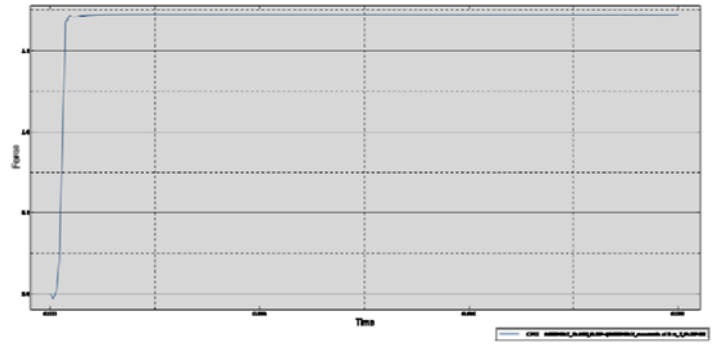

Figure 2-14. 2C ABAQUS friction force result

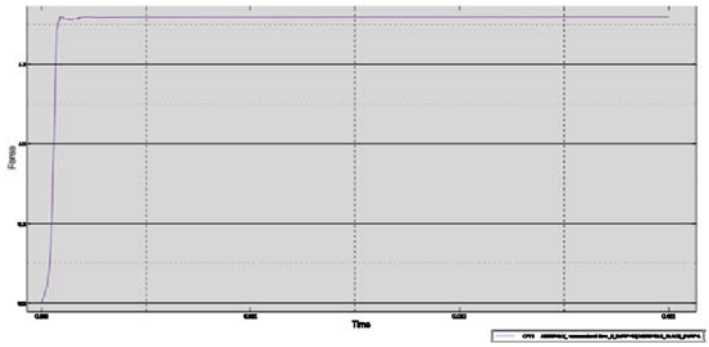

Figure 2-15. 3A ABAQUS friction force result

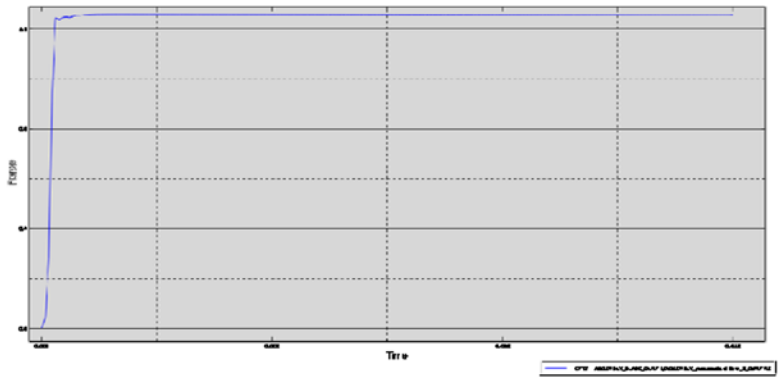

Figure 2-16. 3B ABAQUS friction force result

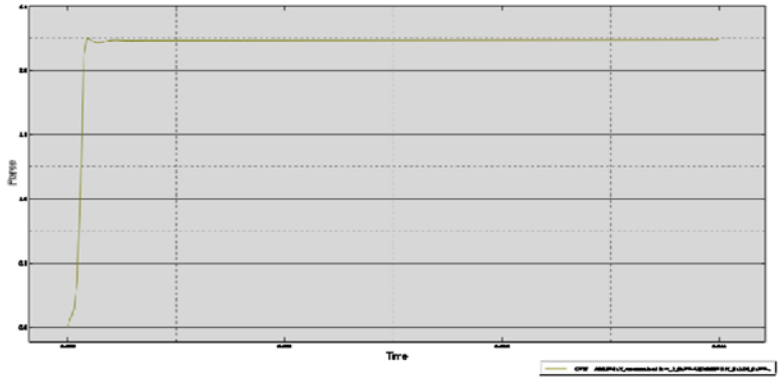

Figure 2-17. 3C ABAQUS friction force result

2.4 Results Comparison and Conclusion

To deliver a clean view and to compare experimental results to FEA results, all the results are shown together for each type of connector, as seen in Figures 2-18 to 2-22. Table 2-5 shows a detailed comparison.

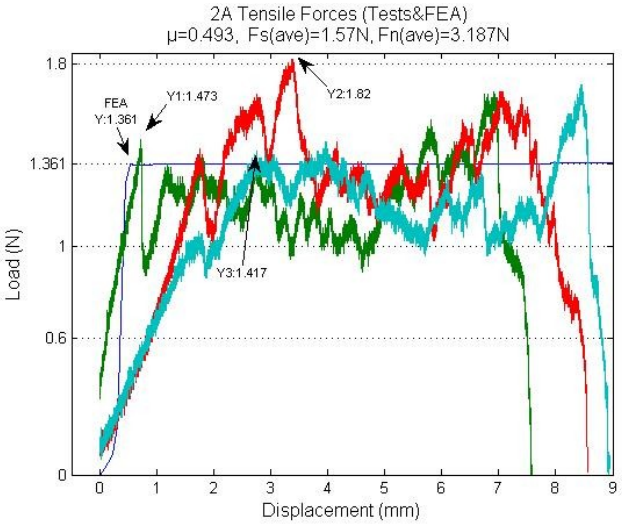

Figure 2-18. 2A friction forces comparison

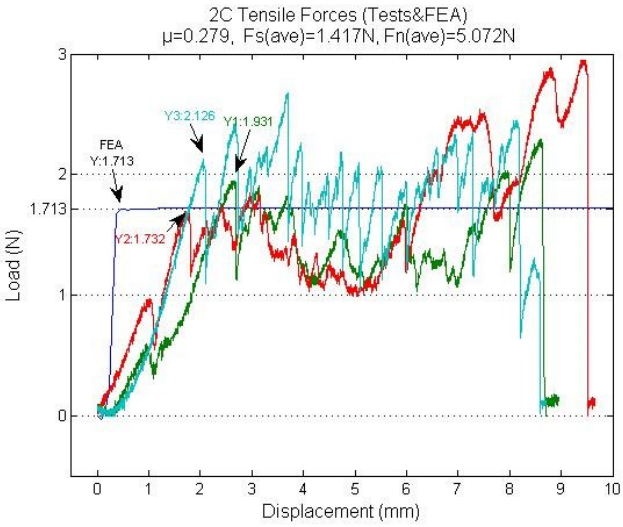

Figure 2-19. 2C friction forces comparison

According to the results comparison, the FEA results reach the static friction much faster and their values are slightly lower than the experimental values with an almost same deviation percentage.

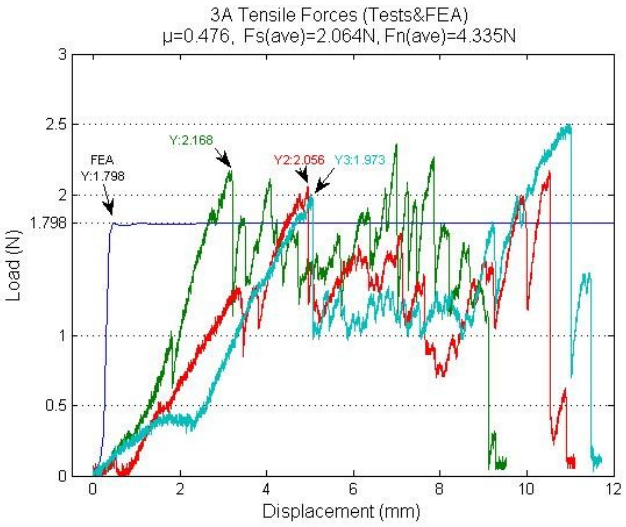

Figure 2-20. 3A friction forces comparison

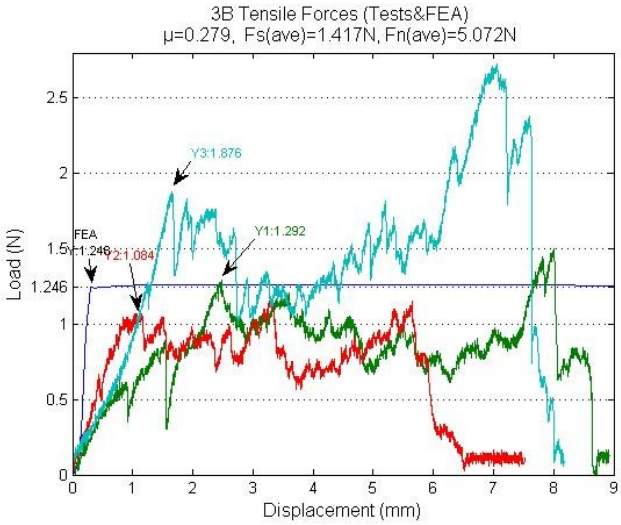

Figure 2-21. 3B friction forces comparison

According to the curve comparisons, the FEA curves always stay in the midriff of the other three experimental curves. This indicates that for the FEA results mostly match the experimental results.

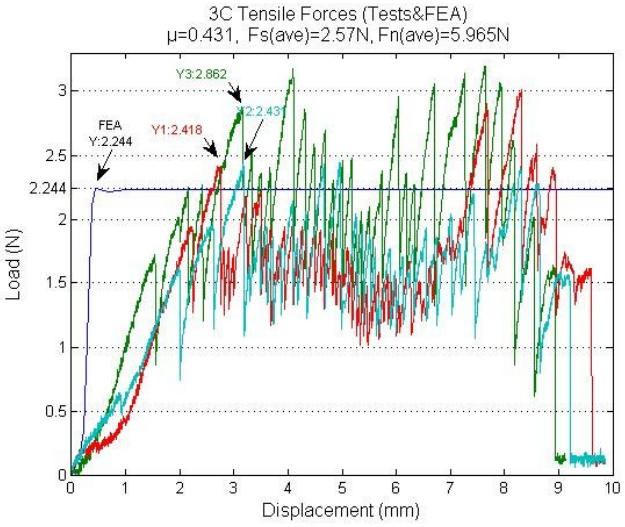

Figure 2-22. 3C friction forces comparison

Table 2-5. Friction force results (average) comparison

	2A	2C	3A	3B	3C
Fs (N)	1.57	1.927	2.064	1.417	2.75
Fn (N)	3.187	5.215	4.335	5.072	5.965
μ	0.493	0.369	0.476	0.279	0.431
FEA Fs (N)	1.361	1.713	1.798	1.246	2.244
$\frac{\left\|F_s^{Exp} - F_s^{FEA}\right\|}{F_s^{Exp}} \times 100\ \%$	15.4%	12.5%	14.8%	13.7%	22.5%

In the experimental situation, conditions are quite complex. Stick-slip, asperities on the contacting surfaces of the connector, test setup differences, and deviation in measurements will all affect the test outcomes.

Chapter 3 A Study of The Frequency Response of Single Blade/Receptacle Connector Pairs

3.1 Introduction

Vibration induced fretting corrosion is one of the major failure mechanisms of electrical connectors. In Chapter One, the details of importance, necessity, and current studies of fretting corrosion have been discussed. In practice, the first mode of natural frequencies, also called the fundamental frequency, is where major oscillation kinetic energy and distortion will appear. As a result, vibration induced fretting corrosion under the first mode natural frequency is a first consideration for most designs. Traditionally, to determine the fretting propensity of particular types of connectors, numerous destructive experiments are required, which necessitates a major commitment of cost and time. Additionally, some minor physical differences in samples and test setup influences the accuracy and the convergence of results. According, a simulation-based method is an effective method for the study of the single blade-receptacle connector vibration induced fretting. Previously, Flowers, Xie, Chen, and Yang [23,30-33] worked on a series of interesting behaviors of vibration induced fretting degradation, focusing on the threshold level of vibration amplitude for the onset of fretting, the electrical resistance, and mathematical model of the connector motion under fretting [30] [31] [32] [33].

In the present study, the primary objective is to predict and validate the frequency response of the blade/receptacle/wiring system. By employing experimental tests, three

dimensional modeling and FEA simulation technology, this section considers the relative motion transfer function of the connector system. Previously, Xie and Chen [30] [31] proposed a two dimensional model of the commercial single blade/receptacle connector system using ANSYS and ABAQUS for fretting propensity evaluation. Using the material property data from experimental tests and ABAQUS simulation results in Chapter Two, three dimensional (3-D) ANSYS models were developed and validated using the results from experimental tests. The details of this work are described in the sections below.

3.2 Experimental Configuration

3.2.1 Experimental Samples

The single blade/receptacle pair shown in Figure 3-1 consists of two parts, the blade and receptacle. The receptacle has a spring component inside the rectangular hull body serves to clamp the inserted blade and receptacle together. Opposite the spring there is a elevated flat section of the inside the hull wall called a "bathtub." The gap between the spring and the bathtub is smaller than the height of the blade, forcing the spring element to bend. This serves to hold the blade, creating the contact force between the blade and the receptacle. A mated connector pair is presented in Figure 3-2. The structural drawings of the receptacle are shown in Figure 3-3. Table 3-1 summarizes the details of structural properties of each type of receptacle.

Figure 3-1 Receptacle and blade

Figure 3-2 Mated connector pair

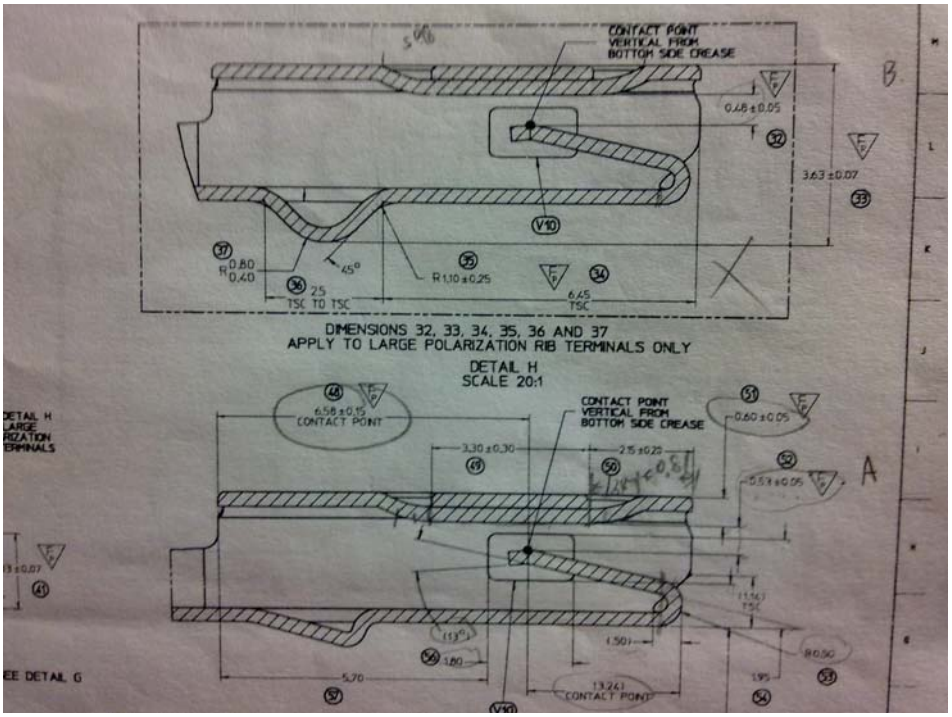

Figure 3-3 Cross-sectional view of receptacles

Table 3-1 Material and physical properties of each type of receptacles

Sample Type	Finish	Gap Size (mm)	Deflection (mm)	Normal Force (N)	Friction Coefficient
2C	2	0.43	0.37	5.215	0.369
3A	3	0.53	0.27	4.335	0.476
3B	3	0.48	0.32	5.072	0.279
3C	3	0.43	0.37	5.965	0.431

Referring to the previous work done by F. Xie, C. Chen, and H. Yang [30] [31] [32], the vibration generated by the shaker head produced very little fretting corrosion on the connector pair interface when a single strand wire was the connection path between a fixture and connector pair. Large plastic deformation and bending of the wire was induced by the vibration, which absorbed a large part of kinetic energy rather than inducing relative motion of the connector pair and fretting. So, increasing the stiffness of wire lead is desirable to enhance the relative motion for the purposes of this study. The previous two methods to help generate fretting were adding mass to the wire and stiffening the wire. For the purpose of this study, the both methods were employed. Using thermal shrink tubing, two additional strands were joined to the initial single strand. The wire lengths of the connector samples were 2cm, 4cm, 6cm and 8cm, as shown in Figure 3-4. Also, in order to facilitate the measurement of the movements of the connected parts laser Vibrometers, rubber seal bands and washers were attached to the blades and receptacles to provide a surface to affix laser reflectors.

Figure 3-4 Receptacle samples with modified wires joined by thermal shrink tubing

3.2.2 Experimental Equipment

In the frequency response transfer function tests and relative motion under fretting tests, the following equipment were used. A Keithley Model 2010 multimeter is used to measure connector resistance values and will be described further in chapter 4. Polytec laser vibrometers systems are used detect the displacements by reflecting laser beam on a specified target surface. An HP 35665A dynamic signal analyzer is used to generate the different types of drive signals (sinusoidal and random noise) for the shaker system and also to provide a means of measuring and recording the frequency response and displacement. An LDS PA500L Amplifier and LDS V408 Shaker constitute the vibration system.

3.2.2.1 Polytec Laser Vibrometer System

A Polytec Laser Vibrometer system is used for non-contact displacement measurements. The system consists of two parts, a Polytec OFV 353 laser sensor head and a Polytec OFV2610 controller, as shown in Figure 3-5 [36]. To identify the relative motion transfer function, two vibrometer systems were used in the experiment. The system provides the means for a displacement according to the fringe counter principle. The output is an analog voltage signal which describes the motion amplitude of the object. The signal can be transferred to HP 35665A dynamic signal analyzer to be viewed on an oscilloscope screen and also can be processed as needed. The decoder specification of the displacement is listed in Table 3-2.

Table 3-2 Displacement decoder specifications of the Polytec Laser Vibrometer

Measurement Range	Full Scale Output (Peak to Peak)	Resolution	Max. Vibration Frequency	Max. Velocity	Max. Acceleration
μm/V	Mm	μm	KHz	m/s	g
20	0.32	0.08	20	1.6	20,000
80	1.3	0.32	20	1.6	20,000
320	5.2	1.3	20	1.6	20,000
1280	20.5	5	20	1.6	20,000
5120	82	20	20	1.6	20,000

Figure 3-5 Polytec Laser Vibrometer

3.2.2.2 HP 35665A Dynamic Signal Analyzer

The HP 35665A Dynamic Signal Analyzer [37] is a two-channel Fast Fourier Transform (FFT) spectrum/network analyzer, shown in Figure 3-6. For the single-channel mode, the frequency range is from 0.19531 Hz to 102.4 kHz. For the two-channel mode, the frequency range is from 0.0097656 Hz to 51.2 kHz. The internal signal source of the analyzer provides random noise, burst random noise, periodic chirp, pink noise, and fixed sine. All the measured data can be saved to an external 3.5-inch disk drive, or an HP SS-80 disk drive, or can be printed out. The important parameters of the analyzer used in this study are listed below:

- Input Noise Level: <-140db
- Full Span FFT Noise Floor: <-76db (-85db typical)
- FFT Cross-Channel Gain Accuracy: ±0.04db (0.46%)
- FFT Cross-Channel Phase Accuracy: ±0.5 degree
- Minimum Frequency Resolution: 122 μ Hz (Two Channel Mode)

Figure 3-6 HP 35665A Dynamic Signal Analyzer

3.2.2.3 LDS Vibration System

The LDS shaker system is controlled by the HP 35665A Analyzer. The time-domain signals, which contain frequency-domain characters, are transmitted to the amplifier to drive the shaker with an amplified current and electromotive force signal. The system serves as a closed-loop control system. An accelerometer is mounted in the payload, sensing the vibration on the shaker and generating an analog signal back to the vibration control system. The time-domain analog feedback signal is converted into the frequency-domain by FFT. By comparing to the original frequency-domain signal characteristics, the vibration control system adjusts the output signal accordingly to maintain the desired response. The connection layout for a typical vibration system [39] [40] is shown in Figure 3-7.

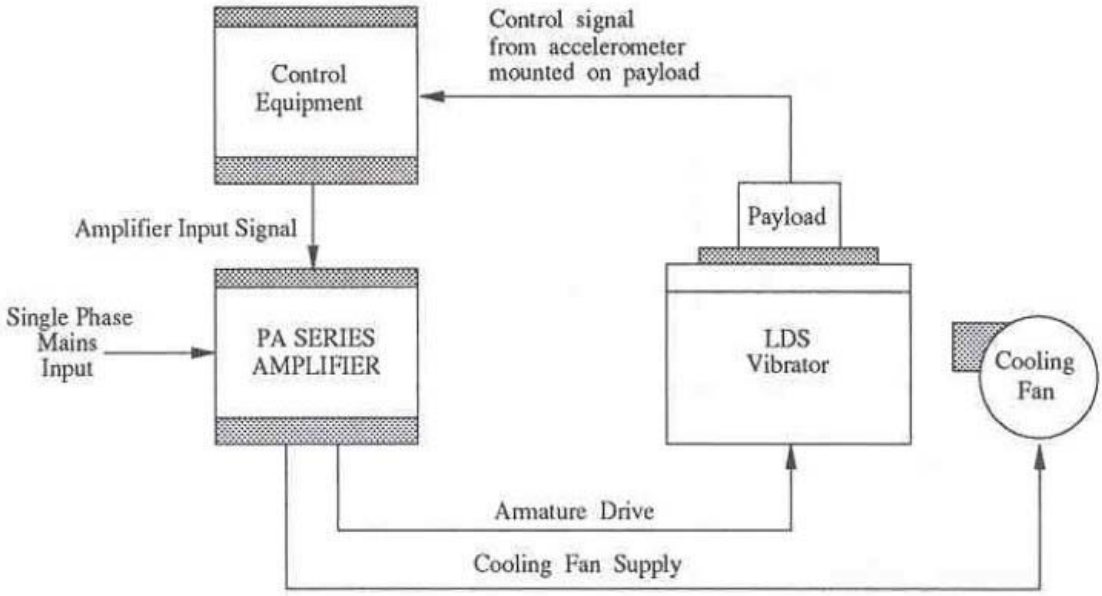

Figure 3-7 Schematic diagram of vibration system

The LDS PA 500L amplifier and V408 shaker used in this study are shown in Figure 3-8 and Figure 3-9.

Figure 3-8 LDS PA 500L Amplifier

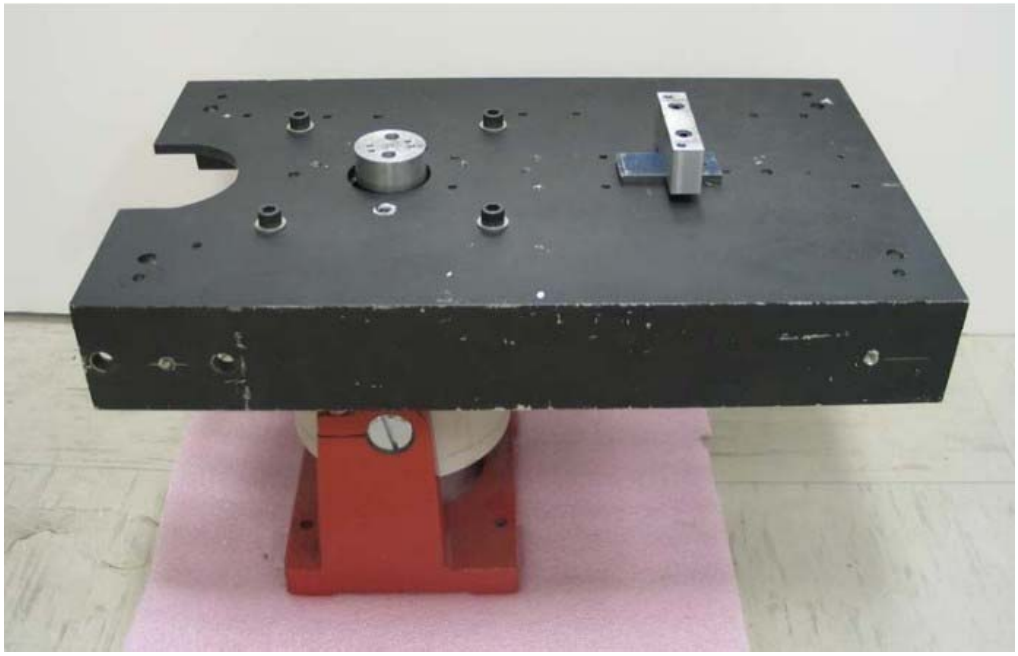

Figure 3-9 LDS V408 shaker

3.3 Experimental Study on the Frequency Response of Single Blade/Receptacle Connector Pairs with Various Types and Cable Lengths

3.3.1 Experimental Setup

In Figure 3-10, the basic setup of blade/receptacle for the transfer function measurement is shown. The rear part of the blade is fixed to the shaker head as the vibrating excitation input point. The metal part of the blade rear is clamped by the fixture, making a metal-to-metal stiff contact, to provide a effective kinetic energy transfer with minimum energy loss. The receptacle part is mated with the blade first and then fixed on the shaker

frame with a rack and movable fixture. The rack is mounted rigidly to the frame. The movable fixture can be moved along the rack track to accommodate different wire lengths. Both sides maintain have a section of free wire out of the fixture to allow the electrical resistance measurements required for the fretting studies.

Under an axial direction random vibration, there are two distinct bending outputs and mode shapes. In this work, the first mode frequency of vibration on two major output deformation directions is the main objective. The directions are the axial direction and the transverse direction as well as the direction perpendicular to the strengthened wire plan. In order to measure the transfer function in two directions, three laser reflectors are used in this section. The input only has one direction, the axial direction. Therefore, the input reflector, named Input A, is stuck on the washer of the blade. For the receptacle, the axial direction and the direction perpendicular to the strengthened wire plan should be monitored. The Output A reflector is stuck in the washer of the receptacle for the axial motion output. The Output T reflector is stuck on the hull of receptacle, which is parallel to the strengthened wire plane, for the transverse motion output. Figure 3-11 shows the whole setup of the transfer function test.

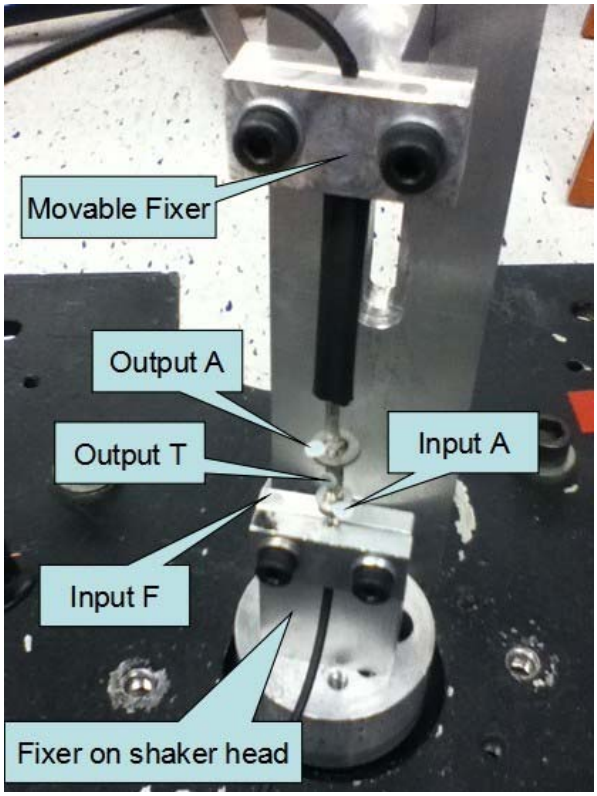

Figure 3-10 Basic setup of blade/receptacle for the transfer function measurement

Figure 3-11 Photograph of equipment setup for transfer function test

3.3.2 Transfer Function Measurement

The relative movement between contacting terminals is widely considered as the primary cause of fretting corrosion. Previously, Flowers and his co-workers [23] [24] [25] [26] proposed electrical measurement methods and test processes based on their study which were employed to find the transfer functions and fretting thresholds. The transfer function of the connector sample is determined by comparing the output response at the receptacle interface to the input excitation at the blade interface. The ratio of the steady-state output to the input amplitude under a given excitation frequency band is the magnitude of the transfer function in the frequency domain.

The transfer function is a functional relationship between the magnitude (M) and the phase (Φ) of the input and the corresponding output in the frequency domain from the dynamic modeling perspective. As an example, a transfer function magnitude of 1 with 0 phase shift indicates that the relative motion between the input and output is synchronous, with no delay. A transfer function magnitude of 2 with a 45° phase angle indicates that the output motion is twice as large as the input motion and it lags the response 45° to the input. In general, most dynamic systems have peak amplitudes at one or more resonant frequencies under input excitations. Typically, the phase switch is close to 90°at or near resonant frequencies, and on both sides of the resonant frequencies the phase shift has a larger or smaller value, which depends on whether the end product is lagging or exceeding. To identify the transfer function in a mathematical way, the complex number is utilized where the actual part is M cos (Φ) and the imaginary part is M sin (Φ). Therefore, the transfer function is expressed by equation 3-1:

$$\text{Transfer Function} = M \cdot \cos(\phi) + i \cdot M \cdot \sin(\phi) \text{ or } M\angle\phi \quad (3\text{-}1)$$

Based on the transfer function above, the relative motion between the two half-interfaces are defined by:

$$Z_F = \sqrt{[1 - M\cos(\phi)]^2 + [M\sin(\phi)]^2} \quad (3\text{-}2)$$

Where Z_F is the relative motion, and M cos (Φ) and M sin (Φ) are the real part and imaginary part of the transfer function. Figure 3-12 and Figure 3-13 are examples of the transfer function and phase response of the connector sample.

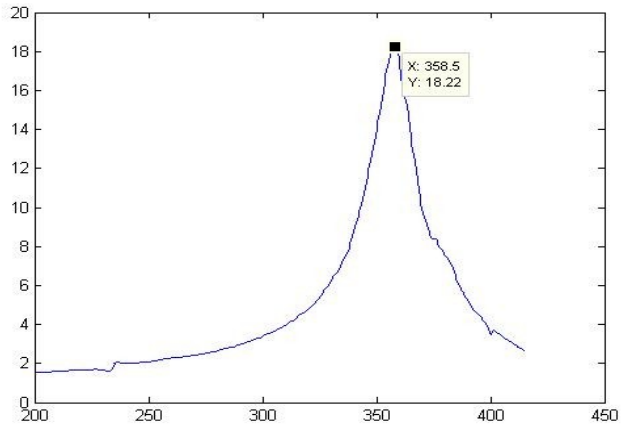

Figure 3-12 2C transverse transfer function with 4cm cable length

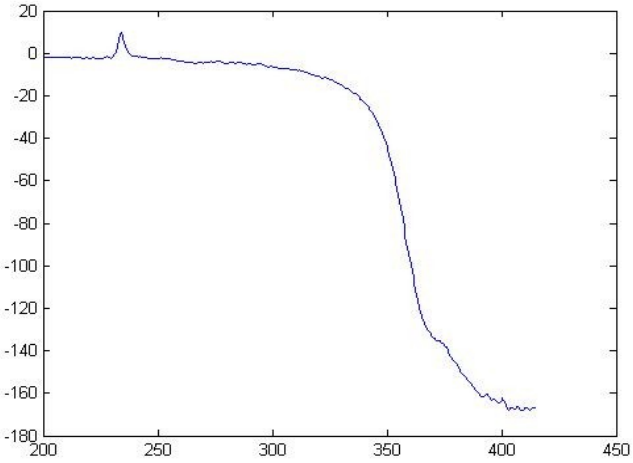

Figure 3-13 2C transverse phase with 4cm cable length

3.3.3 Experimental Results

The actual samples are non-linear and numerous factors could influence the test results, such as the small structural difference between samples, the accuracy of mounting, the equipment and other environmental issues. So in general, each result will be somewhat different from others. For accurate consideration, five samples of each type of the connector along the axial and transverse directions were tested in this study with different cable lengths of 2cm, 4cm, 6cm and 8cm. The detailed results are shown in Figure 3-14 to Figure 3-21 and Appendix D.

3.3.3.1 Results of Type 2C with Cable Lengths of 2cm, 4cm, 6cm and 8cm

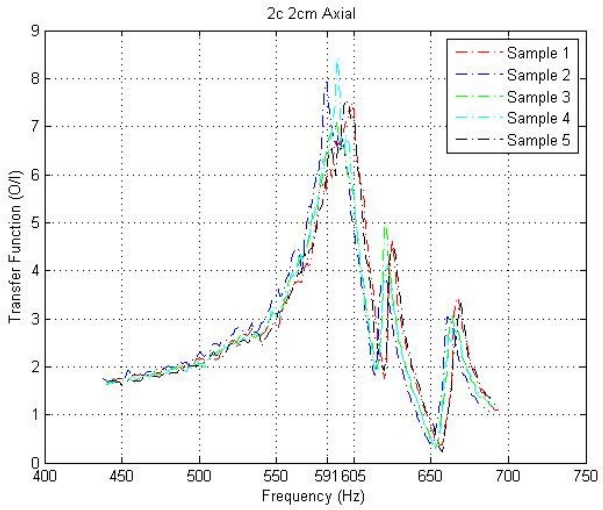

Figure 3-14 Experimental results of 2C 2cm axial transfer function

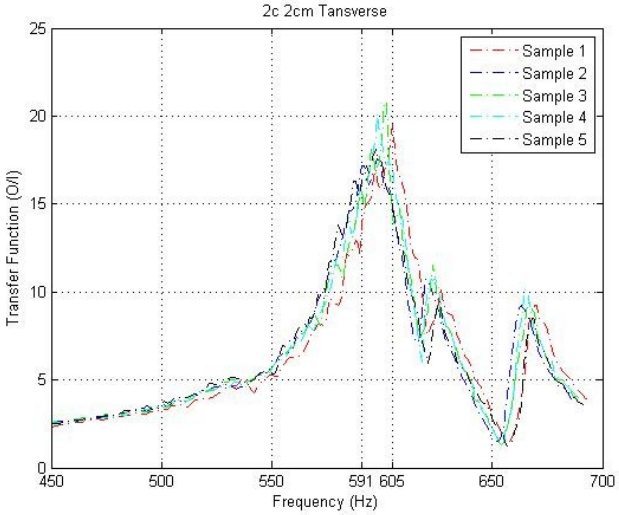

Figure 3-15 Experimental results of 2C 2cm transverse transfer function

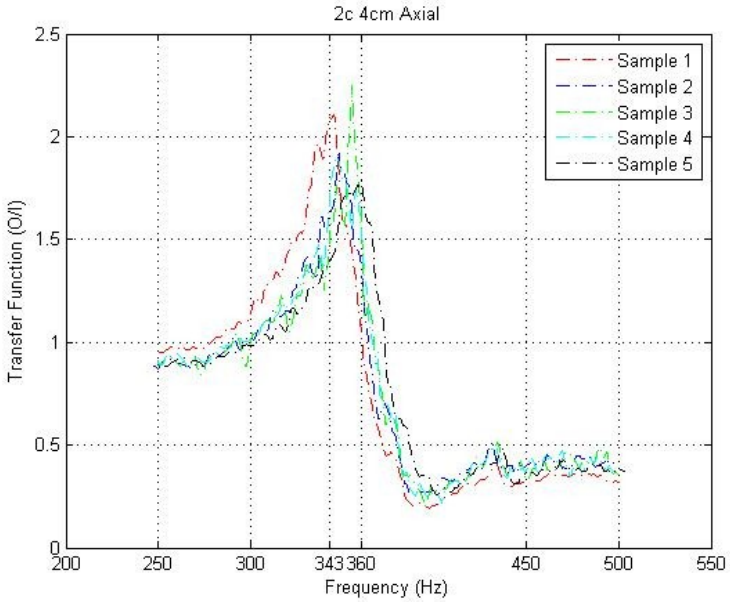

Figure 3-16 Experimental results of 2C 4cm axial transfer function

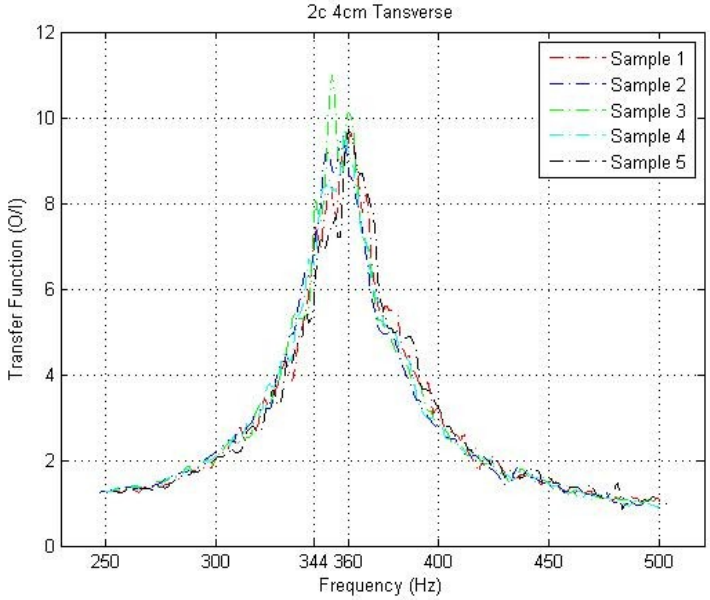

Figure 3-17 Experimental results of 2C 4cm transverse transfer function

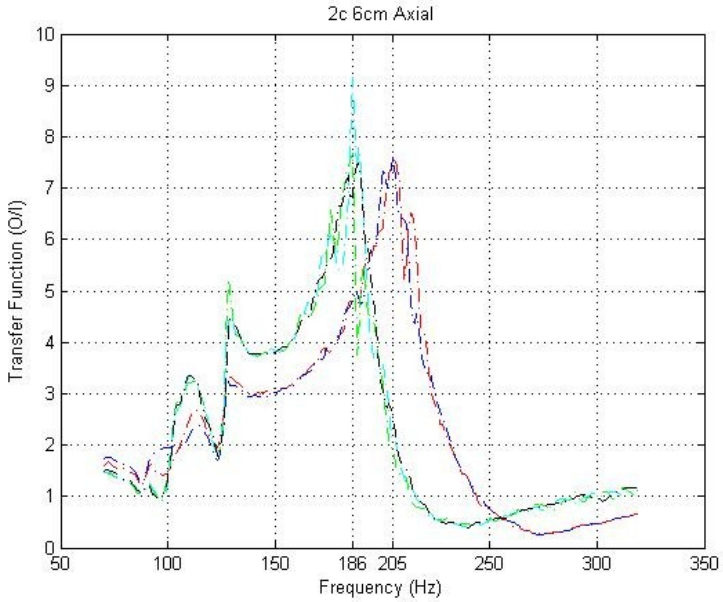

Figure 3-18 Experimental results of 2C 6cm axial transfer function

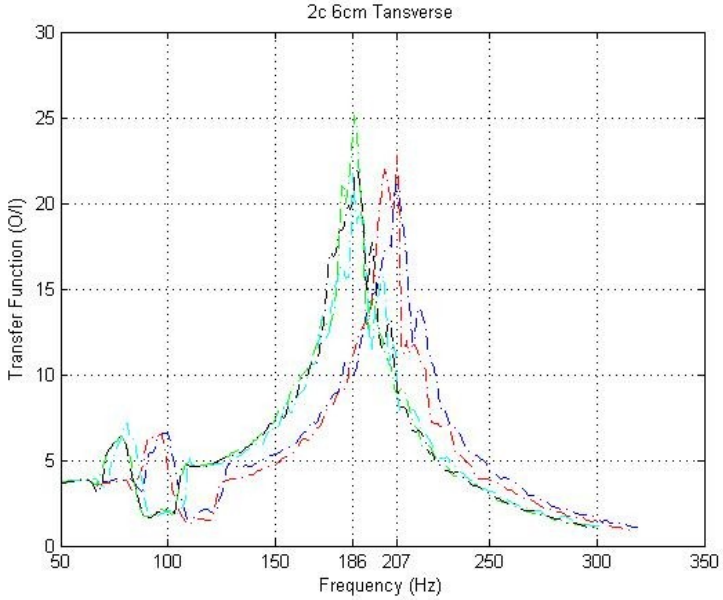

Figure 3-19 Experimental results of 2C 6cm transverse transfer function

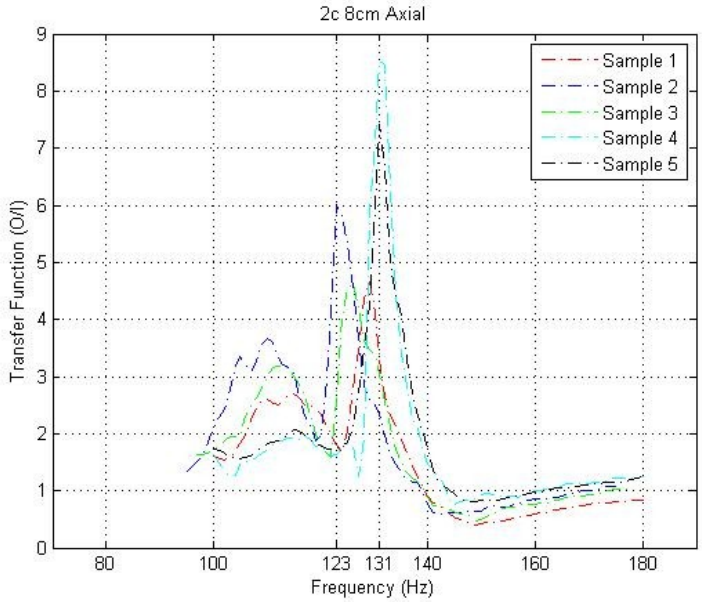

Figure 3-20 Experimental results of 2C 8cm axial transfer function

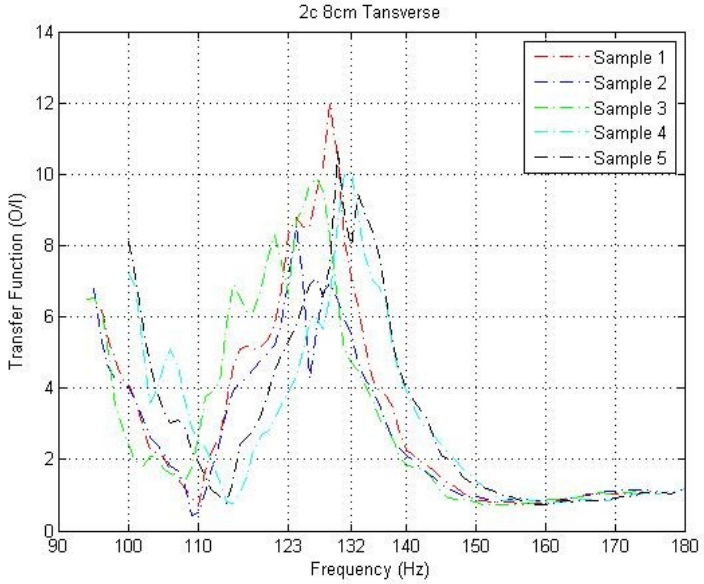

Figure 3-21 Experimental results of 2C 8cm transverse transfer function

Every result curve of each sample in the figures is the mean value. The natural frequencies of type 2C 2cm samples are from 591Hz to 605Hz. The magnitude of the transfer function is the ratio between output motion and input motion. From the results in the above

figures, the transfer function magnitude in the transverse direction is 2 to 3 times bigger than the one in the axial direction. The reason is the whole connector and the wire sample on the fixture can be treated as a thin-long column with a high slenderness ratio. The axial vibrating excitation from the shaker makes the thin-long connector sample buckle at its natural frequencies. Its motion in the experimental test looks like a vibrating string with a slight bending shape along the transverse direction. This phenomenon happens to all samples with different wire lengths. The natural frequencies in both axial and transverse directions are the same for the same type of samples. The natural frequencies of connector samples decreases as the wire length increases. In the 2C case, the natural frequencies are 344Hz - 366Hz at 4cm, 186Hz - 207Hz at 6cm, and 123Hz -131Hz at 8cm. According to the 3A, 3B and 3C experimental results shown in Appendix E, all of the connector types have a tendency to decrease frequency with increasing wire length. The trend is very obvious but not linear and for different connector types with same wire lengths, the natural frequencies are not the identical, but they are relatively close to each other. So an important conclusion can be drawn that the wire length and connector physical properties are the grounds for natural frequency changing, and the wire length plays the dominant role.

3.4 Three Dimensional Modeling and FEA Analysis of the Frequency Response of Single Blade/Receptacle Connector Pairs with Various Types and Cable Lengths

In this study, the aim is not only to understand the fretting corrosion data of electronic connectors resulting from experimental tests, but also to acquire a fuller comprehension of the morphological attributes of the connector for its further design

optimization to prevent or minimize fretting corrosion. As noted in previous chapters, due to the limits of the material samples and experimental tests, the details of the driving mechanism are not easily observed. A finite element simulation is an excellent alternative method to examine visually unobservable behaviors, such as the deformation of specified points on the structure, and relative motion between contacting surfaces.

3.4.1 Three Dimensional Finite Element Model

An ANSYS harmonic finite element three dimensional (3D) model was developed to simulate the transfer function results based on the same sample structures, the experimental configurations, and material properties. Some two dimensional simulations were done by F. Xie and C. Chen for the other connector studies. Their work provided meaningful examples of combining the FEA techniques and experimental tests together. Compared to the two dimensional model, the three dimensional model requires considerably more elements and larger computation resources, but provides more details of the model structure and dynamic behavior.

3.4.1.1 Geometric Model and Meshing

The 3D geometric model was created according to the drawings of the single blade/receptacle connector pair. A part of the drawing is shown in the Figure 3-3. Figure 3-22 and Figure 3-24 show the assembled single blade/receptacle connector pair 3-D model and the meshed model. In Figure 3-22, on the left is the blade with screw nut and washer; the beige color part on the right is stiffened wire; the rest of the part on the right are the crimp

and the receptacle with washer. Inside the receptacle, the spring and the bathtub are shown in the section view of Figure 3-23. The scale of the geometric model is the same as that of the sketch drawings. The thickness of the connector part wall is 0.28mm, which does not include the blade thickness. The wire material properties are a composite of the copper wire and rubber insulation layer. According to the previous work done by F. Xie, C. Chen and R. D. Ibrahim [30] [31] [44], the rubber layer's density and Young's Modulus are negligible compared to the copper cord and are ignored. However, the densities had to be adapted somewhat to match the mass of the original 3D samples.

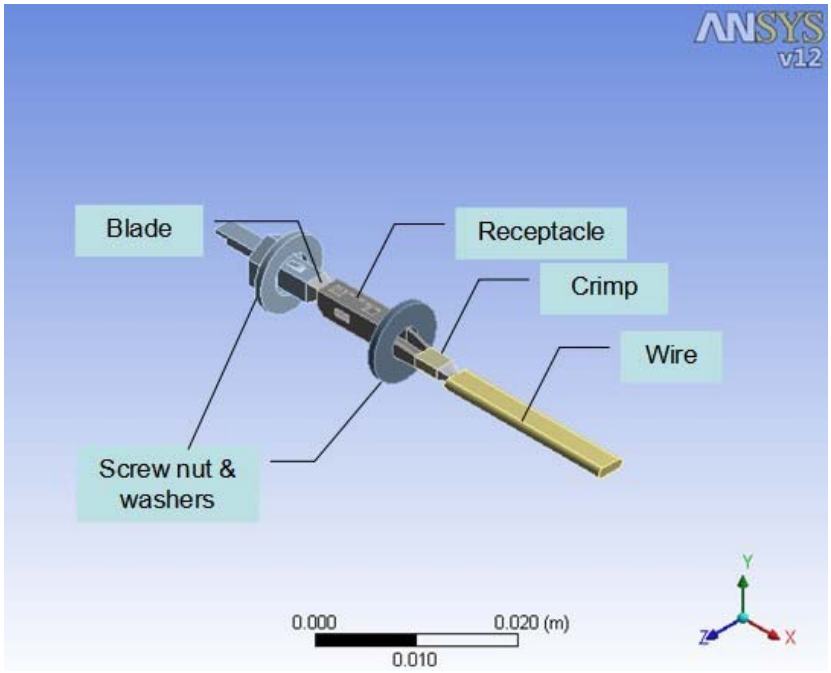

Figure 3-22 Assembly view of 3D connector model with 2cm wire

In order to perform the finite element simulation, mesh grids are generated from the samples. In general, TET-HEX combination grid units were utilized for the complex structure of the connector pair. The mapped method was applied to the uniformed structures to

simplify mesh grids. Some other mesh techniques are employed for the three dimensional model: the Advanced Size Function: Curvature; the Initial Size Seed: Active Assembly; the Curvature Normal Angle is 70.3950 ° ; the Growth Rate Default is 1.850; the Transition Ratio: 0.272; the Growth Rate: 1.2; the Pinch Tolerance: 1.615e-5m.

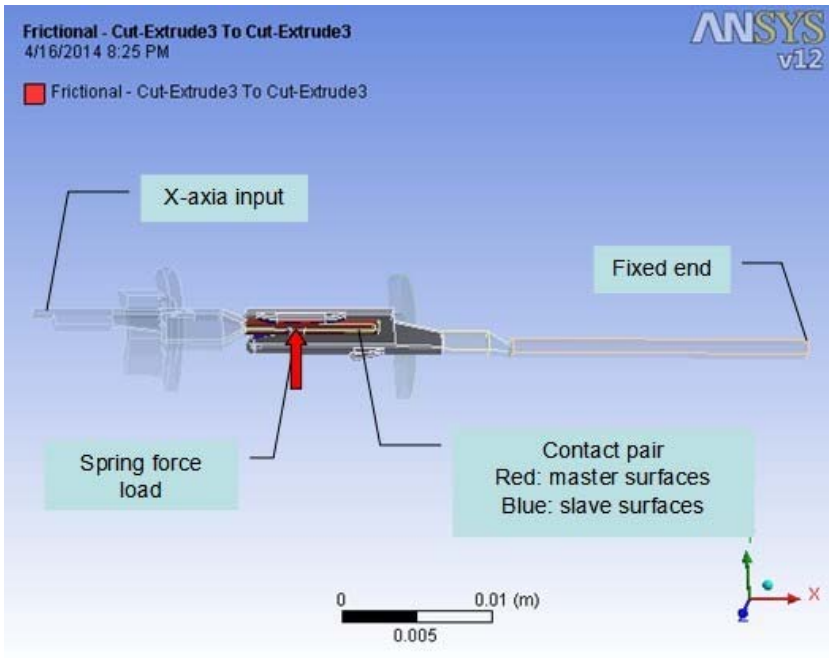

Figure 3-23 Section view of 3D connector model of boundary conditions, loads and contacts information

3.4.1.2 Material Properties

According to the sketch drawings, data sheets and discussions shown above, the Young's Modulus and the densities of each part of the connector and accessories on the connector are listed in Table 3-3.

Table 3-3 Material and dimensional properties of the model components

Components	Thickness	Density	Young's Modulus	Poisson's Ratio
Blade front part	0.8mm	8910kg/m^3	130GPa	0.3
Blade rear part	0.28mm	6974kg/m^3	130GPa	0.3
Receptacle	0.28mm	8910kg/m^3	130GPa	0.3
Spring in receptacle	0.28mm	8910kg/m^3	130GPa	0.3
Wire	1.1mm	4564kg/m^3	9GPa	0.3
Screw nut and washer	-	12876kg/m^3	195GPa	0.3

3.4.1.3 Contact Control

A contact pair was created between the blade front part and the inside structures of the receptacle. The master contact surfaces were the top and bottom surfaces of the blade front part. The slave contact surfaces included the curved tip of the spring, which had a contact with the underside surface of the blade, and the flat step surfaces which had a contact with the upper surface of the blade.

The contact type was set as a frictional contact using penalty contact methods and self-controlled damping. The coefficient of friction values are from the experimental results of Chapter 2, Table 2-.5.

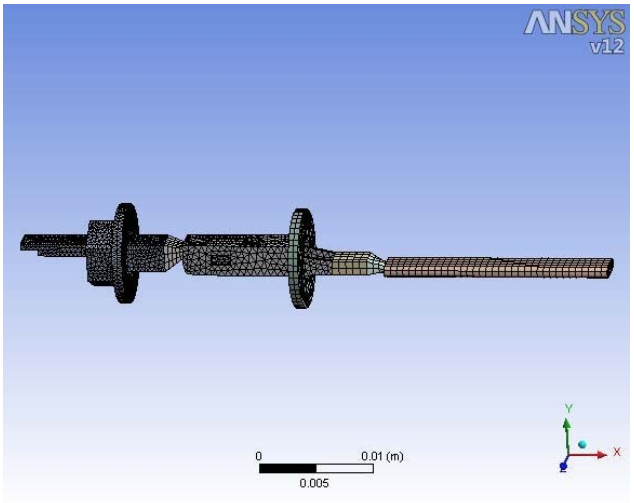

Figure 3-24 Mesh grids of a 2cm wire length 3D model

3.4.1.4 Load and Boundary Conditions

The spring force load was added to the underside of the spring tip to simulate the clamp force from the receptacle. In total, four different values of the spring force were acquired from Chapter 2, Table 2-5.

According to the actual experimental setup shown in Figure 3-10, the end of the wire was set to a Fixed End boundary condition with 0 degrees of motion, to simulate that the wire end was clamped by the fixture. The end of the blade was set to a periodic distance input along the X-axis with 1 degree of freedom and a chosen input frequency.

3.4.2 ANSYS Harmonica Simulation Setup

The frequency bands of each type and wire length situations are the same as the results in Chapter 3.3.2, which makes it convenient to compare the FEA results and the experimental results. To determine the transfer function results, the input and output data

were also assembled by the FEA Post-Processor. The monitored positions are the same as for the experimental points, such as Input A, Output A and Output T. Equation 3-1 was then employed to generate FEA simulation transfer functions.

3.4.3 3-D FEA Transfer Function Simulation Results

The FEA transfer functions are shown in Figure 3-25 to 3-32 and Appendix E.

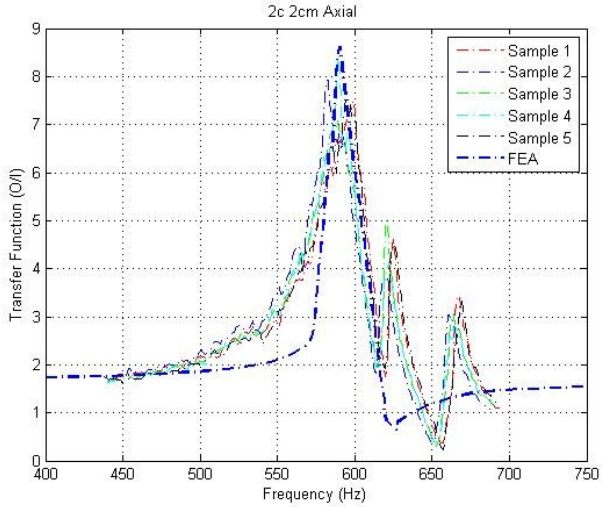

Figure 3-25 Simulation results comparison of 2C 2cm axial transfer function

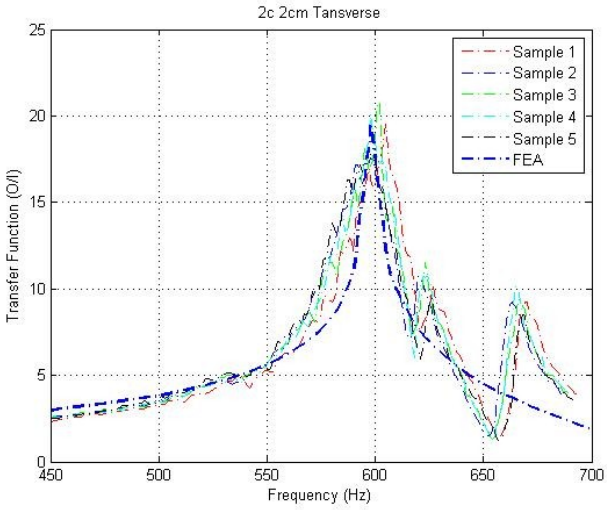

Figure 3-26 Simulation results comparison of 2C 2cm transverse transfer function

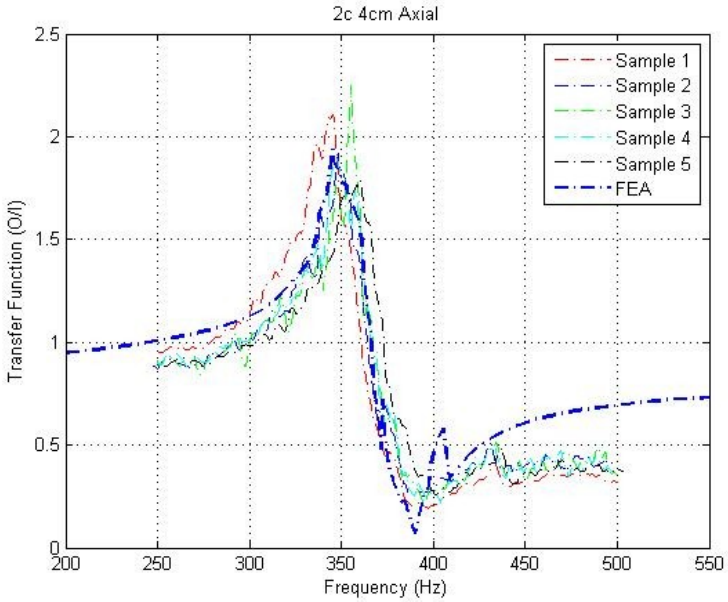

Figure 3-27 Simulation results comparison of 2C 4cm axial transfer function

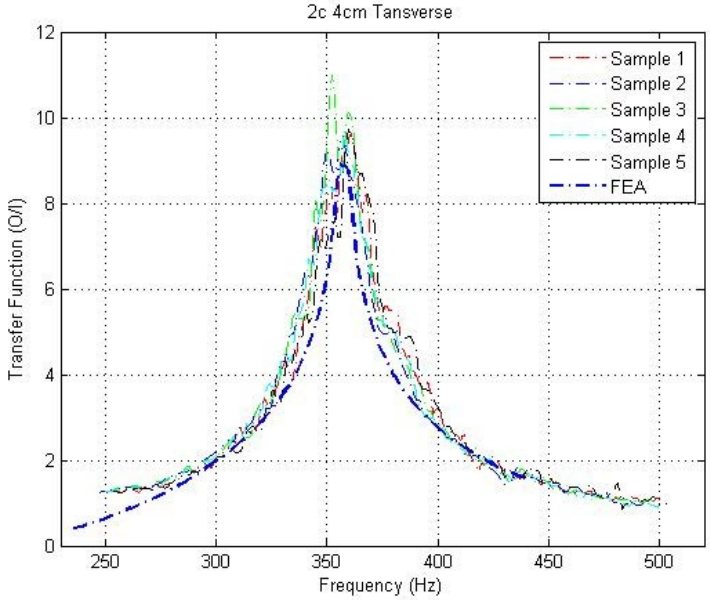

Figure 3-28 Simulation results comparison of 2C 4cm transverse transfer function

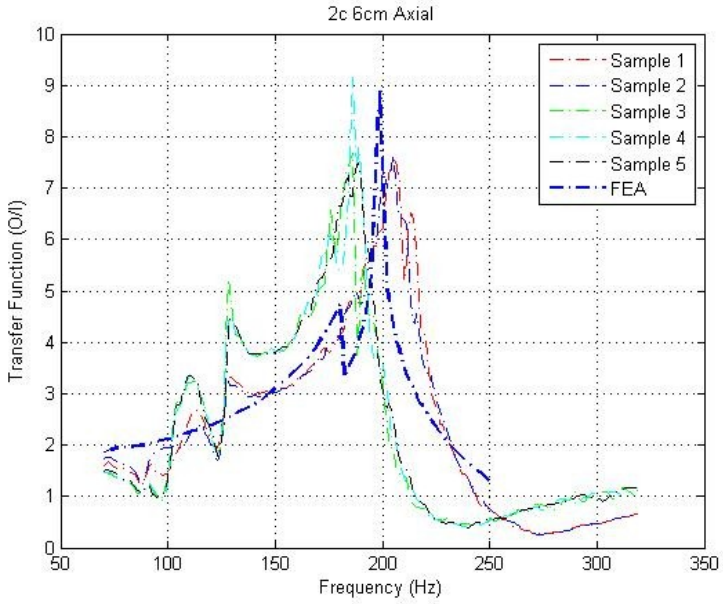

Figure 3-29 Simulation results comparison of 2C 6cm axial transfer function

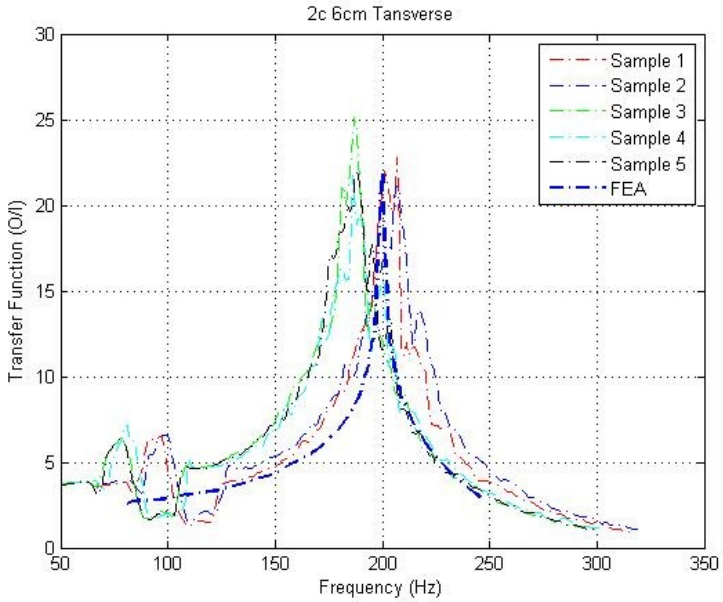

Figure 3-30 Simulation results comparison of 2C 6cm transverse transfer function

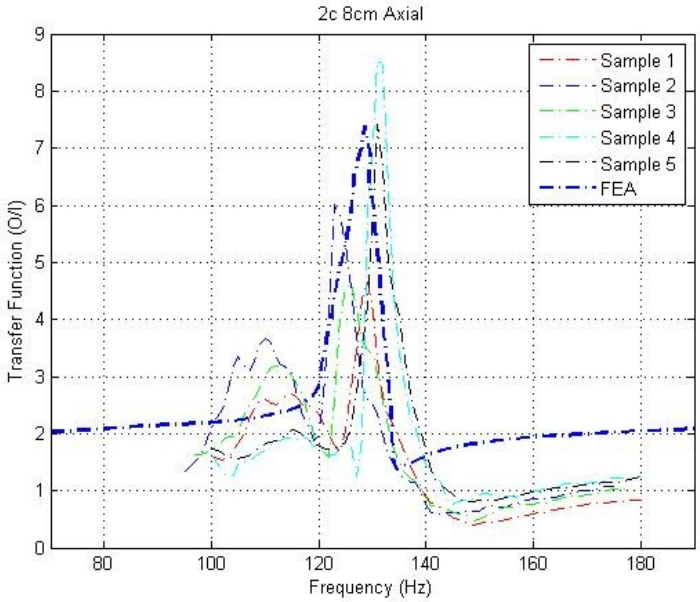

Figure 3-31 Simulation results comparison of 2C 8cm axial transfer function

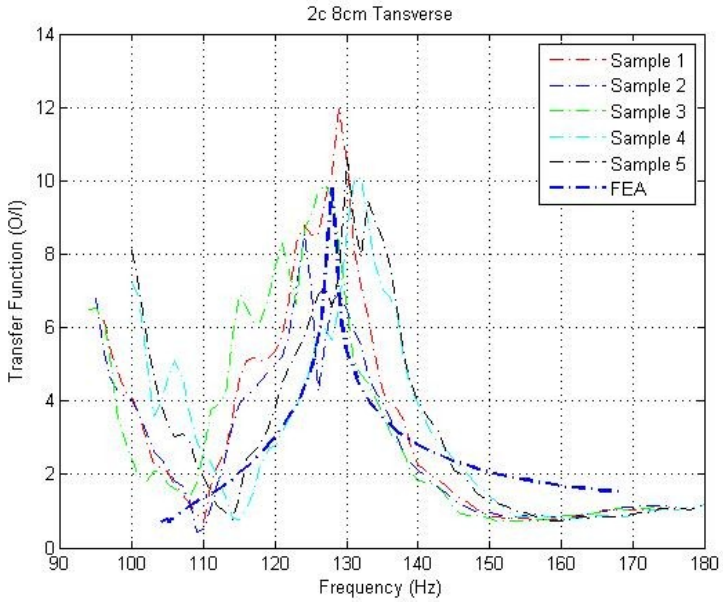

Figure 3-32 Simulation results comparison of 2C 8cm transverse transfer function

The FEA transfer function results match very well with the experimental results. The frequency range and transfer function magnitude range are close to each other. That means the experimental results verify the FEA results. In some cases, such as the 2C 4cm and 6cm

axial results, some small peaks appear around the major natural frequency peak in both experimental and FEA simulation results.

In those cases, the deviation of measurement can be excluded for smaller peaks in the experimental results. Generally, a linear simple structure transfer function curve would be simple and smooth, without small peaks or "jerking" behavior. The connector samples are much more complex with a variety of nonlinear effects, particularly friction. This complex structure makes the whole system more non-linear, and results in the small peaks and jerking in the transfer function curve.

3.5 Summary and Discussion

A study of the vibration induced frequency response and transfer function of a single blade-receptacle pair was presented in this chapter. A series of both experimental tests and 3D FEA simulations were used to determine the natural frequencies of different types of connectors with various lengths of wire. The stiffened wire on the receptacle provided a strong enough cantilever wire condition to prevent the vibration being absorbed by the wiring and not being transferred to the blade/receptacle pair. According to the experimental setup, the previous results in Chapter 2, and the sketch drawings, the details of the structures, assembly, contact conditions, material properties, load and boundary conditions were used in the 3D FEA model, and the respective FEA transfer functions were acquired from the simulations.

The purpose of this chapter is to identify the relationship between natural frequency and connector type and as well as wire length. A given connector system is most susceptible to vibration induced fretting corrosion when the excitation is at its the natural frequency. Accordingly, the results of this chapter provide the input frequencies for the fretting corrosion threshold study described in the next chapter. The details of the experimental frequency results and FEA frequency results are listed in Table 3-4. Figures 3-33 to 3-36 show the corresponding box plots of the results.

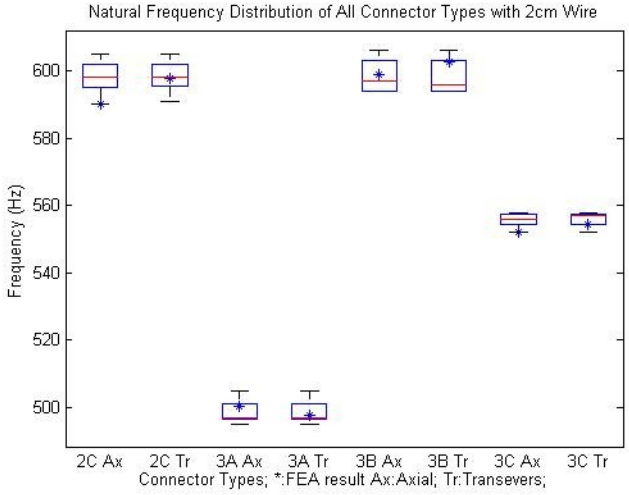

Figure 3-33 Natural Frequency Distribution of All Connector Types with 2cm Wire Length

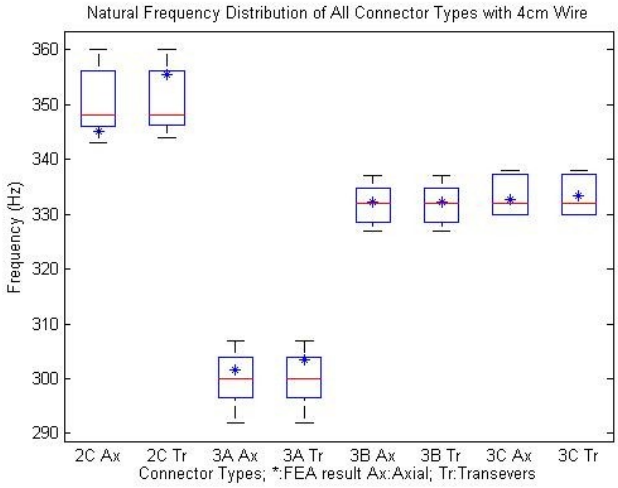

Figure 3-34 Natural Frequency Distribution of All Connector Types with 4cm Wire Length

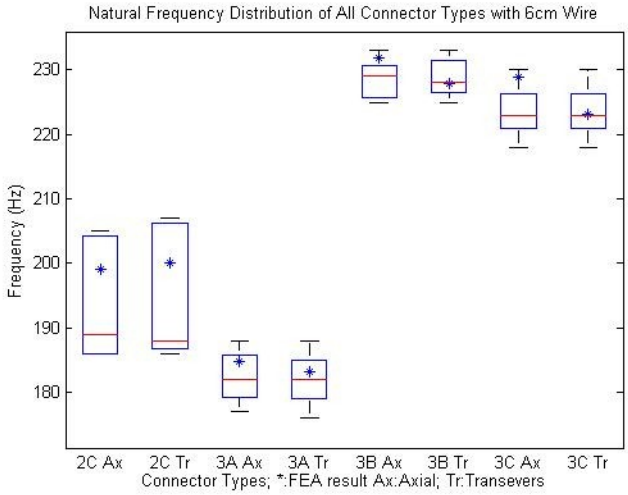

Figure 3-35 Natural Frequency Distribution of All Connector Types with 6cm Wire Length

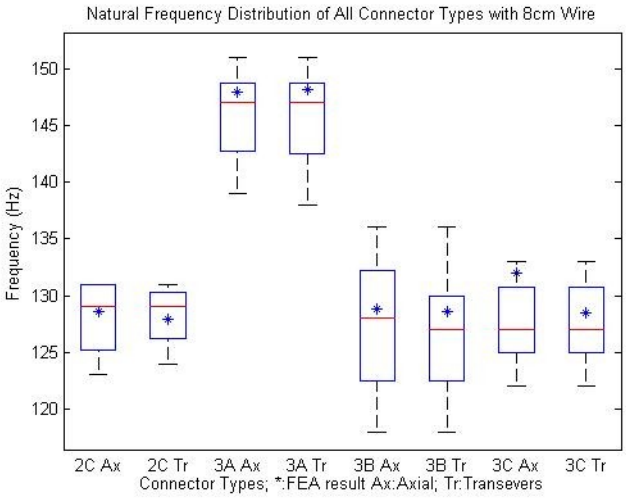

Figure 3-36 Natural Frequency Distribution of All Connector Types with 8cm Wire Length

Table 3-4 Natural frequencies (Hz) of experimental tests and FEA simulations

Type\Sample			1	2	3	4	5	Ave.	FEA	Type\Sample			1	2	3	4	5	Ave.	FEA
2C	2cm	A	590	597	598	601	605	598.2	590.2	3B	2cm	A	594	594	597	602	606	598.6	598.8
		T	591	597	598	601	605	598.4	597.6			T	594	594	596	602	606	598.4	602.7
	4cm	A	343	347	348	355	360	350.6	345.2		4cm	A	327	329	332	334	337	331.8	332.1
		T	344	347	348	355	360	350.8	355.4			T	327	329	332	334	337	331.8	332.2
	6cm	A	186	186	189	204	205	194	199		6cm	A	225	226	229	230	233	228.6	231.8
		T	186	187	188	206	207	194.8	200			T	225	227	228	231	233	228.8	227.9
	8cm	A	123	126	129	131	131	128	128.6		8cm	A	118	124	128	131	136	127.4	128.8
		T	124	127	129	130	131	128.2	127.9			T	118	124	127	128	136	126.6	128.6
3A	2cm	A	495	497	497	500	505	498.8	500.3	3C	2cm	A	552	555	556	557	558	555.6	552.1
		T	495	497	497	500	505	498.8	497.7			T	552	555	557	557	558	555.8	554.4
	4cm	A	292	298	300	303	307	300	301.6		4cm	A	330	330	332	337	338	333.4	332.6
		T	292	298	300	303	307	300	303.4			T	330	330	332	337	338	333.4	333.4
	6cm	A	177	180	182	185	188	182.4	184.8		6cm	A	218	222	223	225	230	223.6	228.8
		T	176	180	182	184	188	182	183.1			T	218	222	223	225	230	223.6	223.1
	8cm	A	139	144	147	148	151	145.8	147.9		8cm	A	122	126	127	130	133	127.6	132
		T	138	144	147	148	151	145.6	148.1			T	122	126	127	130	133	127.6	128.5

From the figures, type 3A has the lowest natural frequencies with the wire length from 2cm to 6cm, but has the highest with the wire length of 8cm. For the other three types, in the 2cm wire length condition, the frequencies for 2C and 3B are relatively close to each other and have the highest natural frequency. The frequencies for 3C are in the middle range of those observed. In the 4cm wire length condition, the frequencies for 2C are highest. Those for 3B and 3C are in the middle range of those observed and relatively close to each other. In the 6cm wire length condition, the frequencies for 2C are in the middle of the observed range. Those for 3B and 3C's are highest and close to each other. On the 8cm wire length condition, the frequencies for 2C, 3B and 3C are close to each other and are at the lowest values for those observed.

Chapter 4 The Fretting Corrosion Input Threshold Study of Single Blade/Receptacle Connector Pairs

4.1 Introduction

Fretting degradation has been recognized as a fatal problem in the mechanical field, and it was first identified nearly 70 years ago [2]. Since then it has become a subject of considerable research interest for engineers and researchers. In the previous chapters, the importance and current status of fretting degradation or fretting corrosion have been discussed. The previous work in Chapter 2 and Chapter 3 identified the static friction coefficients of the connector pairs, spring forces, and the natural frequencies of the sample connectors based on the transfer function, which are the most important parameters for determining the fretting corrosion of electrical connectors.

According to the previous work of G. Flowers, F. Xie, C. Chen and H. Yang [30] [31] [32], there is a threshold level of input excitation. For vibration levels below that threshold, fretting corrosion does not occur. If the vibration levels are above the threshold, then fretting corrosion will occur. The experimental results of those studies showed that, for the primary mode of connector rocking-type interface motion, the relative moment at the location served as a good indicator of the expected fretting rate. An approximate relative motion threshold for the start of fretting corrosion was proposed based on analysis of experimental data.

The work in this chapter focuses on identifying the input vibration amplitude thresholds for four types of sample connectors with different wire lengths. To identify and

monitor when fretting corrosion occurs on the electrical connectors, a Keithley Model 2010 multimeter was used. When the fretting corrosion starts, the electrical resistance increases with time. According to the experience from the experimental tests, the electrical resistance value is generally around 0.05Ω at the beginning of fretting. The FEA dynamic simulation is used in this chapter to evaluate the performance inside the connector pair when it is subjected to a sinusoidal single-frequency excitation. Data and parameters from the experimental work in the previous chapters are used in the 3D FEA model. ABAQUS models show both motions of specified points on the blade and the receptacle contact region along the input direction axis. By comparing the motion amplitudes between points on the blade and the receptacle, the relative motion distances under fretting condition are obtained. The details of the study are presented in the followed sections.

4.2 Experimental Configuration

4.2.1 Experimental Samples

All four types of connector pair samples, 2C, 3A, 3B, and 3C, were tested in this fretting corrosion input threshold study. Each sample type had four different wire lengths, 2cm, 4cm, 6cm, and 8cm, respectively. Accordingly, there were sixteen sample configurations for these test.

4.2.2 Experimental Equipment

4.2.2.1 Keithley Model 2010 Multimeter

The Model 2010 is a $7^{1/2}$-digit high-performance digital multimeter [45]. It has 0.0018% basic DV voltage accuracy and 0.0032% basic resistance accuracy. It is used to measure the contact resistance in the four-wire mode. In this mode, it can measure the resistance from 1uΩ to 120MΩ. The circuit used for measuring the resistance is shown in Figure 4-1.

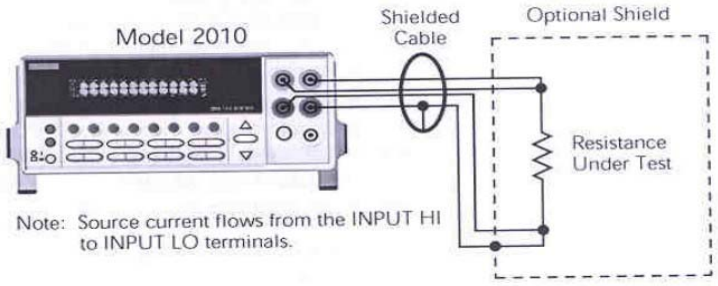

Figure 4-1 Four-wire resistance measurements using a Keithley Model 2010 multimeter

The key condition of the measurement of the contact resistance is dry circuit testing. Many low resistance measurements are made on contact devices such as switches and relay contacts. The purpose of this testing is to determine whether oxidation has increased the resistance of the contacts. If the voltage across the contacts during the test is too high, the oxidation will be punctured and render the test meaningless. Dry circuit testing limits the measurement voltage to 20mV or less.

4.3 Experimental Study on Fretting Corrosion Input Threshold of a Single Blade/Receptacle Connector Pairs with Various Types and Cable Lengths

4.3.1 Experimental Setup

In the fretting corrosion input threshold study, the experimental setup is the same as the one in the frequency response of the connector pair tests in Chapter 3. The mounting method is exactly the same as in section 3.3.1. In the experimental tests, each fretting test started after its corresponding transfer function test, and no dismounting or extra setup was needed. The reason for this same setup is that the actual samples are nonlinear and a slight change of setup or other interferences will make the natural frequency of the sample deviate. So the original setup was the key stage to ensure the accuracy of whole test results. For the setup details please refer to Figure 3-12 in Chapter 3.

4.3.2 Input Source of Vibration

In order to measure the fretting behavior of each experimental connector sample, fixed sine mode vibration was applied at the corresponding natural frequency of each sample. A reflector was attached to the shaker head and a single channel laser vibrometer was used to monitor the input excitation, including the frequency and the amplitude. The excitation frequency was the corresponding natural frequency of each sample and the HP 35665A Dynamic Signal Analyzer was used to drive the LDS amplifier-shaker system. The natural frequencies are shown in Table 3-4. The vibration amplitude can be adjusted using controls on both the HP 35665A Dynamic Signal Analyzer and LDS PA 500L Amplifier. The input vibration amplitude was set to 0 mV_{RMS} at the beginning of each test, and increased gradually.

4.3.3 Electrical Resistance Measurement and Results

The fixed sine vibrations with specific frequencies and amplitudes is related to the g-level on the shaker head which is the main feedback signal to the amplifier. The equation of the g-level, sinusoidal frequency and peak-to-peak amplitude is defined as:

$$g_{RMS} = \frac{0.707 \times \frac{amplitude(mm)_{peak-peak}}{2} \times (2 \times \pi \times f)^2}{9.81 \times 1000} \text{ (g)} \qquad (4\text{-}1)$$

As an important parameter of the vibration system, the g-level was detected by the sensor inside the shaker head without monitoring equipment. The known amplitude and the frequency of the sinusoidal vibration can be utilized to obtain the g-level using to Equation 4-1.

The electrical resistance is the criterion to detect the fretting corrosion in this study. As mentioned in section 4.3.2, the electrical resistance rose in pace with the vibration amplitude increasing gradually. Before the fretting started, the electrical resistance changed very slowly when the vibration amplitude increased. According to many tests, the fretting has a critical point. Before this point, there is no fretting. The resistance was very unstable, rapidly moving up and down, when it was approaching the fretting critical point. When the input excitation amplitude passed the threshold, the fretting started and the resistance rose up rapidly even when the input amplitude did not increase anymore. So, this input amplitude is the input threshold investigated in this study. The test results of the thresholds and g-levels with corresponding sample types and frequencies are listed in Table 4-1, and all the results are the mean value of each situation. Figure 4-2 and Figure 4-2 show the results of Table 4-1.

According to Figure 4-2, the thresholds of type 2C,3A,3B and 3C have the tendency to increase in pace with the increasing wire length. For 3A and 3B, the smallest input threshold is at the 2cm wire length. The type C's smallest input threshold is at 4cm. Throughout all four types of the connector, their threshold is very near to each other at 4cm. Referring to the g-levels in Figure 4-3, the results are less than 10 g and do not receive the same propensity. At 4cm wire length the g-level value of all four types are close to each other as well. With all the results at 4cm wire length, a bold conclusion can be made: all the four types of connectors have a similar frequency response property and fretting performance at 4cm. It is a meaningful conclusion for the commercial connectors, especially for the nonlinear actual productions in the industry. For the designers and manufacturers, this similarity of the property and the fretting performance makes it much easier to optimize the design and avoid failure of the connectors.

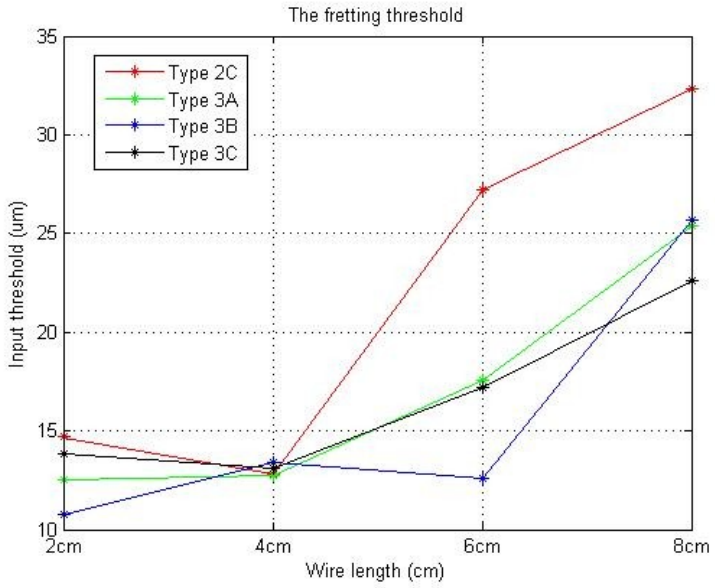

Figure 4-2 Fretting threshold results of all types of connector

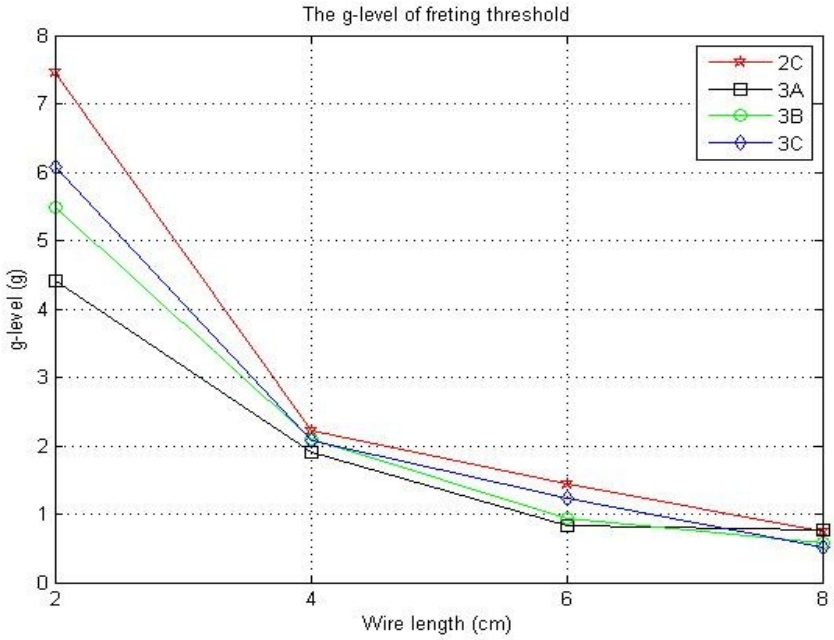

Figure 4-3 G-level of fretting threshold

Table 4-1 The average results of input threshold and g-level

Sample		Frequency/Ave (Hz)	Input Threshold/Ave (um)	g-level (g)	Sample		Frequency/Ave (Hz)	Input Threshold/Ave (um)	g-level (g)
2C	2cm	598.3	14.68	7.468	3B	2cm	598.5	10.78	5.488
	4cm	350.7	12.82	2.213		4cm	331.8	13.39	2.095
	6cm	194.4	27.25	1.445		6cm	228.7	12.6	0.937
	8cm	128.1	32.32	0.754		8cm	127	25.7	0.589
3A	2cm	498.8	12.49	4.416	3C	2cm	555.7	13.85	6.078
	4cm	300	12.75	1.912		4cm	333.4	13.12	2.073
	6cm	182.2	17.54	0.827		6cm	223.6	17.17	1.230
	8cm	145.7	25.4	0.766		8cm	127.6	22.58	0.522

4.4 Three Dimensional Modeling and FEA Simulation of Fretting Corrosion Input Threshold of a Single Blade/Receptacle Connector Pairs with Various Types and Cable Lengths

In the previous chapters, the critical issues which can induce the fretting corrosion of the electrical connector have been studied, such as the friction forces, friction coefficients, normal spring forces, transfer functions of the frequency response and the input thresholds of the fretting corrosion. All these works can be used to describe the performance of the electrical connector and predict the fretting corrosion. However, to reach a better understanding of the mechanism of the contact fretting corrosion of the electrical connector pair, the relative motion between the blade and the receptacle under fretting must be studied. Due to the limitation of the experimental tests, it is not generally possible to observe the relative motion between the blade and the receptacle at such a small scale and high frequency inside a very small and complicated structure. Another approach for such a difficult studying configuration is with the help of the FEA software.

The vibration induced fretting motion is classified as the explicit dynamic problem in the Finite Element field. To produce an accurate simulation, the 3D model is a viable solution with enough moderate calculation speed and accuracy of the complicated system. Based on the reason above and the work in previous chapters, a highly detailed 3D FEA model was developed in ABAQUS according to the sketch drawings of the connector, like the one in Chapter 3. A number of periodic explicit dynamic simulations were implemented to detect the relative motion between the contacting two parts. The detailed content is described in this chapter.

4.4.1 Three Dimensional Finite Element Model

4.4.1.1 Geometric Model and Meshing

Just like the model in Chapter 3, the 3D models of all types of the connectors were imported into the ABAQUS operating system. Unlike the transfer function simulation in ANSYS, the whole simulations were explicit dynamic problems. The calculation method used the General Dynamic (ABAQUS Explicit), and step control was also created. According to the test parameters in Chapter 3 and the previous sections in Chapter 4, the vibration frequencies are very high for generating the fretting motion. The frequencies are from 127 Hz to 598 Hz. Because the 3D dynamic FEA simulation causes many computing resources and takes too much time, and only a few of the cycles of the vibrating motion can give a clear view of the relative motion, so the step is set very short to save calculation time. For the lower frequency samples the step-time was set to 0.01s, and for the higher frequency samples the step time enlarged to 0.02s.

The explicit dynamic mesh grids were developed for the vibration simulation. The solid C3D8R elements have been utilized in the assembly model. Differing from the wire length, the mesh grid values are various, from 1500 level to 3200 level. The details are shown in Figure 4- 4.

4.4.1.2 Material Properties

The material properties are the same values as in the previous chapters. The details of the Young's Modulus and the densities of each part of the connector and accessories on the connector are listed in Table 3-3.

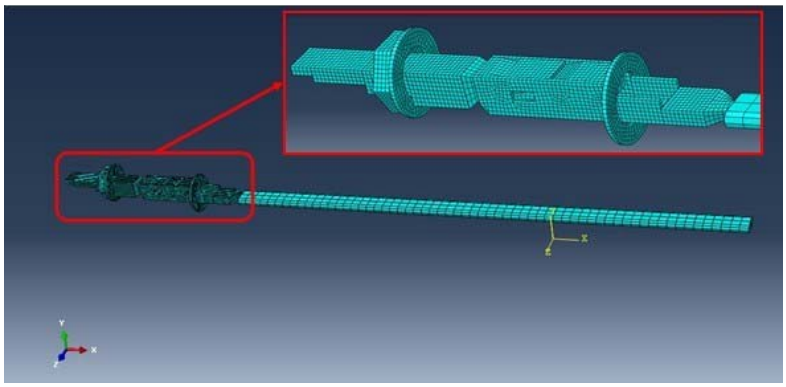

Figure 4- 4 Meshed connector pair model with 8cm length wire

4.4.1.3 Contact Control

The contact occurs between the surfaces of the blade and inside the receptacle. Two contact pairs were created: The master contact surfaces are the upside and underside surfaces of the front part of the blade; the slave contact surfaces include the curved tip of the spring, which has contact with the bottom surface of the blade, and the bathtub surfaces which have contact with the upper surface of the blade. The "Penalty" contact method was used, which employs friction properties of each type of connectors. The highlighted surfaces in the section view of Figure 4-5 are the contact pairs.

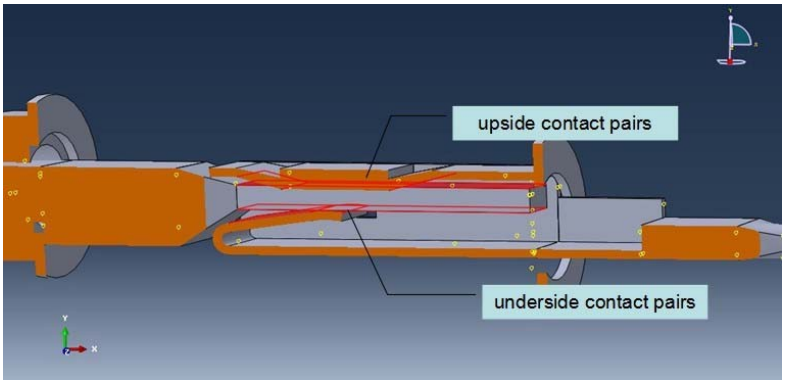

Figure 4-5 Section view of contact pairs

4.4.1.4 Load and Boundary Conditions

The spring force load was added in the spring tip as a "Body Force" to simulate the clamp force from the receptacle. Totally, four different values of the spring force were used from Chapter 2, Table 2-5. In accordance with the physical configuration of the experimental setup, the end of the wire was set to a "Fixed End" boundary condition with 0 degrees of freedom. The end of the blade was subjected to a periodic distance input along the X-axis with a single degree of motion and the input frequencies are set to match the motion produced by shaker head. Figure 4-6 shows the details of the setup. The periodic motion in the simulation is defined by the ABAQUS, as the function listed below:

$$a = A_0 + \sum_{n=1}^{N} [A_n \cos n\omega(t - t_0) + B_n \sin n\omega(t - t_0)] \tag{4-2}$$

where A_0 is the initial amplitude, A_n and B_n are the constant parameters, and ω is the circular frequency which is defined as:

$$\omega = \pi f \tag{4-3}$$

where f is the frequency of the vibration which was determined in Chapter 3. In experimental tests, the sinusoidal excitation was provided by the shaker head for the different frequencies. Therefore, in the particular circumstance of Equation 4-2, $A_0 = 0$, $A_1 = 0$, $B_1 = 1$, n=1. So, Equation 4-2 becomes:

$$a = \sin \omega(t - t_0) \tag{4-4}$$

Equation 4-4 describes the vibratory motions in the fretting input threshold in the previous experimental tests. Table 4-2 gives the circular frequencies in ABAQUS, from Eq. (4-3).

Table 4-2 Comparison table of frequencies

Sample		Frequency/Ave (Hz)	Circular frequency (cycle)	Sample		Frequency/Ave (Hz)	Circular frequency (cycle)
2C	2cm	598.3	1878.662	3B	2cm	598.5	1879.29
	4cm	350.7	1101.198		4cm	331.8	1041.852
	6cm	194.4	610.416		6cm	228.7	718.118
	8cm	128.1	402.234		8cm	127	398.78
3A	2cm	498.8	1566.232	3C	2cm	555.7	1744.898
	4cm	300	942		4cm	333.4	1046.876
	6cm	182.2	572.108		6cm	223.6	702.104
	8cm	145.7	457.498		8cm	127.6	400.664

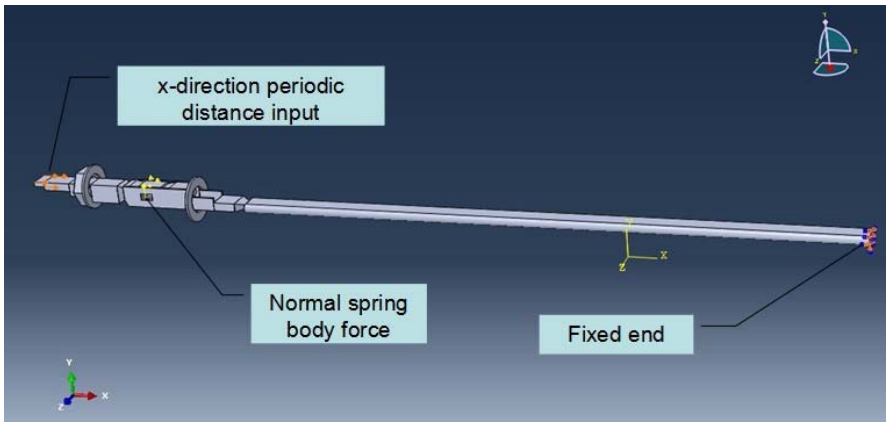

Figure 4-6 Boundary conditions and load setup

4.4.2 3-D FEA Relative Motion Simulation Results

The relative movement between the blade and the receptacle is obtained by the subtraction of the blade motion and the receptacle motion along the “x” direction. To ensure the most accurate results, two points at the contact region were chosen for the displacement “Field

Output." On point is located at the spring tip of the receptacle and the second is at the corresponding point of the blade. Details are shown in Figure 4-7.

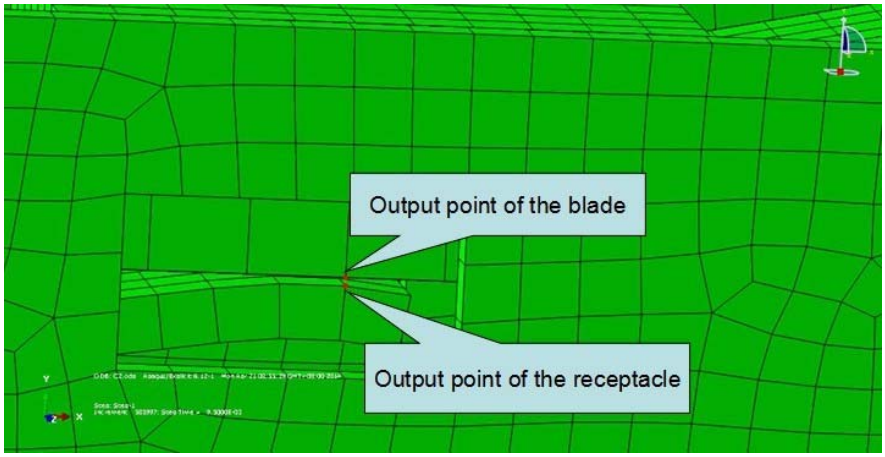

Figure 4-7 Output point of connector pair

Figure 4-8 to Figure 4-11 and Appendix F show the output x-direction displacement plots. From an inspection of these figures, a small delay is observed between the blade output curves and the receptacle curves. The two parts are separate to each other and connected by only normal spring force and friction force between the contacting surfaces. A dynamic damping effect appeared during the vibration process, and ABAQUS calculated the changing damping for every element increment. Both the blade output curves and the receptacle output curves are not regular sine wave in those plots. That is due to the large deformation along the y-direction of the wire. The entire connector undergoes a buckling motion. The pure sine wave input motion from the end of the blade was decomposed into two motions along the x and y directions. At the contact area, this effect became obvious, and progressed the peak-to-peak amplitude on the "x" direction.

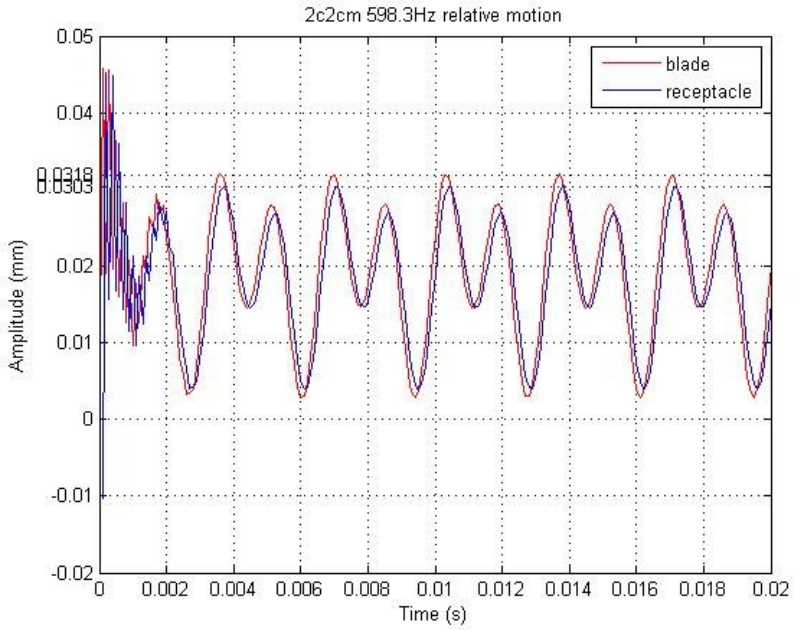

Figure 4-8 Six cycles of the blade and receptacle of 2C 2cm under 598.3Hz

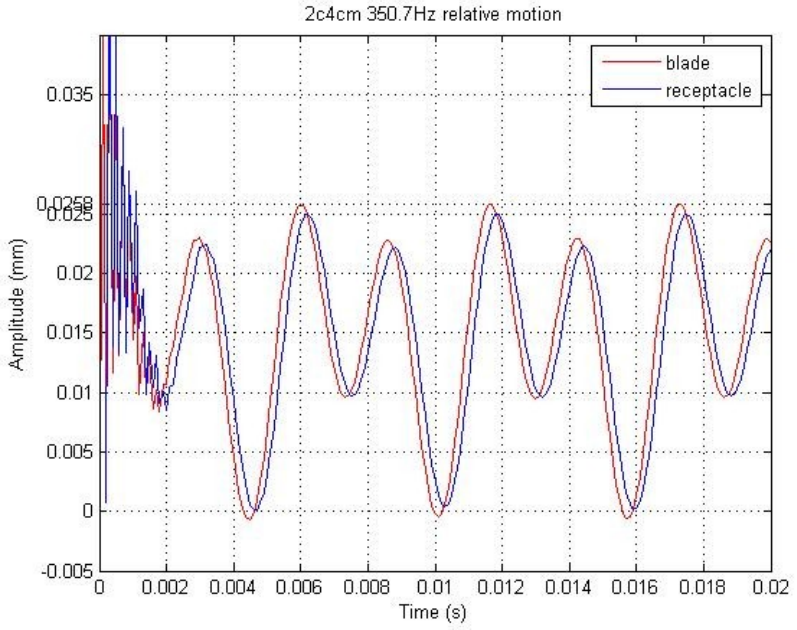

Figure 4-9 Three cycles of the blade and receptacle of 2C 4cm under 350.7Hz

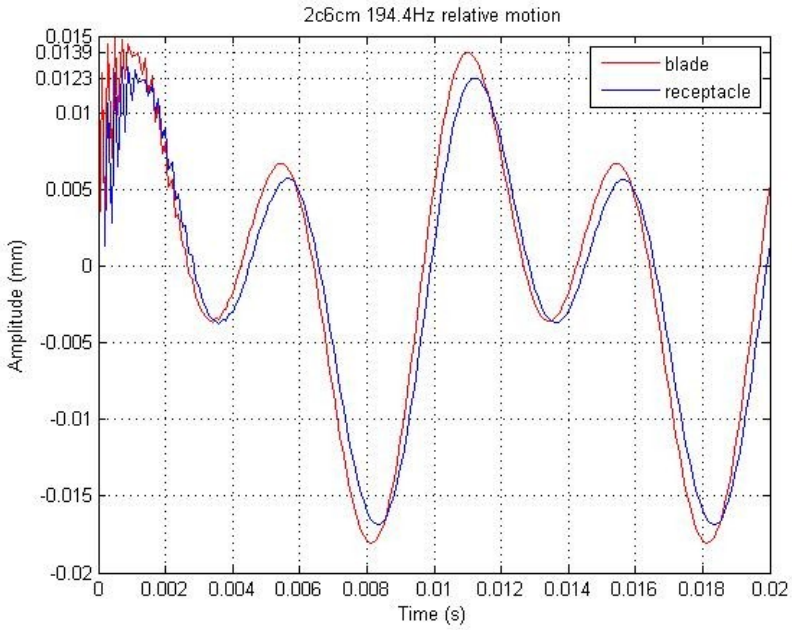

Figure 4-10 Two cycles of the blade and receptacle of 2C 6cm under 194.4Hz

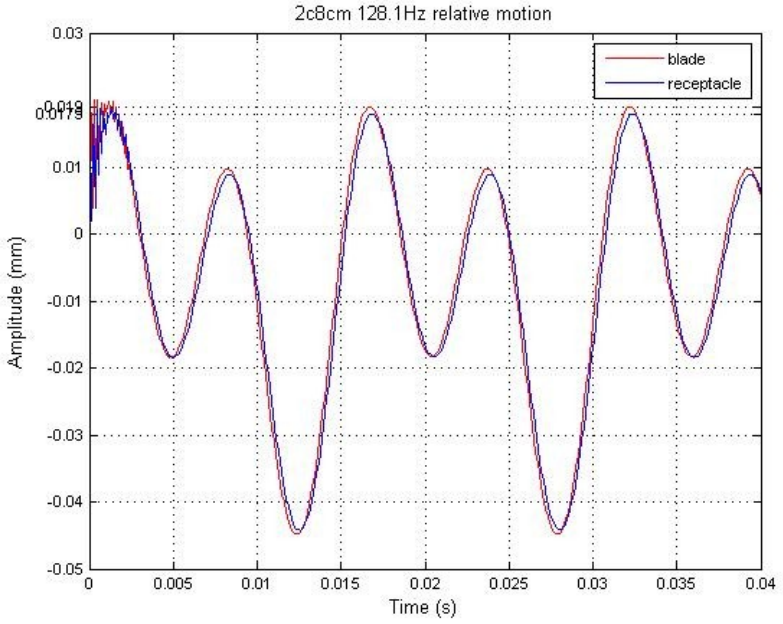

Figure 4-11 Two cycles of the blade and receptacle of 2C 8cm under 128.1Hz

The FEA simulation shows that at the monitored points on the blade tip and corresponding position in the receptacle spring, the output curve is not a pure sinusoidal curve.

According to the simulation, the motion of the connector is buckling and not pure axial motion. A portion of the axial motion is transmitted to the transverse direction, and at the blade/receptacle contacting region this transverse motion is greatest. Therefore, there is some time lag between the blade output and receptacle output. This lag is because those regions are separate to each other; the only link is the friction force between them. The damping generated by the friction force is the reason for the observed delay.

The detailed relative motion values and the responding frequencies of all types of connector are listed in Table 4-3.

Table 4-3 Relative motion of fretting for all connector types

Sample		Frequency/Ave (Hz)	Relative motion (um)	Sample		Frequency/Ave (Hz)	Relative motion (um)
2C	2cm	598.3	1.5	3B	2cm	598.5	1.4
	4cm	350.7	0.8		4cm	331.8	0.8
	6cm	194.4	1.6		6cm	228.7	0.5
	8cm	128.1	1.1		8cm	127	1.0
3A	2cm	498.8	1.5	3C	2cm	555.7	1.5
	4cm	300	0.9		4cm	333.4	0.7
	6cm	182.2	1.0		6cm	223.6	1.4
	8cm	145.7	1.2		8cm	127.6	0.8

The average value of the relative motion for all of the results in Table 4-3 is 1.10625 um. This value is close to the fretting relative threshold value, 1.0 um, which is assumed in previous work in this area [23], [24], [25], [26], [29], [30]. That work identified a threshold point of input excitation which indicated the onset of fretting corrosion. This result confirms that assumption, through a combination of experimental tests and FEA simulations.

4.5 Summary and Discussion

In this chapter, two sections of work have been described. The first section concentrated on determining the input vibration amplitude thresholds which resulted in the onset of fretting corrosion for the four types of connectors with different wire lengths. By using the Keithley Model 2010 multimeter and the shaker system, the experimental tests monitored the electrical resistance when the connectors began to exhibit fretting under single-natural-frequency sinusoidal vibration. The corresponding input amplitudes were recorded as the fretting input thresholds for each type of connector.

In the second section, the FEA models were developed to explore the relative motion between the blade and the receptacle when the fretting was occurring for the connector pair. The ABAQUS Explicit technique was used in this section. The final simulation results demonstrated that due to the soft wire of the connection, the wire buckled when it was under vibration. The large deformation of the wire produced motion orthogonal to the input excitation direction. The relative motion values were obtained by monitoring the motion of two specified points on the blade and the receptacle in the contact area. The mean value of all the relative motion values is 1.10625 um, which is close to the 1um fretting relative motion threshold proposed by G. Flowers.

Chapter 5 Conclusions and Future Work

In this thesis, four experimental studies and three corresponding FEA simulations have been performed on the topic of fretting corrosion in commercial auto electrical connectors. The first two projects were concerned with the frictional property of the connector surfaces and the spring force of the receptacle. The author studies static friction forces and the coefficients of static friction for 5 cases of commercial electrical connectors, which are essential data for finding out natural frequency and predicting fretting corrosion of connectors. Next, the author obtained the coefficients of static friction from experimental test data. The MT-200 tension/torsion experimental test system is employed for the static friction force and spring normal force experimental test. The ABAQUS^{TM} FEA 3-D simulation is also utilized to verify the static friction forces by applying coefficients of static friction and normal military units.

In the third study, a study of the vibration induced frequency response and transfer function on a single blade-receptacle pair was presented. A series of both the experimental tests and 3D FEA simulations were used to see the natural frequencies of different types of connector with various lengths of wire. The strengthened wire on the receptacle provided a strong enough cantilever wire condition to prevent the vibration being absorbed by a soft one. According to the experimental setup, the previous results in Chapter 2, and the sketch drawings provided by connector manufacture, the details of structures, assembly, contact conditions, material properties, load and boundary conditions were reproduced by the 3D FEA model. The respect FEA transfer functions were acquired from the simulations.

Finally, two sections of work have been completed by the author. The first section concentrated on hearing the input thresholds of the vibration amplitude which caused the fretting corrosion on the four types of the connectors with different wire lengths. By using the Keithley Model 2010 multimeter and shaker system, the experimental tests monitored the electrical resistance when the connectors became fretting under the single-natural-frequency sinusoidal vibration. The corresponding input amplitudes were recorded as the fretting input thresholds for each type of connector. In the second portion, the 3D FEA models were produced to identify the relative movement between the blade and the receptacle when the connector pair was under fretting excitation. The ABAQUS Explicit technique was employed in this section. The final simulation results demonstrated that, due to the soft wire of the connection, the wire buckled when it was under vibration. The large deformation of the wire caused a sub-motion, which was perpendicular to the input excitation direction. The relative motion values were obtained by monitoring two close points on the blade and the receptacle at the contact area, whose X- coordinate values were same.

Suggested further research includes

- Refinement of the FEA model for frequency responses and relative motion thresholds.
- Investigation of relative motion under non-resonate frequencies.
- Investigate the transfer functions and input thresholds of the fretting corrosion.
- Develop the 3D simulation of the lateral direction excitation situation.

References

[1]. E.M. Eden, W.N. Rose, and F.L. Cunnungham, The Endurance of Metals, *Proc. Inst. Mech. Engrs.* 1911.

[2]. Tomlinson, Thorpe, and Gough, "An Investigation of The Fretting Corrosion of Closely Fitting Surfaces," *Proc. I. Mech E., Vol.141,* 1939

[3]. Bethune, B., and R. B. Waterhouse. "Electrochemical studies of fretting corrosion." *Wear 12.1,* 1968, pp.27-34.

[4]. E.M. Bock and J.H. Whitley, "Fretting Corrosion in Electric Contacts," *Electric Contacts - 1974, Chicago*, 1974, p.128.

[5]. K. Wright, *Proc. Inst. Mech. Engrs.* (B),1B (11), 556 (1952-1953)

[6]. Clough, Ray W., and James L. Tocher. "Finite element stiffness matrices for analysis of plates in bending." *Proceedings of conference on matrix methods in structural analysis. Vol. 1,* 1965.

[7]. G. Villeneuve, D. Kulkarni, P. Bastnagel, and D. Berry, "Dynamic Finite Element Analysis Simulation of the Terminal Crimping Process," *Electrical Contacts, 1996., Proceedings of the Forty-Second IEEE Holm Conference Joint with the 18th International Conference on Electrical Contacts*, Sept. 1996, pp.156-172.

[8]. A. Monnier, B. Froidurot, C. Jarrige, R.Meyer, and P. Teste, "A Mechanical, Electrical, Thermal Coupled-field Simulation of a Sphere-plane Electrical Contact," *Electrical Contacts, 2005. Proceedings of the Fifty-First IEEE Holm Conference on Electrical Contacts,* Sept. 2005, pp. 224 – 231.

[9]. S. Krumbein, "Contact Properties of Tin Plates," *Electric Contacts* -1974, Chicago, 1974, p.38.

[10]. M. Antler, W.F. Graddick and H.G. Tompkins, "Base Metal Contacts: An Exploratory Study of Separable Connection To Tin-Lead," *Electric Contacts* -1975, Chicago, 1975, p. 25.

[11]. J.H. Whitley, "Investigation of Fretting Corrosion Phenomena in Electric Contacts," *Proc. 8Th Int. Conf. Electrical Contact Phenomena*, Tokyo, 1976, pp. 659-665

[12]. M. Antler, and E.S. Sproles, "Effect of Fretting on the Contact Resistance of Palladium," *IEEE Trans. CHMT*, V.5, N.1, 1982, p. 158.

[13]. J.M. Hooyer and K. Peekstok, "The Influence of Practical Contact Parameters on Fretting Corrosion of Tin-Base Low-Level Connector Contacts," *Electric Contacts* -1987, IEEE - HOLM, Chicago, 1987, p. 43.

[14]. M. Antler, "Survey of Contact Fretting in Electrical Contacts," *Proceedings of the Twenty Ninth IEEE Holm Conference on Electrical Contacts*, 1984, pp. 3-22.

[15]. A. Lee and M.S. Mamrick, "Fretting Corrosion of Tin with Electrical Load," *Proc. 13 International Conference On Electric Contacts*, Lausanne, Switzerland, 1986, pp. 476.

[16]. A. Lee and M.S. Mamrick, "Fretting Corrosion of Tin-Plated Copper Alloy," *IEEE Trans. CHMT* – 10, 1987, pp. 63.

[17]. A.Lee and M.S.Mamrick, "Fretting Corrosion of Tin at Elevated Temperatures" *Proceedings of the Thirty Fourth IEEE Holm Conference on Electrical Contacts*, 1988, pp. 87-91.

[18]. M. Braunovic, "Fretting Damage inTin-Plated Aluminum and Copper Connections," *Electric Contacts,* 1988, IEEE-HOLM, San Francisco, 1988, p. 179.

[19]. J.J. Motine and B.T. Reagor, "Investigation of Fretting Corrosion at Dissimilar Metal Interfaces on Socketed IC Device Applications," *IEEE Trans. CHMT-7*, V.7, N.1, 1984, pp. 61-68.

[20]. M.D. Bryant, "Resistance Buildup in Electrical Connectors Due To Fretting Corrosion of Rough Surfaces," *IEEE Transactions on Components, Packaging, and Manufacturing Technology*, V.17, N.1, March 1994, pp. 86-95.

[21]. R. D. Malucci, "Multispot Model of Contacts Based on Surface Features," *Electric Contacts -1990, IEEE - HOLM*, Montreal, 1990, pp.625.

[22]. R. D. Malucci, "Impact of Fretting Parameters on Contact Degradation," *Proceedings of the Forty-Second IEEE Holm Conference on Electrical Contacts*, 1996, pp. 395-403

[23]. G. T. Flowers, F. Xie, M. Bozack, R. Horvath, R. D. Malucci, and B. Rickett, "Vibration Testing of Fretting Corrosion in Electrical Connectors Subjected to Multi-Frequency and Random Spectral Profiles," *Proceedings of the Forty-Ninth IEEE Holm Conference on Electrical Contacts,* September 8-10, 2003, pp. 45-50.

[24]. G. T. Flowers, F. Xie, M. Bozack, X. Hai, B. Rickett, and R. D. Malucci, "A Study of the Physical Characteristics of Vibration Induced Fretting Corrosion," *Proceedings of the Fiftieth IEEE Holm Conference on Electrical Contacts*, September 20-23, 2004, pp.312-319.

[25]. George T. Flowers, Fei Xie, Michael J. Bozack, and Robert D. Malucci, "Vibration Thresholds for Fretting Corrosion in Electrical Connectors," *IEEE Transactions on Components and Packaging Technologies*, Vol. 27, No. 1, 2004, pp. 65-71.

[26]. George T. Flowers, Fei Xie, Michael J. Bozack, Roland Horvath, Robert D. Malucci, and Bretton I. Rickett. "Modeling early stage fretting of electrical connectors subjected to

random vibration," *IEEE Transactions on Components and Packaging Technologies,* 28.4 (2005): p. 721-727.

[27]. G. Flowers, F. Xie, M. Bozack, B. Rickett, and R. Malucci, "The Influence of Contact Interface Characteristics on Vibration-Induced Fretting Degradation," *Proceedings of the Fifty-First IEEE Holm Conference* on *Electrical Contacts*, September 26-28, 2005, pp.82-88.

[28]. X. Fei. "A study of vibration-induced fretting corrosion for electrical connectors," *Doctoral Dissertation, Auburn University*, 2007.

[29]. Chen Chen, George T. Flowers, Michael Bozack, and Jeffrey Suhling, "Modeling and analysis of a connector system for the prediction of vibration-induced fretting degradation," *Proceedings of the 55th IEEE Holm Conference on Electrical Contacts,* September 14-16, 2009, pp.131-137.

[30]. C. Chen. "A study of the prediction of vibration-induced fretting corrosion in electrical contacts," *Doctoral Dissertation Auburn University*, 2009.

[31]. H. Yang. "Thresholds of Axial Vibration Induced Fretting Corrosion in Electrical Connectors," *Thesis Auburn University*, 2013.

[32]. Fei Xie, George T. Flowers, Chen Chen, Michael Bozack, Jeffrey Suhling, Bretton I. Rickett, Robert D. Malucci, and Charlie Manlapaz, "Analysis and Prediction of Vibration-Induced Fretting Motion in a Blade/Receptacle Connector Pair," *IEEE Transactions on Components and Packaging Technologies*, Vol. 32, No. 3, 2009, pp. 585-592.

[33]. L. Lam, J. W. McBride, C. Maul, and J. K. Atkinson, "Displacement Measurements at the Connector Contact Interface Employing a Novel Thick Film Sensor," *Electrical Contacts, 2005. Proceedings of the Fifty-First IEEE Holm Conference on 26-28 Sept. 2005*, pp.89-96.

[34]. G. Villeneuve, D. Kulkarni, P. Bastnagel, and D. Berry, "Dynamic Finite Element Analysis Simulation of the Terminal Crimping Process," Electrical Contacts, 1996., Proceedings of the Forty-Second IEEE Holm Conference Joint with the 18th International Conference on Electrical Contacts, Sept. 1996, pp. 156-172.

[35]. A. Monnier, B. Froidurot, C. Jarrige, R.Meyer, and P. Teste, "A Mechanical, Electrical, Thermal Coupled-field Simulation of a Sphere-plane Electrical Contact," *Electrical Contacts, 2005. Proceedings of the Fifty-First IEEE Holm Conference* on26-28 Sept. 2005, pp. 224-231.

[36]. S.V. Angadi, W.E. Wilson, R.L. Jackson, Flowers, G.T. and B.I. Rickett, "A Multi-Physics Finite Element Model of an Electrical Connector Considering Rough Surface Contact," *Proceedings of the 54th IEEE Holm Conference on Electrical Contacts*, October 27-29, 2008, pp.168-177.

[37]. John A. Schey. "Tribology in metalworking: friction, lubrication, and wear." *Journal of Applied Metalworking* 3.2 (1984): p.173.

[38]. A.T. Male, "A method for the determination of the coefficient of friction of metals under conditions of bulk plastic deformation." *J. Inst. Metal. 93* (1964): p.38-p.46.

[39]. Laser Vibrometer User Manual, Controller OFV-2610/2620, Sensor Head OFV-353, POLYTEC Co., Germany

[40]. HP 35665A Dynamic Signal Analyzer Installation and Verification Guide, Hewlett-Packard Company, USA, 1991

[41]. Installation and Operating Manual PA 500/1000L-CE Amplifiers, LDS Company, USA

[42]. Installation and Operating Manual V400 Series Vibrators, LDS Company, USA

[43]. Model 2010 Multimeter User's Manual, Keithley Instruments, Inc., USA, 1999.

Appendix A Log File of 2C2cm ANSYS Harmonica Simulation

```
/batch
/config,noeldb,1     ! force off writing results to database
*get,_wallstrt,active,,time,wall
! ANSYS input file written by Workbench version 12.0.1 Release
! File used for geometry attach: C:\Fuxi connector\model for ansys\Assem 2C 2cm.SLDASM
/com,--- Data in consistent MKS units.
/units,MKS
/nopr
/track,-1
/wb,file,start              !  signify a WB generated input file
/prep7
! Turn off shape checking because checks already performed inside WB mesher.
! See help system for more information.
SHPP,OFF,,NOWARN
/nolist
etcon,set             ! allow ANSYS to choose best KEYOP's for 180x elements
/com,********** Nodes for the whole assembly **********
nblock,3
(1i8,3e20.9e3)
       1  -2.557331435E-004    1.530384357E-003    1.454492897E-003
       2  -7.025385153E-004    1.609297184E-003    1.577380605E-003
......
   14222    6.193148450E-003    2.145028085E-003    1.015439873E-005
   14223    5.796154288E-003    2.246130190E-003   -1.030715149E-004
-1
/wb,elem,start            !  set before creation of elements
/com,********** Elements for Body 1 "Cut-Extrude2" **********
et,1,186
keyo,1,2,1
eblock,10
(15i8)
    4553      1      1      1      0     48     54     93     90     51     55    113    112   1695   1712
       0      0      0      0      0   1797   1696   1702   1714   1833   1703   1694   1710   1804   1798
......
    4608      1      1      1      0     11     22     16     16     91     52     72     72   1596   1611
       0      0      0      0      0     16   1595   1706   1705     72   1760   1597   1624   1612   1612
-1
/com,********** Elements for Body 2 "Boss-Extrude13" **********
et,2,187
eblock,10
(15i8)
       1      2      1      2      0    261    605    604   1220   2883   5216   2882   2888   5223   5219
......
    6212      5      4      5      0   9280   9281   9668   9674   9379   9380   9442   9441  10947  10951
       0      0      0      0      0  11802  10949  11242  11246  11371  11243  10948  10950  11374  11372
-1
/com,********** Elements for Body 6 "Loft1" **********
et,6,186
keyo,6,2,1
```

```
eblock,10
(15i8)
   5821      6      4      6      0   9454   9457   9458   9462   9455   9456   9459   9463   11397  11403
      0      0      0      0      0  11406  11398  11399  11402  11408   11400  11396  11401  11404  11412
......
   5824      6      4      6      0   9382   9385   9384   9383   9462   9458   9461   9465   11249  11254
      0      0      0      0      0  11252  11248  11406  11405  11411   11413  11251  11257  11255  11253
-1
/com,********** Elements for Body 7 "Boss-Extrude20" **********
et,7,186
keyo,7,2,1
eblock,10
(15i8)
   5825      7      4      7      0   9283   9474   9473   9471   9388   9391   9392   9393   10961  11425
      0      0      0      0      0  11423  10960  11262  11271  11274   11263  10958  11273  11275  11277
......
   5830      7      4      7      0   9282   9475   9468   9466   9389   9390   9399   9398   10957  11419
      0      0      0      0      0  11417  10955  11265  11269  11285   11267  10954  11270  11287  11286
-1
/com,********** Elements for Body 8 "Boss-Extrude26" **********
et,8,187
eblock,10
(15i8)
   4609      8      4      8      0   9999   10018  10090  10004  13128  13313  13131  13126  13177  13180
......
   5820      8      4      8      0  10009  10010  10045  10295  13229  13248  13234  13241  13254  13518
-1
/com,********** Elements for Body 9 "Boss-Extrude21" **********
et,9,186
keyo,9,2,1
eblock,10
(15i8)
   6213      9      4      9      0   9331   9836   9837   9332   9374   9448   9452   9373   11120  12098
      0      0      0      0      0  11123  11118  11228  11385  11227  11224  11119  11386  11394  11122
......
   6217      9      4      9      0   9332   9840   9839   9839   9373   9451   9450   9450   11125  12102
      0      0      0      0      0   9839  11124  11226  11389   9450  11225  11122  11392  11390  11390
-1
/wb,elem,end              !  done creating elements
/com,********** Send User Defined Coordinate System(s) **********
csys,0
/com,********** Set Reference Temperature **********
tref,22.
/wb,mat,start             !  starting to send materials
/com,********** Send Materials **********
MP,DENS,1,8910.,          ! kg m^-3
MP,ALPX,1,1.2e-005,     ! C^-1
MP,C,1,434.,      ! J kg^-1 C^-1
MP,KXX,1,60.5,            ! W m^-1 C^-1
MP,MURX,1,10000.,
MP,RSVX,1,1.7e-007,     ! kg m^3 A^-2 s^-3
MP,EX,1,129740000000.,            ! Pa
MP,NUXY,1,0.3,
```

```
MP,DENS,2,8910.,        ! kg m^-3
MP,ALPX,2,1.2e-005,    ! C^-1
MP,C,2,434.,     ! J kg^-1 C^-1
MP,KXX,2,60.5,          ! W m^-1 C^-1
MP,MURX,2,10000.,
MP,RSVX,2,1.7e-007,    ! kg m^3 A^-2 s^-3
MP,EX,2,129740000000.,          ! Pa
MP,NUXY,2,0.3,

MP,DENS,3,8910.,        ! kg m^-3
MP,ALPX,3,1.2e-005,    ! C^-1
MP,C,3,434.,     ! J kg^-1 C^-1
MP,KXX,3,60.5,          ! W m^-1 C^-1
MP,MURX,3,10000.,
MP,RSVX,3,1.7e-007,    ! kg m^3 A^-2 s^-3
MP,EX,3,129740000000.,          ! Pa
MP,NUXY,3,0.3,

MP,DENS,4,7850.,        ! kg m^-3
MP,ALPX,4,1.2e-005,    ! C^-1
MP,C,4,434.,     ! J kg^-1 C^-1
MP,KXX,4,60.5,          ! W m^-1 C^-1
MP,MURX,4,10000.,
MP,RSVX,4,1.7e-007,    ! kg m^3 A^-2 s^-3
MP,EX,4,200000000000.,          ! Pa
MP,NUXY,4,0.3,

MP,DENS,5,7850.,        ! kg m^-3
MP,ALPX,5,1.2e-005,    ! C^-1
MP,C,5,434.,     ! J kg^-1 C^-1
MP,KXX,5,60.5,          ! W m^-1 C^-1
MP,MURX,5,10000.,
MP,RSVX,5,1.7e-007,    ! kg m^3 A^-2 s^-3
MP,EX,5,200000000000.,          ! Pa
MP,NUXY,5,0.3,

MP,DENS,6,7850.,        ! kg m^-3
MP,ALPX,6,1.2e-005,    ! C^-1
MP,C,6,434.,     ! J kg^-1 C^-1
MP,KXX,6,60.5,          ! W m^-1 C^-1
MP,MURX,6,10000.,
MP,RSVX,6,1.7e-007,    ! kg m^3 A^-2 s^-3
MP,EX,6,200000000000.,          ! Pa
MP,NUXY,6,0.3,

MP,DENS,7,7850.,        ! kg m^-3
MP,ALPX,7,1.2e-005,    ! C^-1
MP,C,7,434.,     ! J kg^-1 C^-1
MP,KXX,7,60.5,          ! W m^-1 C^-1
MP,MURX,7,10000.,
MP,RSVX,7,1.7e-007,    ! kg m^3 A^-2 s^-3
MP,EX,7,200000000000.,          ! Pa
MP,NUXY,7,0.3,
```

```
MP,DENS,8,7850.,          ! kg m^-3
MP,ALPX,8,1.2e-005,     ! C^-1
MP,C,8,434.,      ! J kg^-1 C^-1
MP,KXX,8,60.5,            ! W m^-1 C^-1
MP,MURX,8,10000.,
MP,RSVX,8,1.7e-007,     ! kg m^3 A^-2 s^-3
MP,EX,8,200000000000.,            ! Pa
MP,NUXY,8,0.3,

MP,DENS,9,7850.,          ! kg m^-3
MP,ALPX,9,1.2e-005,     ! C^-1
MP,C,9,434.,      ! J kg^-1 C^-1
MP,KXX,9,60.5,            ! W m^-1 C^-1
MP,MURX,9,10000.,
MP,RSVX,9,1.7e-007,     ! kg m^3 A^-2 s^-3
MP,EX,9,200000000000.,            ! Pa
MP,NUXY,9,0.3,

/wb,mat,end               !  done sending materials
!************************ Model Summary *********************
!Cut-Extrude2, AU Blade, matid, 1
!Boss-Extrude13, AU Blade, matid, 2
!Cut-Extrude3, AU Blade, matid, 3
!Boss-Extrude24, Structural Steel, matid, 4
!Boss-Extrude22, Structural Steel, matid, 5
!Loft1, Structural Steel, matid, 6
!Boss-Extrude20, Structural Steel, matid, 7
!Boss-Extrude26, Structural Steel, matid, 8
!Boss-Extrude21, Structural Steel, matid, 9
!************************ End Model Summary ********************
! get the diagonal of the bounding box. Needed later for other things
*get,_xmin,node,,mnloc,x
*get,_ymin,node,,mnloc,y
*get,_zmin,node,,mnloc,z
*get,_xmax,node,,mxloc,x
*get,_ymax,node,,mxloc,y
*get,_zmax,node,,mxloc,z
_ASMDIAG=(_xmax-_xmin)*(_xmax-_xmin)+(_ymax-_ymin)*(_ymax-_ymin)+(_zmax-_zmin)*(_zmax-
_zmin)
_ASMDIAG=SQRT(_ASMDIAG)
/wb,contact,start         !  starting to send contact
/com,********** Create Contact "Frictional - Cut-Extrude3 To Boss-Extrude26" **********
/com,           Real Contact Set For Above Contact Is 11 & 10
*set,tid,11
*set,cid,10
r,tid
r,cid
et,tid,170
et,cid,174
eblock,10
(15i8)
   6218     11     11     11      0   1202   1204   1215   1215   8096   8101   1215   8097
.....
   6701     11     10     11      0  10005   9999  10032  10032  13127  13130  10032  13186
```

```
-1
keyo,cid,12,0             ! standard contact
mp,mu,cid,0.279! unitless
keyo,cid,2,1              ! penalty function only
keyo,cid,9,0              ! use real geometry with stepped effects
keyo,cid,7,0              ! No Prediction
rmod,tid,3,1.      ! FKN
rmod,tid,5,0.      ! ICONT
rmod,tid,6,0.      ! PINB
rmod,tid,10,0.     ! CNOF
rmod,tid,12,0.     ! FKT
rmod,cid,3,1.      ! FKN
rmod,cid,5,0.      ! ICONT
rmod,cid,6,0.      ! PINB
rmod,cid,10,0.     ! CNOF
rmod,cid,12,0.     ! FKT
/com,********** Create Contact "Contact Region 12" **********
/com,           Real Contact Set For Above Contact Is 13 & 12
*set,tid,13
*set,cid,12
r,tid
r,cid
et,tid,170
et,cid,174
eblock,10
(15i8)
   6702     13     13     13      0    220    227    228    228   2667   2703    228   2668
......
   6801     13     12     13      0     13     25     26     14   1603   1629   1606   1602
-1
keyo,cid,12,5             ! bonded always
keyo,cid,2,1              ! penalty function only
keyo,cid,9,1              ! ignore initial gaps/penetration
keyo,cid,7,0              ! No Prediction
rmod,tid,3,1.      ! FKN
rmod,tid,5,0.      ! ICONT
rmod,tid,6,0.      ! PINB
rmod,tid,10,0.     ! CNOF
rmod,tid,12,0.     ! FKT
rmod,cid,3,1.      ! FKN
rmod,cid,5,0.      ! ICONT
rmod,cid,6,0.      ! PINB
rmod,cid,10,0.     ! CNOF
rmod,cid,12,0.     ! FKT
/com,********** Create Contact "Contact Region 13" **********
/com,           Real Contact Set For Above Contact Is 15 & 14
*set,tid,15
*set,cid,14
r,tid
r,cid
et,tid,170
et,cid,174
eblock,10
(15i8)
```

```
   6802     15     15     15      0    634    635    660    660   5413   5420    660   5415
......
   6885     15     14     15      0     51     55    113    112   1702   1714   1833   1703
-1
keyo,cid,12,5            ! bonded always
keyo,cid,2,1             ! penalty function only
keyo,cid,9,1             ! ignore initial gaps/penetration
keyo,cid,7,0             ! No Prediction
rmod,tid,3,1.      ! FKN
rmod,tid,5,0.      ! ICONT
rmod,tid,6,0.      ! PINB
rmod,tid,10,0.     ! CNOF
rmod,tid,12,0.     ! FKT
rmod,cid,3,1.      ! FKN
rmod,cid,5,0.      ! ICONT
rmod,cid,6,0.      ! PINB
rmod,cid,10,0.     ! CNOF
rmod,cid,12,0.     ! FKT
/com,********** Create Contact "Contact Region 20" **********
/com,           Real Contact Set For Above Contact Is 17 & 16
*set,tid,17
*set,cid,16
r,tid
r,cid
et,tid,170
et,cid,174
eblock,10
(15i8)
   6886     17     17     17      0   9460   9464   9463   9459  11410  11414  11408  11407
......
   6899     17     16     17      0   9373   9452   9453   9451  11227  11393  11391  11226
-1
keyo,cid,12,5            ! bonded always
keyo,cid,2,1             ! penalty function only
keyo,cid,9,1             ! ignore initial gaps/penetration
keyo,cid,7,0             ! No Prediction
rmod,tid,3,1.      ! FKN
rmod,tid,5,0.      ! ICONT
rmod,tid,6,0.      ! PINB
rmod,tid,10,0.     ! CNOF
rmod,tid,12,0.     ! FKT
rmod,cid,3,1.      ! FKN
rmod,cid,5,0.      ! ICONT
rmod,cid,6,0.      ! PINB
rmod,cid,10,0.     ! CNOF
rmod,cid,12,0.     ! FKT
/com,********** Create Contact "Contact Region 14" **********
/com,           Real Contact Set For Above Contact Is 19 & 18
*set,tid,19
*set,cid,18
r,tid
r,cid
et,tid,170
et,cid,174
```

```
eblock,10
(15i8)
   6900     19     19     19      0    687    688   1183   1183   5720   5734   1183   5726
......
   7143     19     18     19      0   9916   9936   9935   9935  12727  12835   9935  12726
-1
keyo,cid,12,5            ! bonded always
keyo,cid,2,1             ! penalty function only
keyo,cid,9,1             ! ignore initial gaps/penetration
keyo,cid,7,0             ! No Prediction
rmod,tid,3,1.      ! FKN
rmod,tid,5,0.      ! ICONT
rmod,tid,6,0.      ! PINB
rmod,tid,10,0.     ! CNOF
rmod,tid,12,0.     ! FKT
rmod,cid,3,1.      ! FKN
rmod,cid,5,0.      ! ICONT
rmod,cid,6,0.      ! PINB
rmod,cid,10,0.     ! CNOF
rmod,cid,12,0.     ! FKT
/com,********** Create Contact "Contact Region 21" **********
/com,           Real Contact Set For Above Contact Is 21 & 20
*set,tid,21
*set,cid,20
r,tid
r,cid
et,tid,170
et,cid,174
eblock,10
(15i8)
   7144     21     21     21      0   9867   9992   9993   9993  12359  13091   9993  12360
......
   7163     21     20     21      0   9391   9396   9469   9474  11272  11282  11420  11273
-1
keyo,cid,12,5            ! bonded always
keyo,cid,2,1             ! penalty function only
keyo,cid,9,1             ! ignore initial gaps/penetration
keyo,cid,7,0             ! No Prediction
rmod,tid,3,1.      ! FKN
rmod,tid,5,0.      ! ICONT
rmod,tid,6,0.      ! PINB
rmod,tid,10,0.     ! CNOF
rmod,tid,12,0.     ! FKT
rmod,cid,3,1.      ! FKN
rmod,cid,5,0.      ! ICONT
rmod,cid,6,0.      ! PINB
rmod,cid,10,0.     ! CNOF
rmod,cid,12,0.     ! FKT
/com,********** Create Contact "Contact Region 22" **********
/com,           Real Contact Set For Above Contact Is 23 & 22
*set,tid,23
*set,cid,22
r,tid
r,cid
```

```
et,tid,170
et,cid,174
eblock,10
(15i8)
   7164     23     23     23      0   9387   9382   9385   9386  11250  11249  11256  11258
......
   7171     23     22     23      0   9475   9468   9399   9390  11419  11287  11269  11270
-1
keyo,cid,12,5            ! bonded always
keyo,cid,2,1             ! penalty function only
keyo,cid,9,1             ! ignore initial gaps/penetration
keyo,cid,7,0             ! No Prediction
rmod,tid,3,1.      ! FKN
rmod,tid,5,0.      ! ICONT
rmod,tid,6,0.      ! PINB
rmod,tid,10,0.     ! CNOF
rmod,tid,12,0.     ! FKT
rmod,cid,3,1.      ! FKN
rmod,cid,5,0.      ! ICONT
rmod,cid,6,0.      ! PINB
rmod,cid,10,0.     ! CNOF
rmod,cid,12,0.     ! FKT
/com,********** Create Contact "Contact Region 11" **********
/com,          Real Contact Set For Above Contact Is 25 & 24
*set,tid,25
*set,cid,24
r,tid
r,cid
et,tid,170
et,cid,174
eblock,10
(15i8)
   7172     25     25     25      0   9895   9896   9902   9902  12606  12613   9902  12607
......
   7233     27     26     27      0   9330   9326   9325   9324  11107  11103  11100  11101
-1
keyo,cid,12,5            ! bonded always
keyo,cid,2,1             ! penalty function only
keyo,cid,9,1             ! ignore initial gaps/penetration
keyo,cid,7,0             ! No Prediction
rmod,tid,3,1.      ! FKN
rmod,tid,5,0.      ! ICONT
rmod,tid,6,0.      ! PINB
rmod,tid,10,0.     ! CNOF
rmod,tid,12,0.     ! FKT
rmod,cid,3,1.      ! FKN
rmod,cid,5,0.      ! ICONT
rmod,cid,6,0.      ! PINB
rmod,cid,10,0.     ! CNOF
rmod,cid,12,0.     ! FKT
/com,********** Create Contact "Contact Region 16" **********
/com,          Real Contact Set For Above Contact Is 29 & 28
*set,tid,29
*set,cid,28
```

```
r,tid
r,cid
et,tid,170
et,cid,174
eblock,10
(15i8)
   7234     29     29     29      0   9699   9673   9325   9326  11806  11105  11103  11108
......
   7261     29     28     29      0   9332   9837   9836   9331  11123  12098  11120  11118
-1
keyo,cid,12,5            ! bonded always
keyo,cid,2,1             ! penalty function only
keyo,cid,9,1             ! ignore initial gaps/penetration
keyo,cid,7,0             ! No Prediction
rmod,tid,3,1.      ! FKN
rmod,tid,5,0.      ! ICONT
rmod,tid,6,0.      ! PINB
rmod,tid,10,0.     ! CNOF
rmod,tid,12,0.     ! FKT
rmod,cid,3,1.      ! FKN
rmod,cid,5,0.      ! ICONT
rmod,cid,6,0.      ! PINB
rmod,cid,10,0.     ! CNOF
rmod,cid,12,0.     ! FKT
nsel,all
esel,all
/wb,contact,end           !  done creating contacts
/golist
/wb,load,start            !  starting to send loads
/com,********** Fixed Supports **********
CMBLOCK,FIXEDSU ,NODE,      49
(8i10)
     9375     9376     9377     9378     9379     9380     9381     9436
......
    11365    11367    11369    11371    11373    11375    11377    11379
    11381
cmsel,s,FIXEDSU
d,all,all
nsel,all
nsel,all
/com,********** Displacements **********
d,117,ux,1.078e-005,0.
......
d,8600,ux,1.078e-005,0.
/gst,on,on
fini
*get,_numnode,node,0,count
*get,_numelem,elem,0,count
/go
/wb,load,end              !  done creating loads
/com,--- Number of total nodes = %_numnode%
/com,--- Number of contact elements = 1044
/com,--- Number of spring elements = 0
/com,--- Number of solid elements = 6217
```

```
/com,--- Number of total elements = %_numelem%
*get,_wallbsol,active,,time,wall
/solu
antype,harm
harfrq,520.,640.
hropt,full
kbc,1
nsub,50
outres,erase
outres,all,none
outres,nsol,all
/nopr
/gopr
! ********** WB SOLVE COMMAND **********
! check interactive state
*get,ANSINTER_,active,,int
*if,ANSINTER_,ne,0,then
/eof
*endif
solve
fini
*get,_wallasol,active,,time,wall
/post1
esel,all
nsel,all
fini
xmlo,parm
/xml,parm,xml
/gopr
*get,_walldone,active,,time,wall
_preptime=(_wallbsol-_wallstrt)*3600
_solvtime=(_wallasol-_wallbsol)*3600
_posttime=(_walldone-_wallasol)*3600
_totaltim=(_walldone-_wallstrt)*3600
/wb,file,end              ! done with WB generated input
```

Appendix B Inp File of 2C2cm ABAQUS Vibration Simulation

```
*Heading
** Job name: 2c2cm595 Model name: Model-1
** Generated by: Abaqus/CAE 6.12-1
*Preprint, echo=NO, model=NO, history=NO, contact=NO
**
** PARTS
**
*Part, name=Blade1
*Node
      1,  -22.0200005,           0.,  0.939999998
......
     42,  -22.7700005,   -0.3150087, -1.24000001
*Element, type=C3D8R
1,  9, 27, 39, 25,  1, 21, 22, 4
......
*Nset, nset=Set-1, generate
  1,  42,  1
*Elset, elset=Set-1, generate
  1,  12,  1
** Section: Blade
*Solid Section, elset=Set-1, material=Blade
,
*End Part
**
*Part, name=Blade1_3
*Node
      1,  -18.1200008,  -1.10000002,  1.24000001
......
     48,  -22.0200005,           0.,  -1.24000001
*Element, type=C3D8R
 1, 13, 14, 16, 15,  1,  2,  4, 3
......
*Nset, nset=Set-1, generate
  1,  48,  1
*Elset, elset=Set-1, generate
  1,  15,  1
** Section: Blade
*Solid Section, elset=Set-1, material=Blade
,
*End Part
**
*Part, name=Blade1_4
*Node
      1,  -14.8199997, -0.300000012, -0.939999998
......
    110,  -17.2950001,  -1.02999997, -0.939999998
*Element, type=C3D8R
1,  8, 29, 78, 34,  1, 21, 75, 28
......
*Nset, nset=Set-1, generate
```

```
  1,  110,   1
*Elset, elset=Set-1, generate
 1,  40,  1
** Section: Blade
*Solid Section, elset=Set-1, material=Blade
,
*End Part
**
*Part, name=Blade1_5
*Node
      1,  -9.01000023,  -1.30999994, -0.774999976
......
    390,   -11.297143,       -1.245,  0.620000005
*Element, type=C3D8R
 1,  34, 147, 325, 141,   1,  17, 137, 22
......
*Nset, nset=Set-1, generate
  1,  390,   1
*Elset, elset=Set-1, generate
  1,  200,   1
** Section: Blade
*Solid Section, elset=Set-1, material=Blade
,
*End Part
**
*Part, name=cable_1
*Node
      1,           0.,   2.99000001,  -1.10000002
......
    252,          38.,   2.82890868,  -1.48890877
*Element, type=C3D8R
 1,  50, 101, 120,  13,   1,   9,  10,  4
......
*Nset, nset=Set-1, generate
  1,  252,   1
*Elset, elset=Set-1, generate
  1,  120,   1
** Section: wire
*Solid Section, elset=Set-1, material=wire
,
*End Part
**
*Part, name=receptacle
*Node
      1,   16.2299995,   1.66999996,  1.40999997
......
     24,   17.7299995,   2.46986461, -0.512156606
*Element, type=C3D8R
1,  9, 10, 12, 11,  1,  2,  4, 3
......
6, 21, 22, 24, 23, 13, 14, 16, 15
*Nset, nset=Set-1, generate
 1,  24,  1
*Elset, elset=Set-1, generate
 1,  6, 1
** Section: receptacle
```

```
*Solid Section, elset=Set-1, material=receptacle
,
*End Part
**
*Part, name=receptacle_1
*Node
      1,   13.2299995,   1.66999996, -1.39999998
......
     50,   16.2299995,   2.76999998,  1.40999997
*Element, type=C3D8R
 1, 11, 12, 14, 13,  1,  2,  4, 3
......
*Nset, nset=Set-1, generate
  1,  50,  1
*Elset, elset=Set-1, generate
  1,  16,  1
** Section: receptacle
*Solid Section, elset=Set-1, material=receptacle
,
*End Part
**
*Part, name=receptacle_2
*Node
      1,   9.93999958,   2.76999998,         1.12
......
   1132,   0.22360149,   2.23474932, 0.549999952
*Element, type=C3D8R
 1,  10, 148, 505, 135,   1,   2, 119, 126
......
*Nset, nset=Set-1, generate
    1,  1132,     1
*Elset, elset=Set-1, generate
   1,  541,   1
** Section: receptacle
*Solid Section, elset=Set-1, material=receptacle
,
*End Part
**
**
** ASSEMBLY
**
*Assembly, name=Assembly
**
*Instance, name=receptacle, part=receptacle
-17.7300000516075, 2.81937591708968, 1.80000000000057e-05
-17.7300000516075,   2.81937591708968,       1.80000000000057e-05,   -16.7300000516075,   2.81937591708968,
1.79999999999901e-05,         180.
*End Instance
**
*Instance, name=receptacle_1, part=receptacle_1
-17.7300000516075, 2.81937591708968, 1.80000000000057e-05
-17.7300000516075,   2.81937591708968,       1.80000000000057e-05,   -16.7300000516075,   2.81937591708968,
1.79999999999901e-05,         180.
*End Instance
**
*Instance, name=receptacle_2, part=receptacle_2
```

```
-17.7300000516075, 2.81937591708968, 1.80000000000057e-05
-17.7300000516075,  2.81937591708968,  1.80000000000057e-05,  -16.7300000516075,  2.81937591708968,
1.79999999999901e-05,  180.
*End Instance
**
*Instance, name=Blade1, part=Blade1
-8.0200000516075, 2.78937591708969,  1.8e-05
*End Instance
**
*Instance, name=Blade1_3, part=Blade1_3
-8.0200000516075, 2.78937591708969,  1.8e-05
*End Instance
**
*Instance, name=Blade1_4, part=Blade1_4
-8.0200000516075, 2.78937591708969,  1.8e-05
*End Instance
**
*Instance, name=Blade1_5, part=Blade1_5
-8.0200000516075, 2.78937591708969,  1.8e-05
*End Instance
**
*Instance, name=cable_1, part=cable_1
 -3.23181005512652e-07, -1.890000321489,  0.
*End Instance
**
*Nset, nset=Set-2, instance=receptacle_2
  65,  66,  68, 69, 103, 104, 105, 106, 247, 248, 249, 259, 260, 261, 399, 400
 401, 402, 403, 404, 405, 406, 407, 408, 857, 858, 859, 860, 861, 862
*Elset, elset=Set-2, instance=receptacle_2, generate
 315,  322,  1
*Nset, nset=Set-3, instance=Blade1
  2,  3,  5,  6, 10, 12, 13, 17, 18, 19, 26, 29, 32, 37
*Elset, elset=Set-3, instance=Blade1
  2,  4,  7,  8, 10, 12
*Nset, nset=Set-4, instance=Blade1
  1,  2,  3,  5,  6, 10, 12, 13, 14, 17, 18, 19, 21, 26, 29, 31
 32, 33, 37, 41
*Nset, nset=Set-4, instance=Blade1_3, generate
  2,  48,  2
*Nset, nset=Set-4, instance=Blade1_4
  5,  6,  7,  8, 29, 30, 31, 32, 33, 34, 35, 36, 78, 79, 80
*Elset, elset=Set-4, instance=Blade1
  2,  4,  5,  6,  7,  8, 10, 12
*Elset, elset=Set-4, instance=Blade1_3, generate
  1,  15,  1
*Elset, elset=Set-4, instance=Blade1_4, generate
 1,  8, 1
*Nset, nset=Set-5, instance=Blade1, generate
  1,  42,  1
*Nset, nset=Set-5, instance=Blade1_3, generate
  1,  48,  1
*Nset, nset=Set-5, instance=Blade1_4, generate
   1,  110,  1
*Nset, nset=Set-5, instance=Blade1_5
   2,  3,  5,  6,  13,  14,  15,  16,  19,  25,  35,  36,  37,  38,  39, 40
......
```

```
*Elset, elset=Set-5, instance=Blade1, generate
  1,  12,  1
*Elset, elset=Set-5, instance=Blade1_3, generate
  1,  15,  1
*Elset, elset=Set-5, instance=Blade1_4, generate
  1,  40,  1
*Elset, elset=Set-5, instance=Blade1_5, generate
 145,  200,   1
*Nset, nset=Set-6, instance=cable_1
   5,   6,   7,   8,  11,  12,  89,  90,  91,  98,  99, 100
*Elset, elset=Set-6, instance=cable_1
  39,  40,  41,  42, 119, 120
*Nset, nset=Set-7, instance=Blade1
  1,  2,  3,  4,  5,  6,  7, 10, 12, 13, 14, 15, 17, 18, 19, 20
 21, 22, 24, 25, 26, 29, 31, 32, 33, 35, 36, 37, 38, 39, 41, 42
*Nset, nset=Set-7, instance=Blade1_3, generate
  2,  48,  2
*Nset, nset=Set-7, instance=Blade1_4
  5,  6,  7,  8, 12, 13, 19, 20, 29, 30, 31, 32, 33, 34, 35, 36
 50, 51, 52, 62, 63, 64, 78, 79, 80
*Elset, elset=Set-7, instance=Blade1, generate
  1,  12,  1
*Elset, elset=Set-7, instance=Blade1_3, generate
  1,  15,  1
*Elset, elset=Set-7, instance=Blade1_4
  1,  2,  3,  4,  5,  6,  7,  8, 21, 22, 23, 24, 37, 38, 39, 40
*Elset, elset=_m_Surf-1_S1, internal, instance=receptacle, generate
 4,  6, 1
*Surface, type=ELEMENT, name=m_Surf-1
_m_Surf-1_S1, S1
*Elset, elset=_Surf-4_S2, internal, instance=receptacle_2
  81,  82,  83,  84,  85,  86,  87,  88,  89,  90,  91,  92,  93,  94,  95, 96
 259, 260, 261, 262, 263, 264, 265, 266
*Elset, elset=_Surf-4_S5, internal, instance=receptacle_2
 271, 272, 273, 274, 279, 280, 281, 282, 287, 288, 289, 290, 295, 296, 297, 298
 303, 304, 305, 306, 311, 312, 313, 314, 315, 316, 317, 318, 319, 320, 321, 322
*Elset, elset=_Surf-4_S1, internal, instance=receptacle_2, generate
 223,  234,   1
*Surface, type=ELEMENT, name=Surf-4
_Surf-4_S2, S2
_Surf-4_S5, S5
_Surf-4_S1, S1
*Elset, elset=_Surf-3_S4, internal, instance=Blade1_5, generate
  26,  144,   2
*Elset, elset=_Surf-3_S6, internal, instance=Blade1_5, generate
  25,  143,   2
*Surface, type=ELEMENT, name=Surf-3
_Surf-3_S4, S4
_Surf-3_S6, S6
*Elset, elset=_m_Surf-5_S3, internal, instance=receptacle_1, generate
  1,  13,  4
*Surface, type=ELEMENT, name=m_Surf-5
_m_Surf-5_S3, S3
*Elset, elset=_s_Surf-5_S5, internal, instance=receptacle_2
   5,  10,  15,  20,  25,  45,  50,  55,  60,  65, 117, 138, 159, 180, 201, 222
*Surface, type=ELEMENT, name=s_Surf-5
```

```
_s_Surf-5_S5, S5
*Elset, elset=_m_Surf-7_S2, internal, instance=receptacle, generate
 1,  3, 1
*Surface, type=ELEMENT, name=m_Surf-7
_m_Surf-7_S2, S2
*Elset, elset=_s_Surf-7_S5, internal, instance=receptacle_1, generate
  4,  16,  4
*Surface, type=ELEMENT, name=s_Surf-7
_s_Surf-7_S5, S5
*Elset, elset=_m_Surf-9_S5, internal, instance=Blade1_3, generate
  5,  15,  5
*Surface, type=ELEMENT, name=m_Surf-9
_m_Surf-9_S5, S5
*Elset, elset=_s_Surf-9_S3, internal, instance=Blade1
  5,  6,  9, 11
*Elset, elset=_s_Surf-9_S6, internal, instance=Blade1
 1, 3
*Surface, type=ELEMENT, name=s_Surf-9
_s_Surf-9_S3, S3
_s_Surf-9_S6, S6
*Elset, elset=_m_Surf-11_S3, internal, instance=Blade1_3, generate
  1,  11,  5
*Surface, type=ELEMENT, name=m_Surf-11
_m_Surf-11_S3, S3
*Elset, elset=_s_Surf-11_S5, internal, instance=Blade1_4
  7,  8, 28, 32, 36, 40
*Elset, elset=_s_Surf-11_S4, internal, instance=Blade1_4, generate
 12,  24,  4
*Surface, type=ELEMENT, name=s_Surf-11
_s_Surf-11_S5, S5
_s_Surf-11_S4, S4
*Elset, elset=_m_Surf-13_S2, internal, instance=Blade1_5, generate
 145,  152,   1
*Surface, type=ELEMENT, name=m_Surf-13
_m_Surf-13_S2, S2
*Elset, elset=_s_Surf-13_S3, internal, instance=Blade1_4
  1,  2, 25, 29, 33, 37
*Elset, elset=_s_Surf-13_S6, internal, instance=Blade1_4, generate
  9,  21,  4
*Surface, type=ELEMENT, name=s_Surf-13
_s_Surf-13_S3, S3
_s_Surf-13_S6, S6
*Elset, elset=_s_Surf-15_S2, internal, instance=cable_1
  1,  2, 79, 80
*Elset, elset=_s_Surf-15_S1, internal, instance=cable_1
 81, 82
*Surface, type=ELEMENT, name=s_Surf-15
_s_Surf-15_S2, S2
_s_Surf-15_S1, S1
*Elset, elset=_m_Surf-16_S2, internal, instance=cable_1
 1, 2
*Surface, type=ELEMENT, name=m_Surf-16
_m_Surf-16_S2, S2
*Elset, elset=_s_Surf-16_S1, internal, instance=receptacle, generate
 4,  6, 1
*Surface, type=ELEMENT, name=s_Surf-16
```

```
_s_Surf-16_S1, S1
** Constraint: Constraint-1
*Tie, name=Constraint-1, adjust=yes
s_Surf-16, m_Surf-16
** Constraint: Constraint-2
*Tie, name=Constraint-2, adjust=yes
s_Surf-5, m_Surf-5
** Constraint: Constraint-3
*Tie, name=Constraint-3, adjust=yes
s_Surf-7, m_Surf-7
** Constraint: Constraint-4
*Tie, name=Constraint-4, adjust=yes
s_Surf-9, m_Surf-9
** Constraint: Constraint-5
*Tie, name=Constraint-5, adjust=yes
s_Surf-11, m_Surf-11
** Constraint: Constraint-6
*Tie, name=Constraint-6, adjust=yes
s_Surf-13, m_Surf-13
*End Assembly
*Amplitude, name=x2c4cm, definition=PERIODIC
2,          1114.,              0.,         0.01282
            0.,         0.01282,            0.02,         0.01282
*Amplitude, name=x3a4cm, definition=PERIODIC
2,           951.,              0.,         0.01275
            0.,         0.01275,              1.,         0.01275
*Amplitude, name=x3b4cm, definition=PERIODIC
2,          1042.,              0.,         0.01339
            0.,         0.01339,              1.,         0.01339
*Amplitude, name=x3c4cm, definition=PERIODIC
2,          1036.,              0.,         0.01717
            0.,         0.01717,            0.02,         0.01717
**
** MATERIALS
**
*Material, name=Blade
*Density
 8.91e-09,
*Elastic
129742., 0.3
*Material, name=receptacle
*Density
 8.794e-09,
*Elastic
129742., 0.3
*Material, name=wire
*Density
 4.564e-09,
*Elastic
96534., 0.3
**
** INTERACTION PROPERTIES
**
*Surface Interaction, name=x2c
*Friction
 0.369,
```

```
*Surface Interaction, name=x3a
*Friction
 0.476,
*Surface Interaction, name=x3b
*Friction
 0.279,
*Surface Interaction, name=x3c
*Friction
 0.431,
**
** BOUNDARY CONDITIONS
**
** Name: BC-1 Type: Symmetry/Antisymmetry/Encastre
*Boundary
Set-6, ENCASTRE
**
** INTERACTIONS
**
** Interaction: Int-1
*Contact, op=NEW
*Contact Inclusions
Surf-3 , Surf-4
*Contact Property Assignment
 ,  , x3c
** ----------------------------------------------------------------
**
** STEP: Step-1
**
*Step, name=Step-1
*Dynamic, Explicit
, 0.02
*Bulk Viscosity
0.06, 1.2
**
** BOUNDARY CONDITIONS
**
** Name: BC-3 Type: Displacement/Rotation
*Boundary, amplitude=x3c4cm
Set-7, 1, 1, 0.01717
Set-7, 2, 2
**
** LOADS
**
** Name: Load-1   Type: Body force
*Dload
Set-2, BY, 5.072
**
** OUTPUT REQUESTS
**
*Restart, write, number interval=1, time marks=NO
**
** FIELD OUTPUT: F-Output-1
**
*Output, field, time interval=0.0001
*Node Output
A, U, V
```

```
*Element Output, directions=YES
EVF,
**
** HISTORY OUTPUT: H-Output-1
**
*Output, history, variable=PRESELECT
*End Step
```

Appendix C Experimental Results of Receptacle Spring and Friction Force

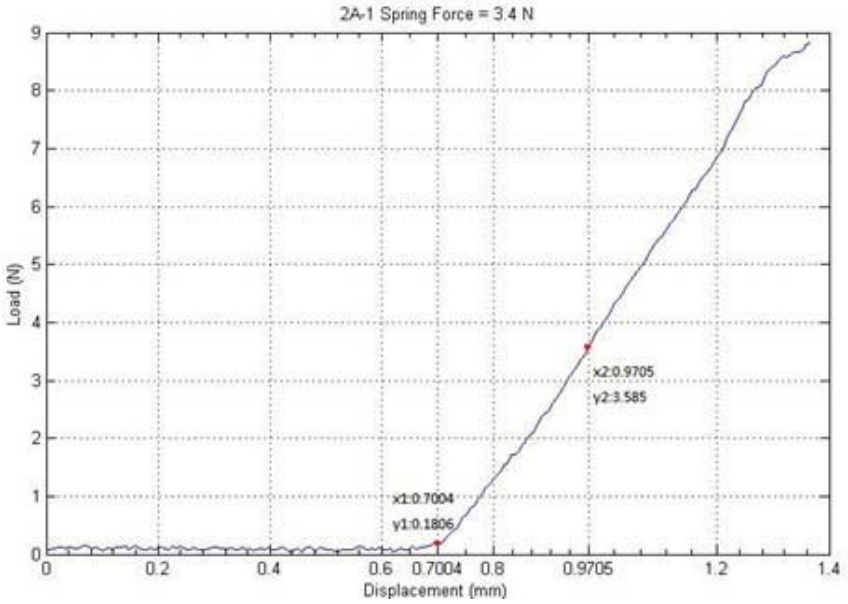

Figure App.C-1. 2A-1 spring normal forces.

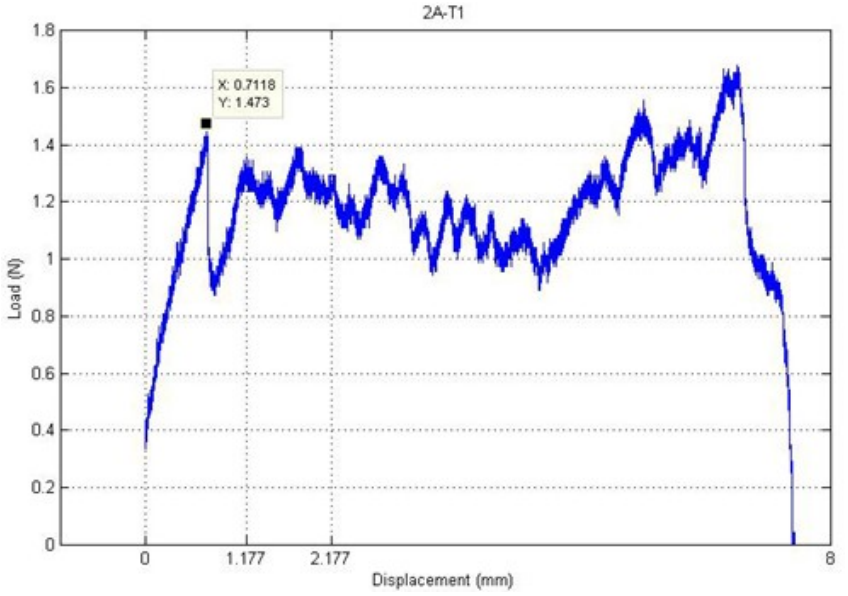

Figure App.C-2. 2A-1 friction forces

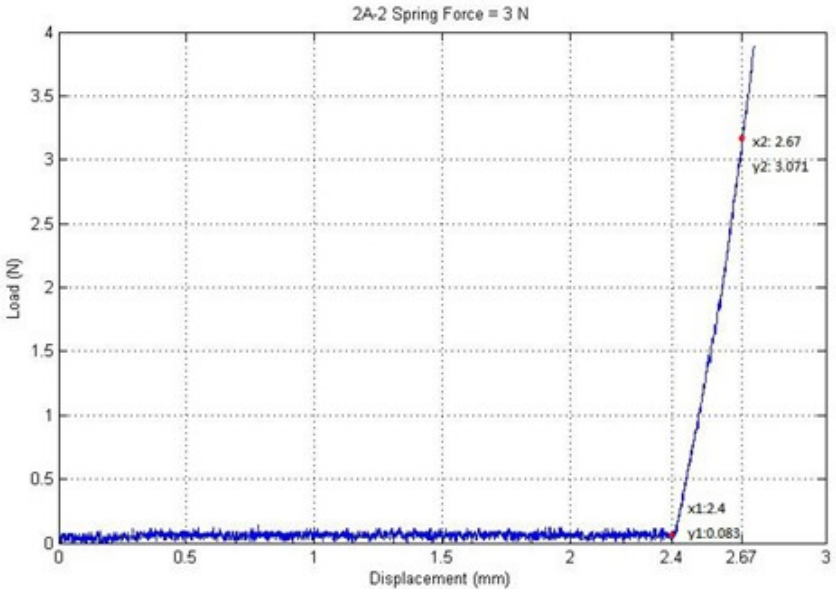

Figure App.C-3. 2A-2 spring normal forces.

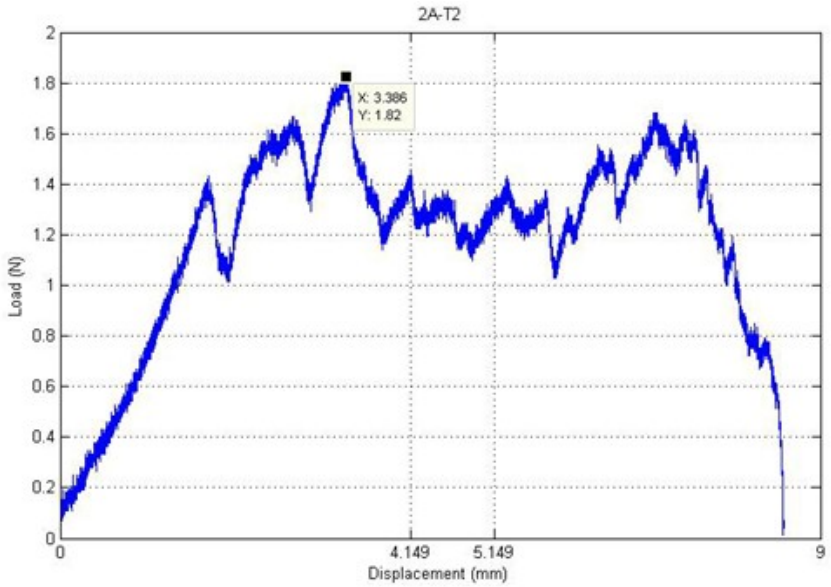

Figure App.C-4. 2A-2 friction forces

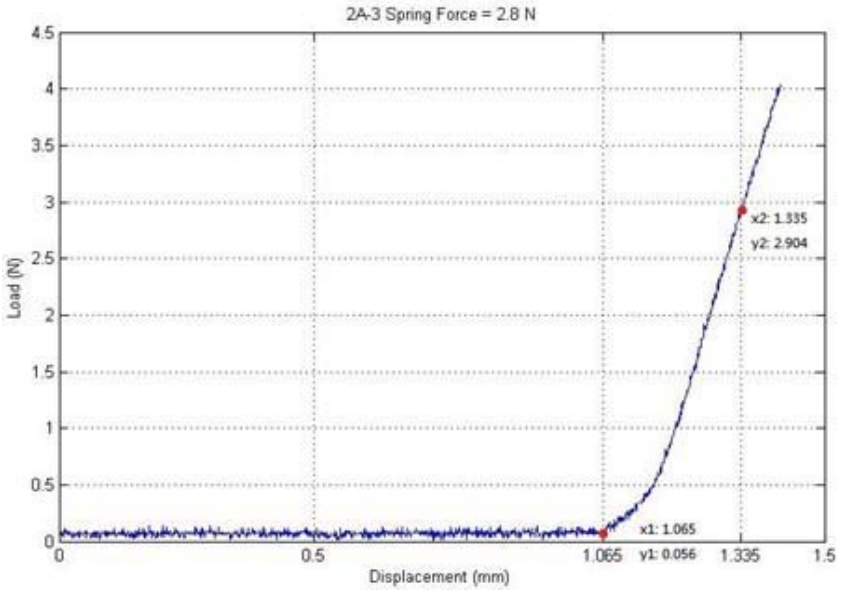

Figure App.C-5. 2A-3 spring normal forces.

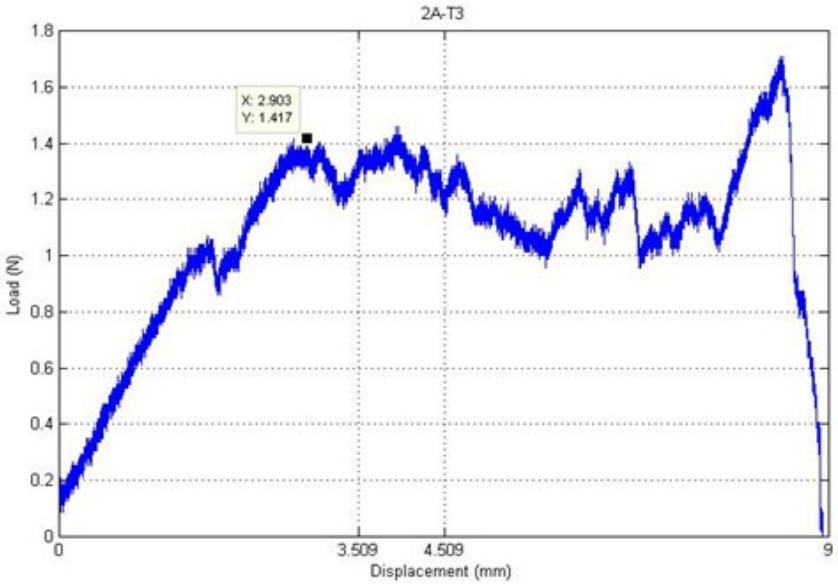

Figure App.C-6. 2A-3 friction forces

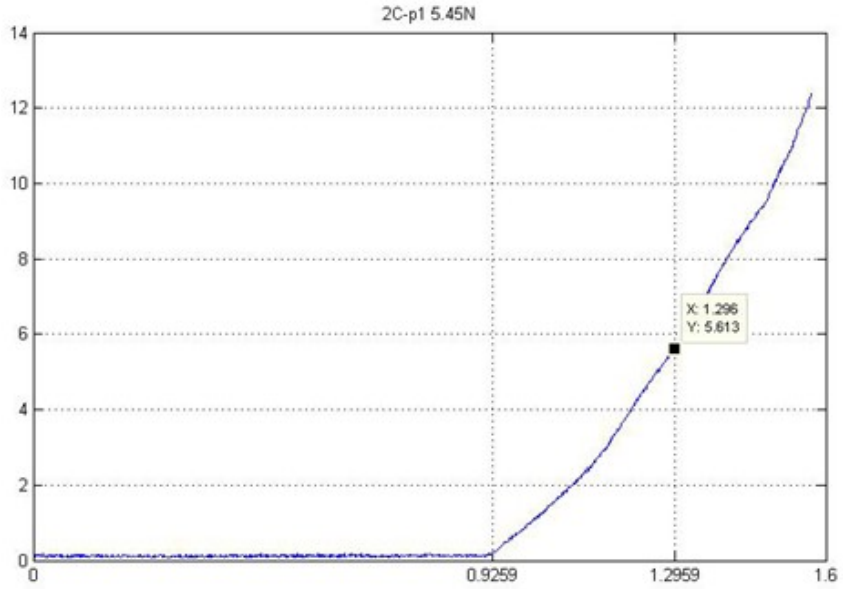

Figure App.C-7. 2C-1 spring normal forces.

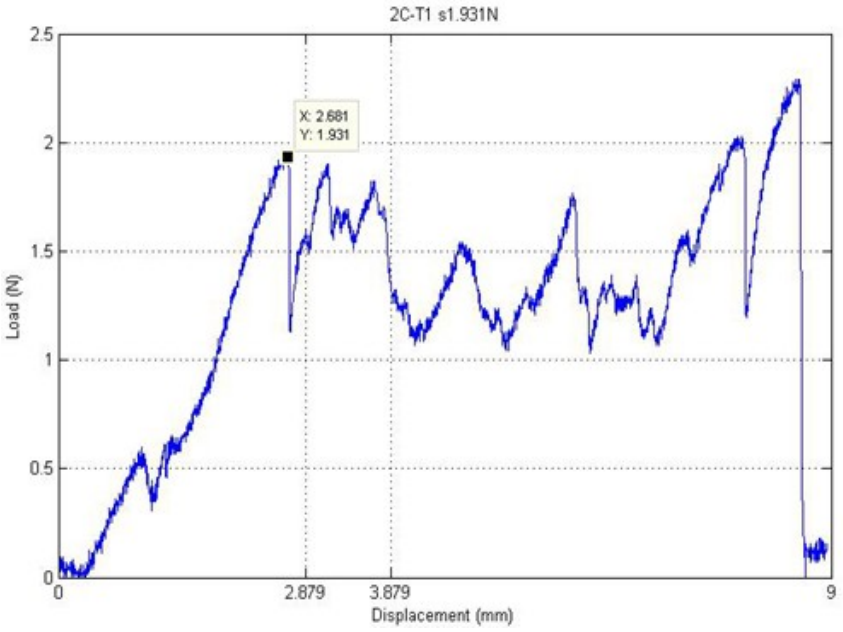

Figure App.C-8. 2C-1 friction forces

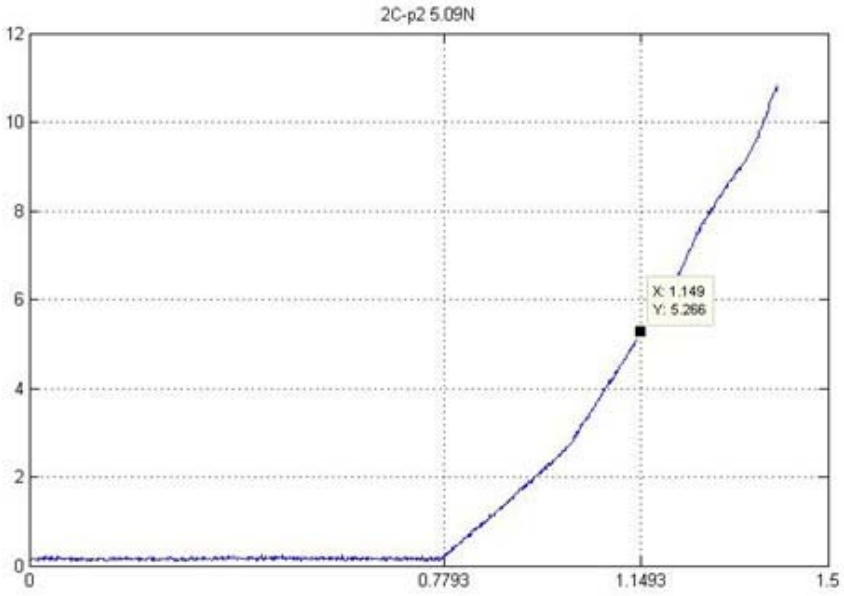

Figure App.C-9. 2C-2 spring normal forces

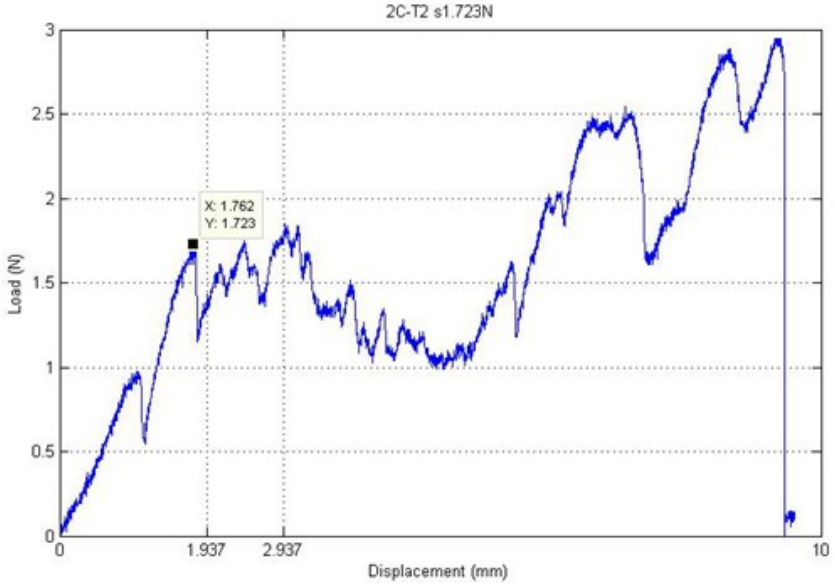

Figure App.C-10. 2C-2 friction forces

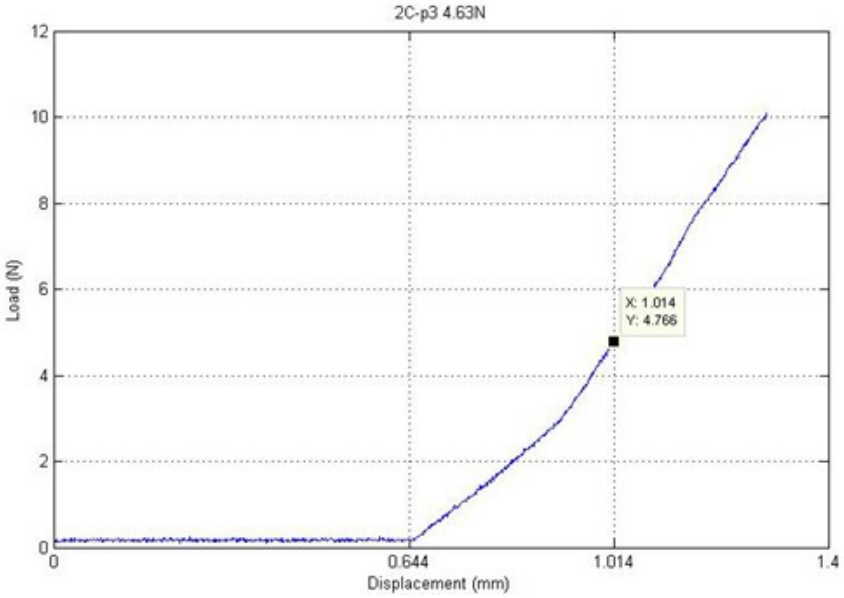

Figure App.C-11. 2C-3 spring normal forces

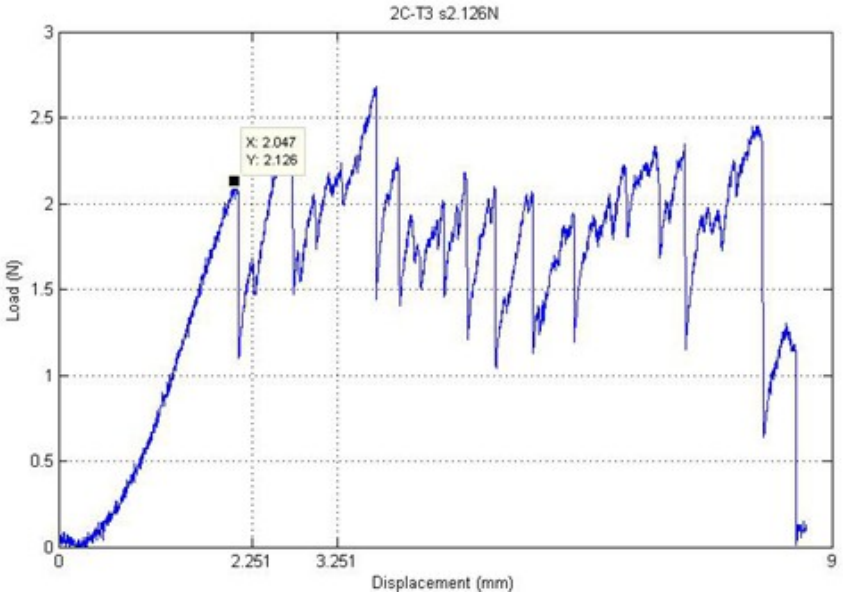

Figure App.C-12. 2C-3 friction forces

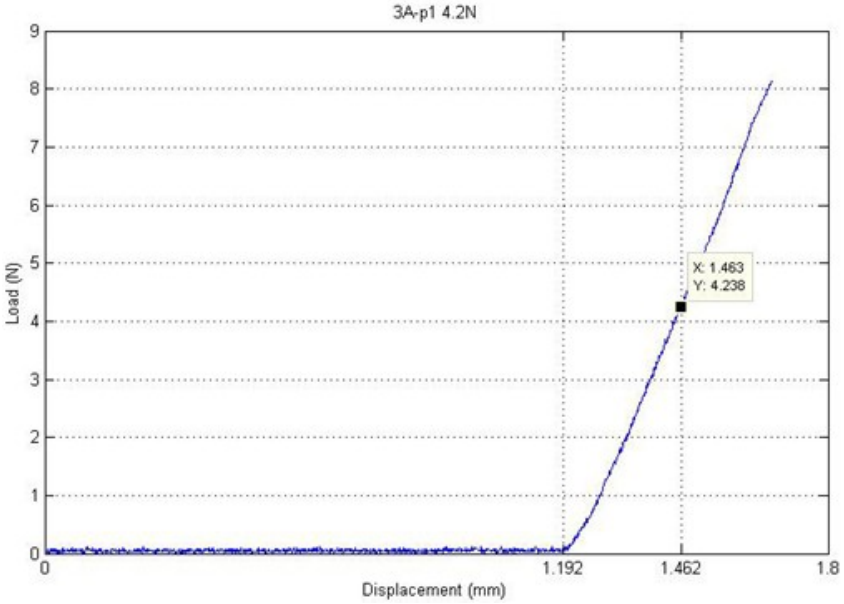

Figure App.C-13. 3A-1 spring normal forces

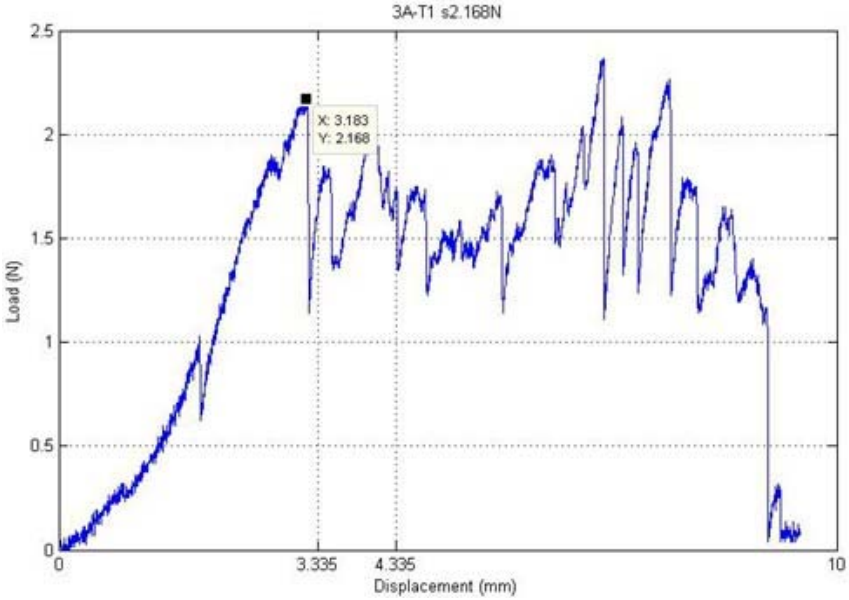

Figure App.C-14. 3A-1 friction forces

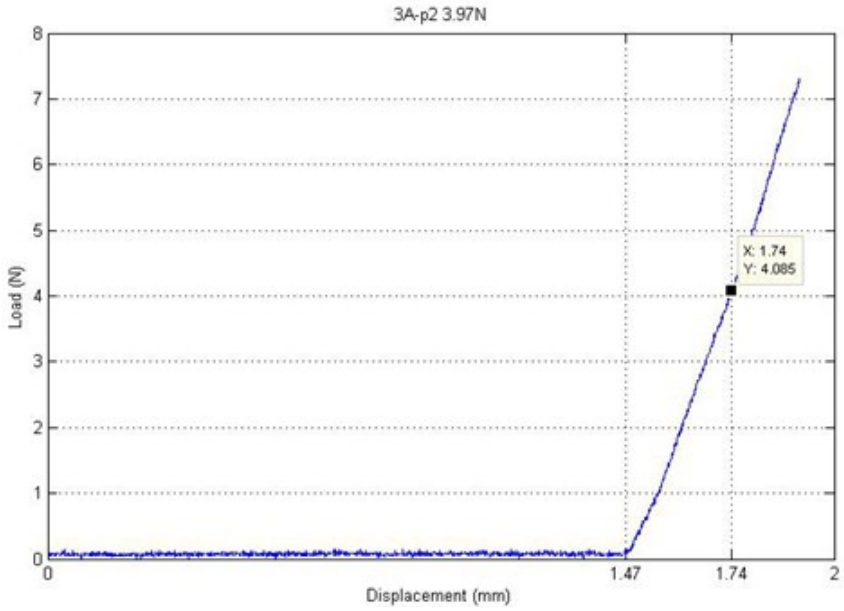

Figure App.C-15. 3A-2 spring normal forces

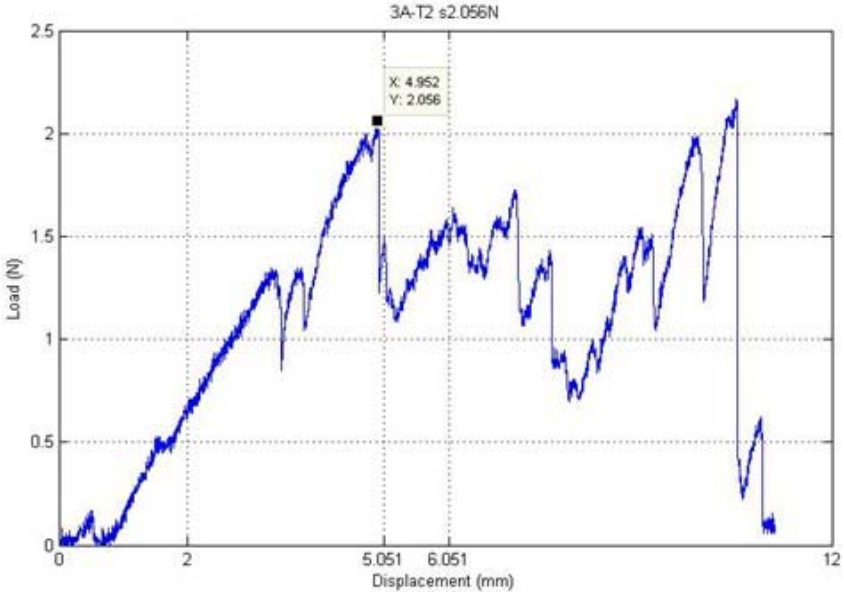

Figure App.C-16. 3A-2 friction forces

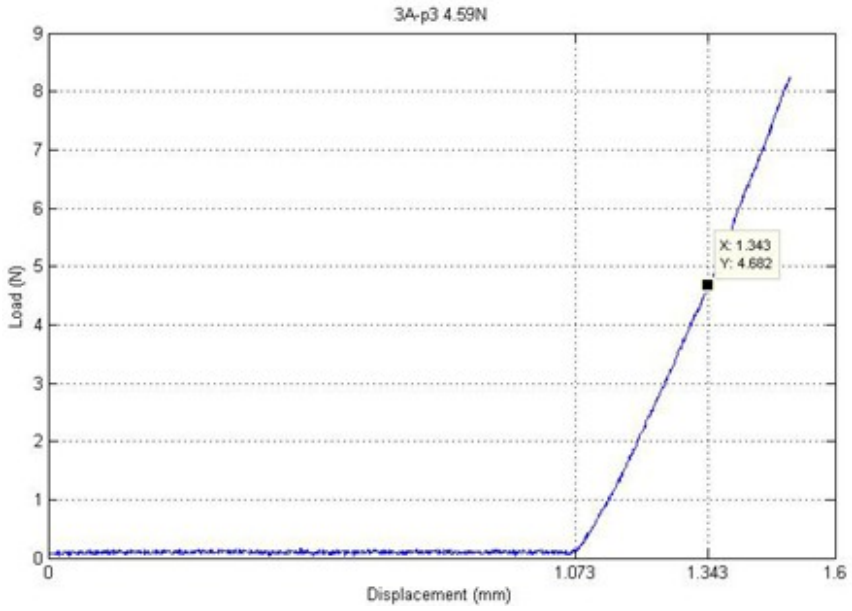

Figure App.C-17. 3A-3 spring normal forces

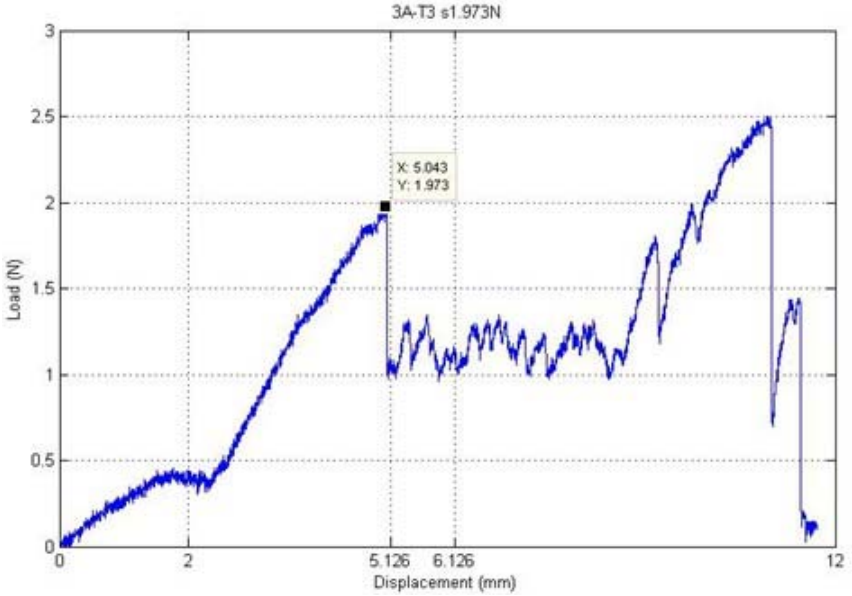

Figure App.C-18. 3A-3 friction forces

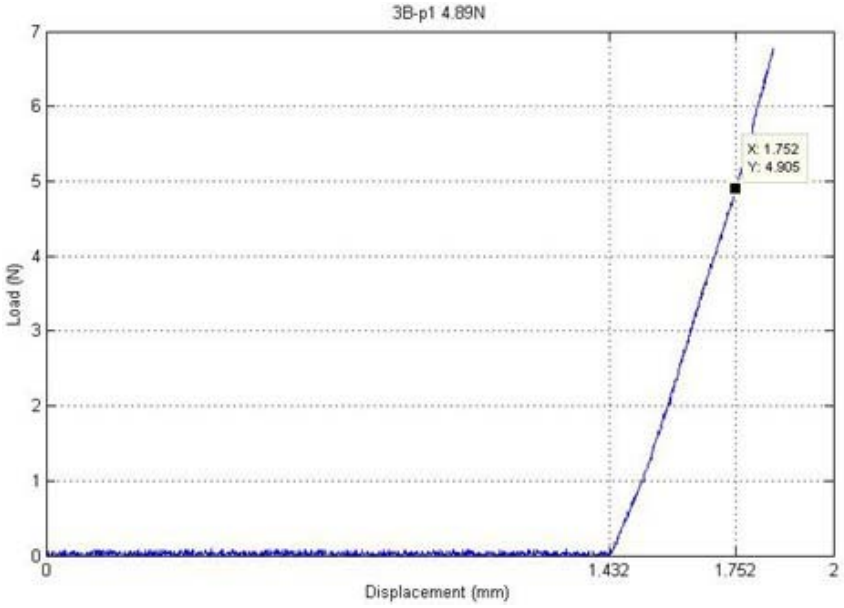

Figure App.C-19. 3B-1 spring normal forces

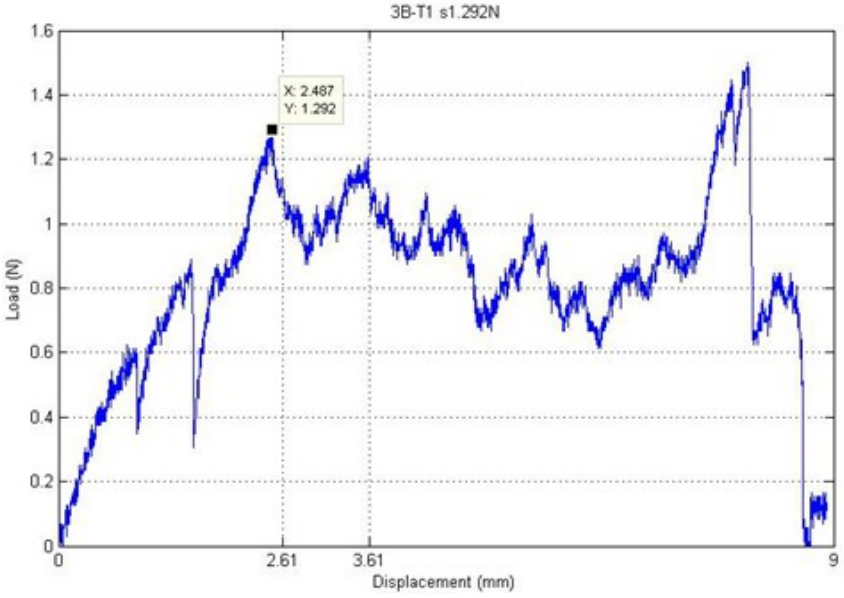

Figure App.C-20. 3B-1 friction forces

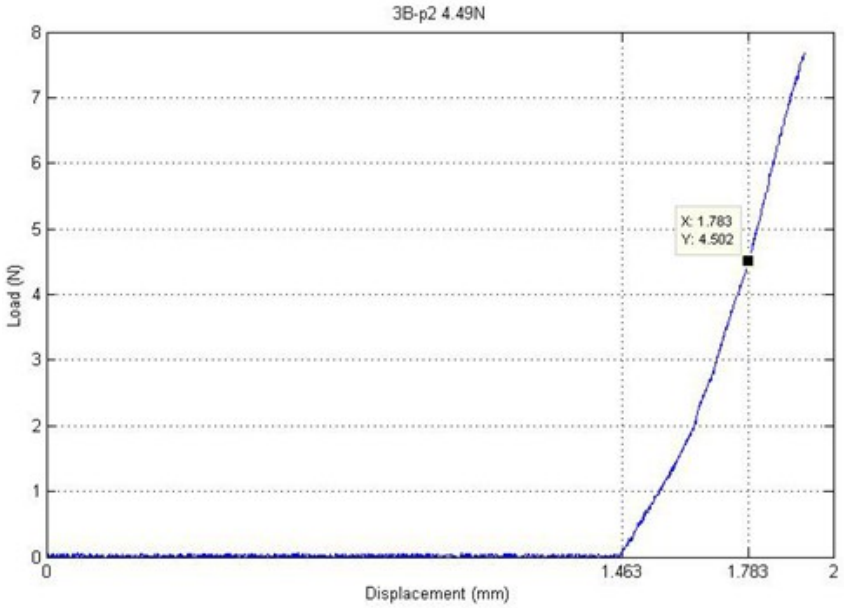

Figure App.C-21. 3B-2 spring normal forces

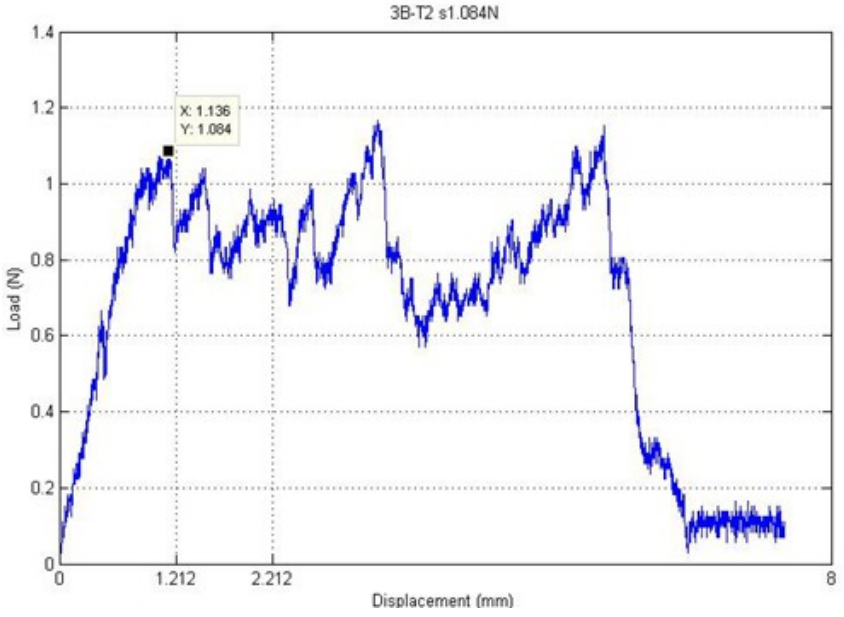

Figure App.C-22. 3B-2 friction forces

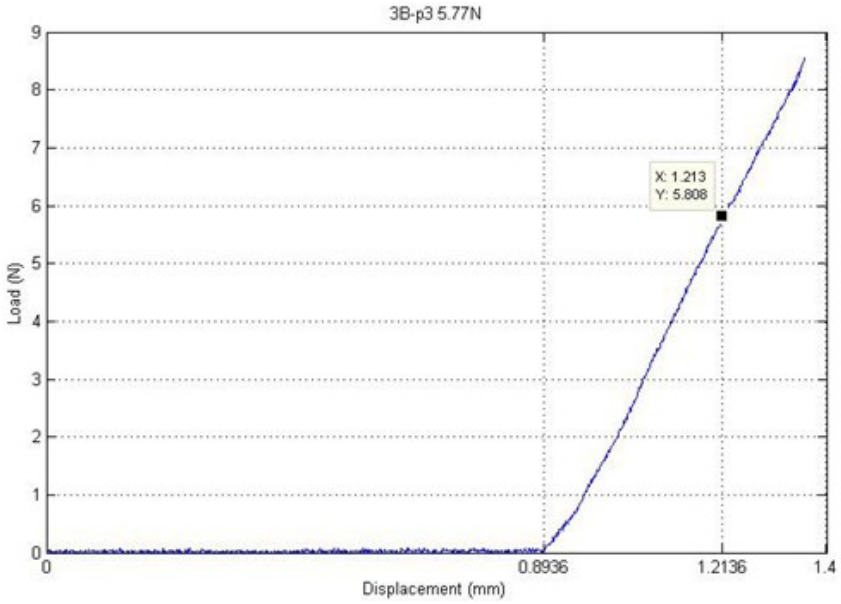

Figure App.C-23. 3B-3 spring normal forces

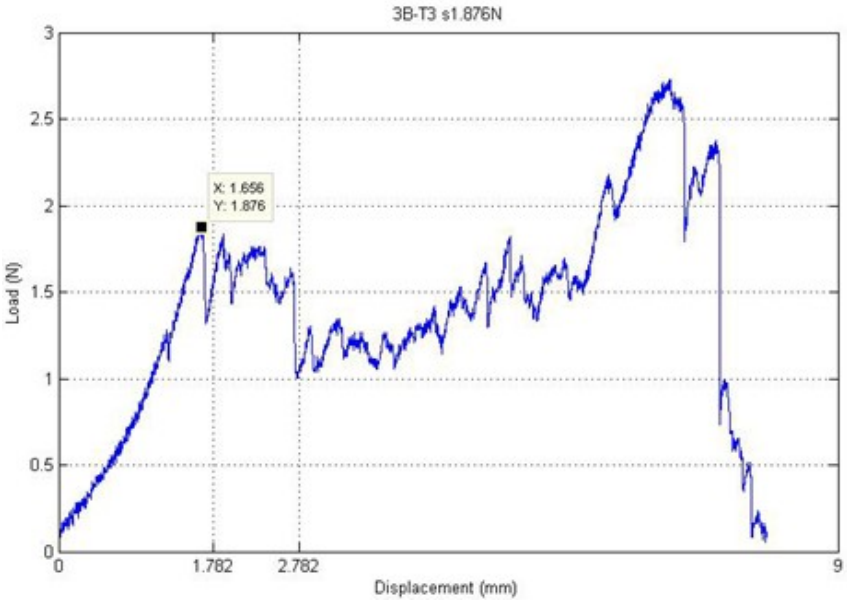

Figure App.C-24. 3B-3 friction forces

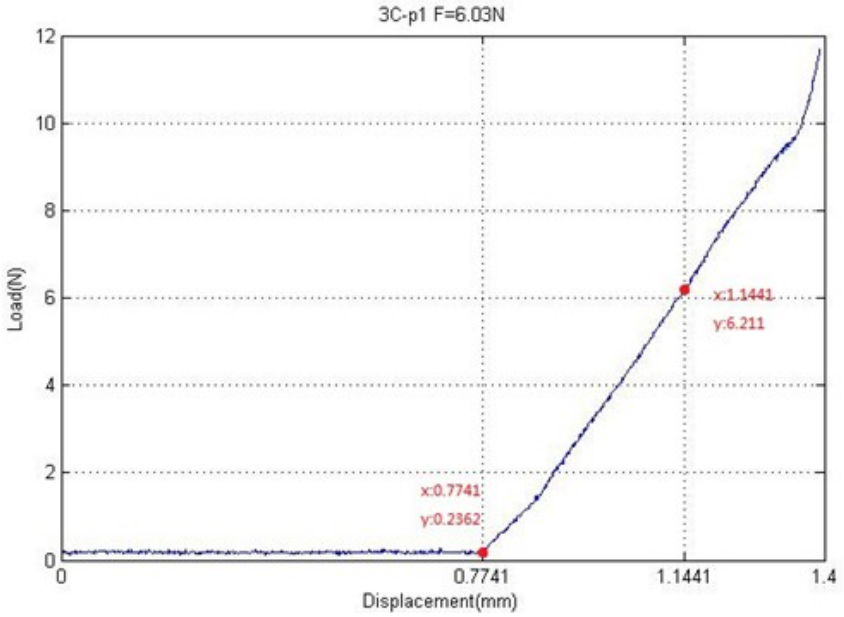

Figure App.C-25. 3C-1 spring normal forces

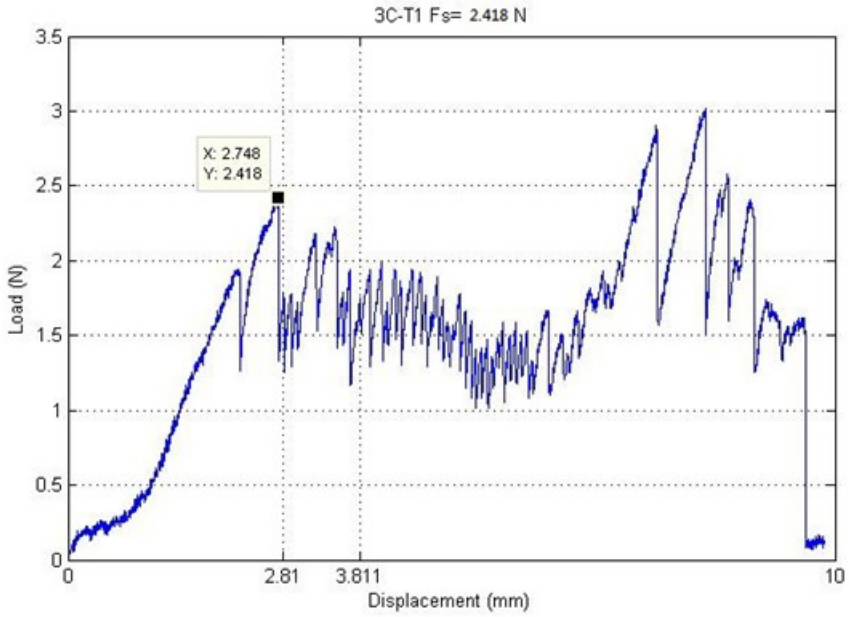

Figure App.C-26. 3C-1 friction forces

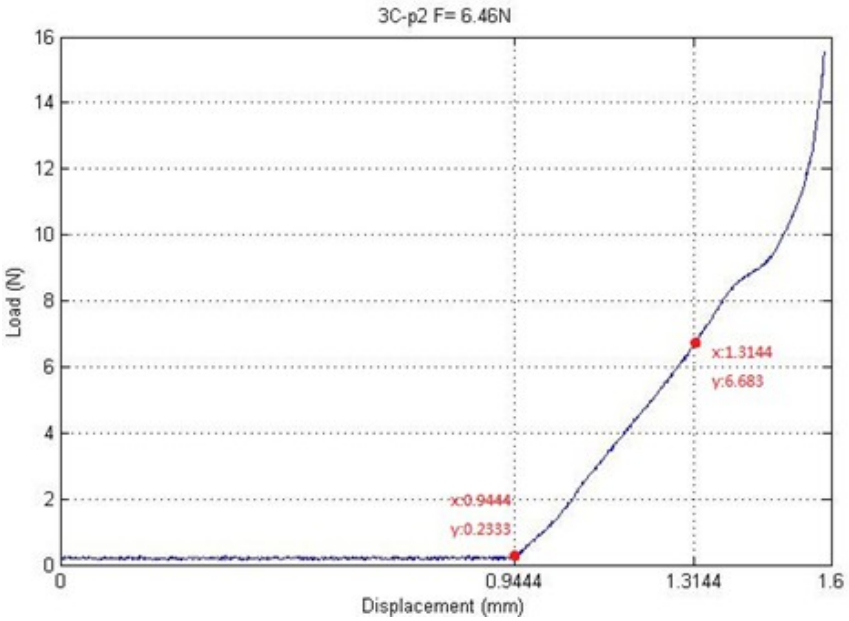

Figure App.C-27. 3C-2 spring normal forces

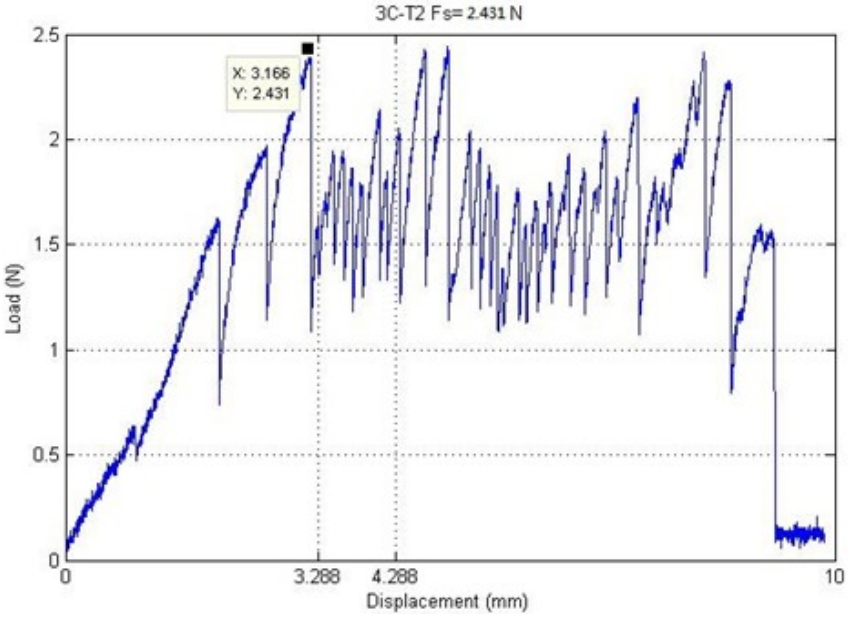

Figure App.C-28. 3C-2 friction forces

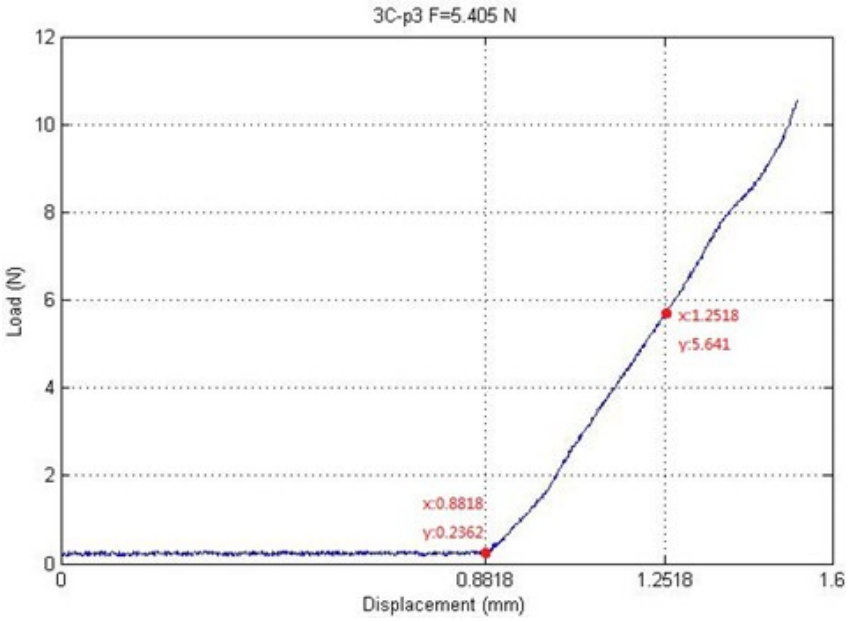

Figure App.C-29. 3C-3 spring normal forces

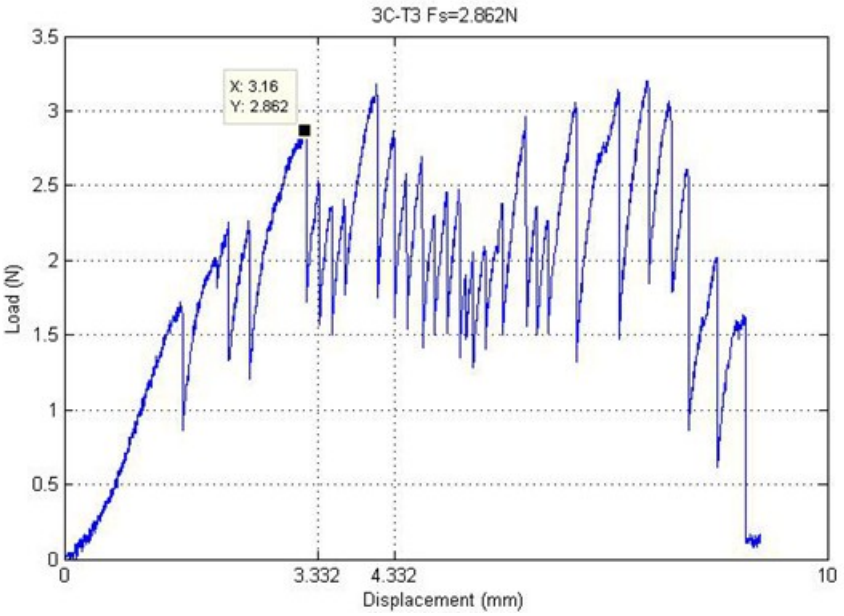

Figure App.C-30. 3C-3 friction forces

Appendix D Experimental Results of Frequency Response

3.3.2.1 Results of Type 2C with Cable Lengths of 2cm, 4cm, 6cm and 8cm

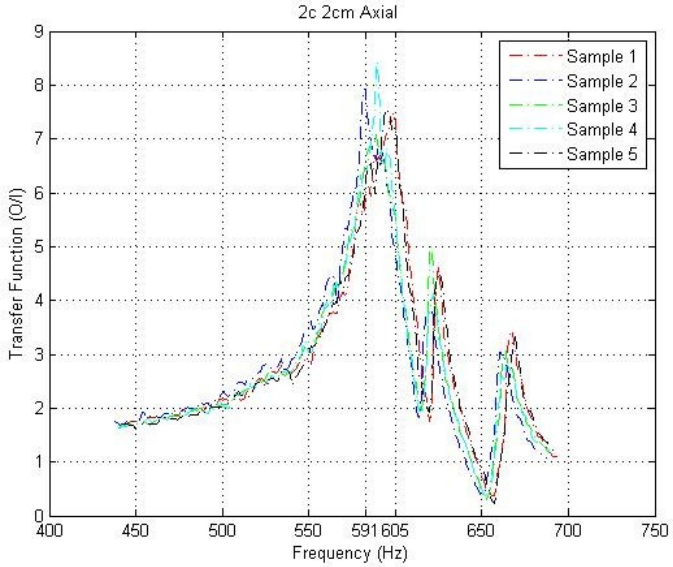

Figure App.D-1 Experimental results of 2C 2cm axial transfer function

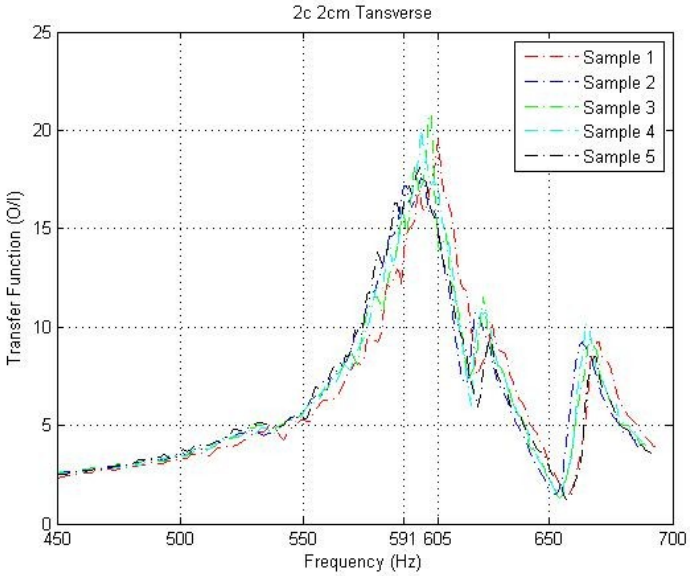

Figure App.D-2 Experimental results of 2C 2cm transverse transfer function

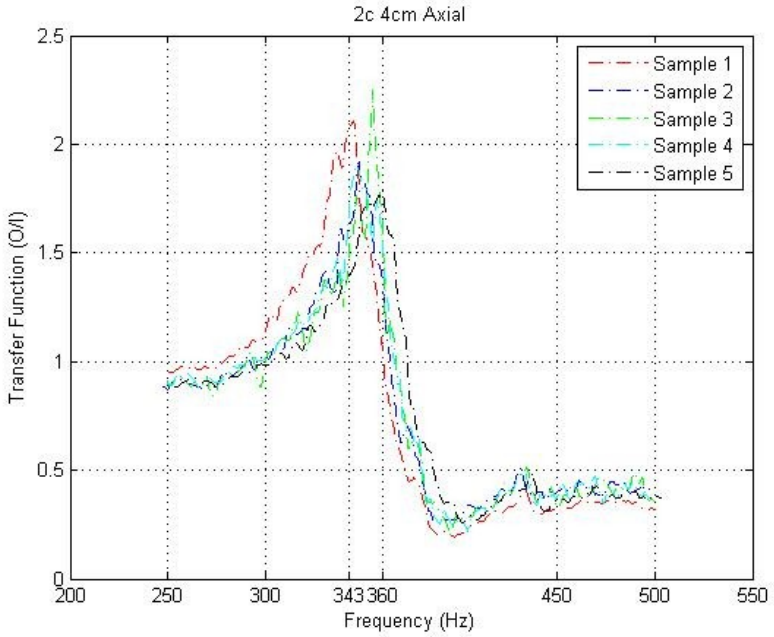

Figure App.D-3 Experimental results of 2C 4cm axial transfer function

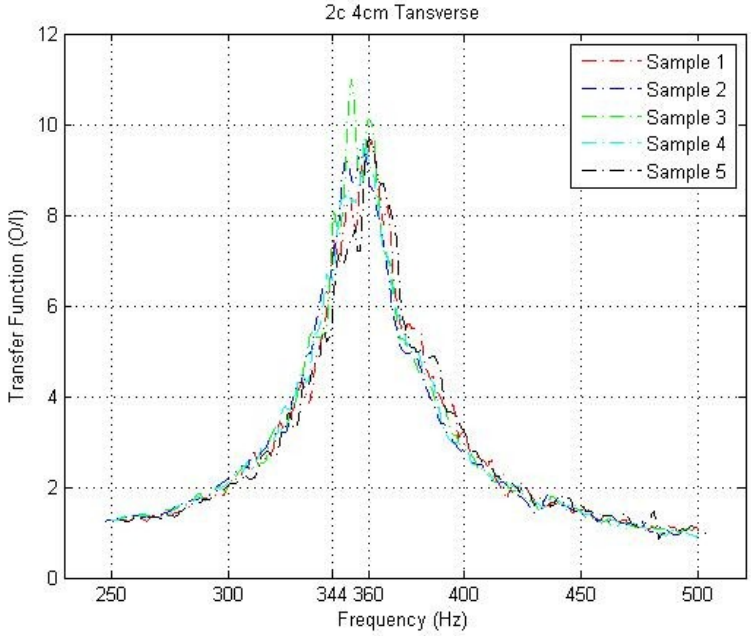

Figure App.D-4 Experimental results of 2C 4cm transverse transfer function

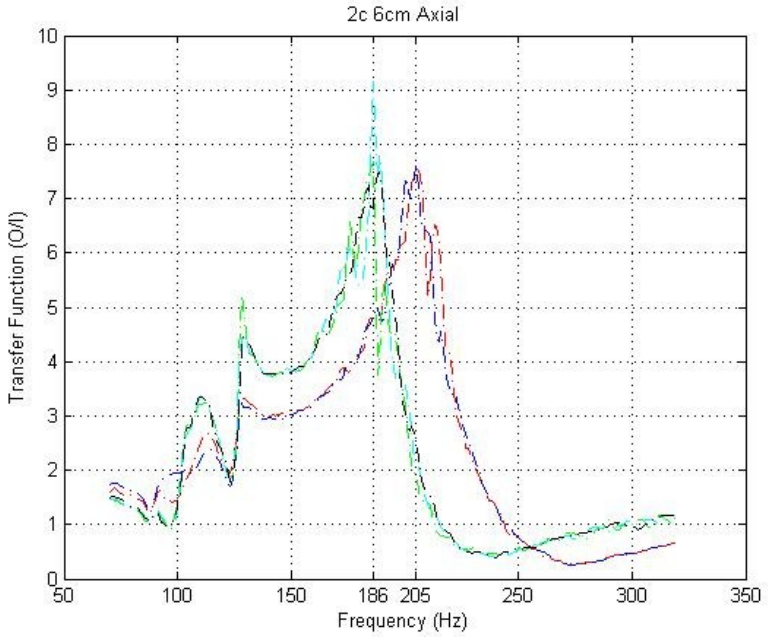

Figure App.D-5 Experimental results of 2C 6cm axial transfer function

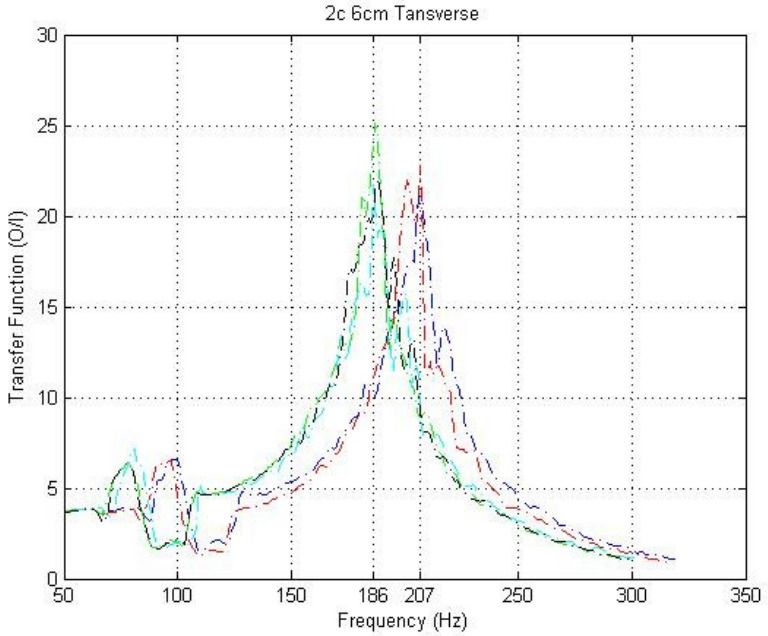

Figure App.D-6 Experimental results of 2C 6cm transverse transfer function

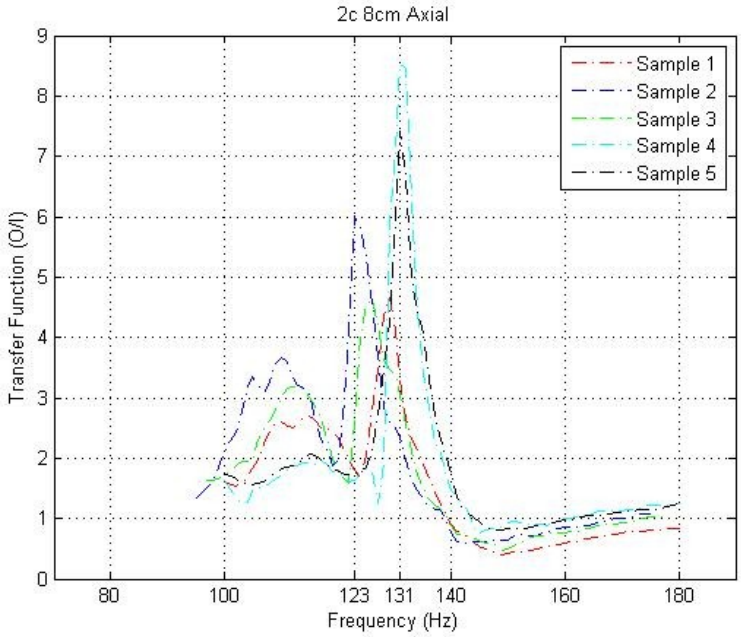

Figure App.D-7 Experimental results of 2C 8cm axial transfer function

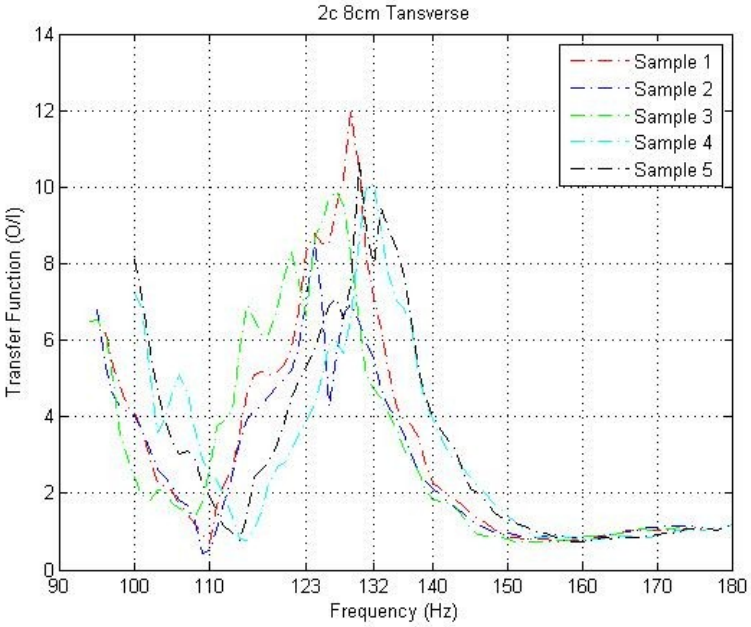

Figure App.D-8 Experimental results of 2C 8cm transverse transfer function

3.3.2.2 Results of Type 3A with Cable Lengths of 2cm, 4cm, 6cm and 8cm

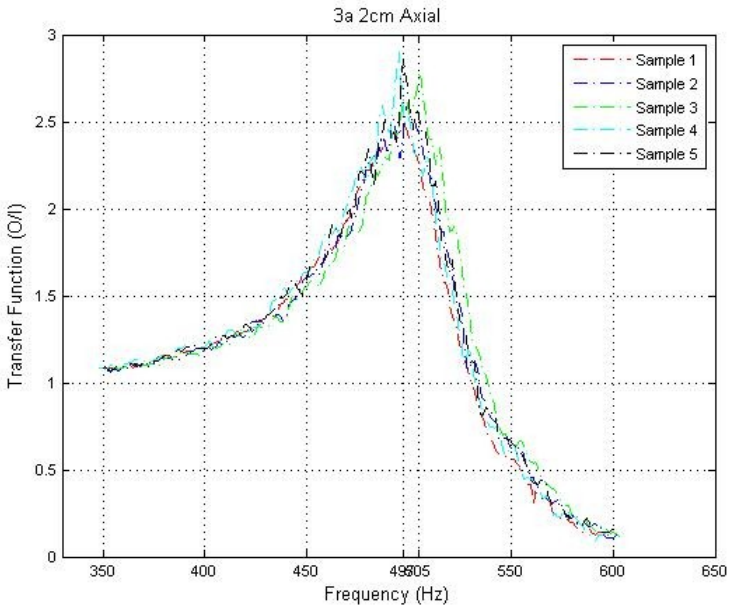

Figure App.D-9 Experimental results of 3A 2cm axial transfer function

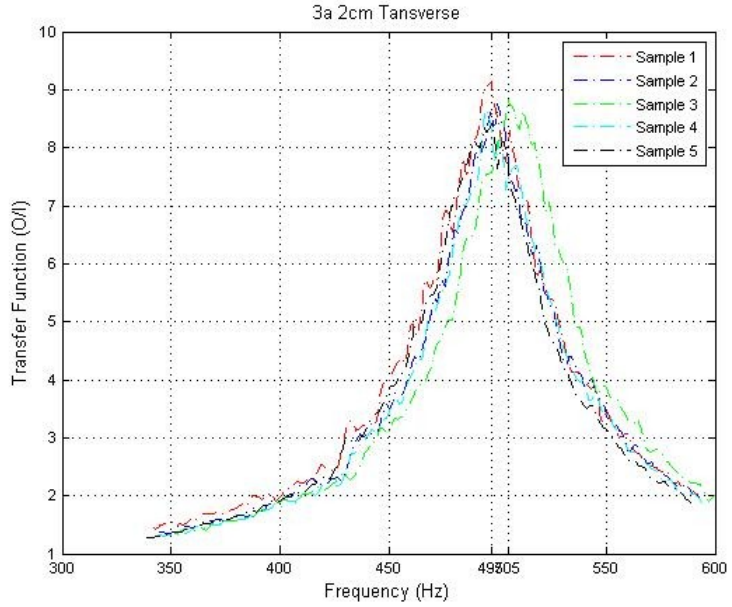

Figure App.D-10 Experimental results of 3A 2cm transverse transfer function

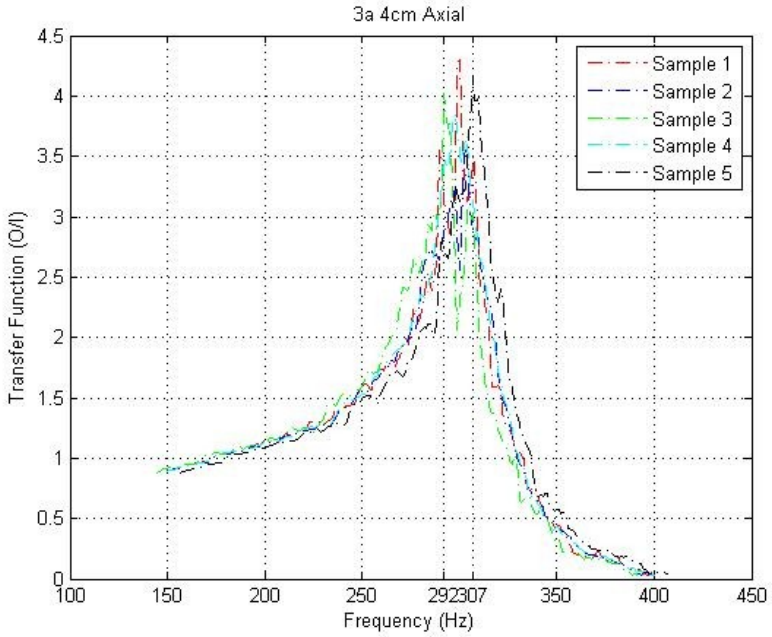

Figure App.D-11 Experimental results of 3A 4cm axial transfer function

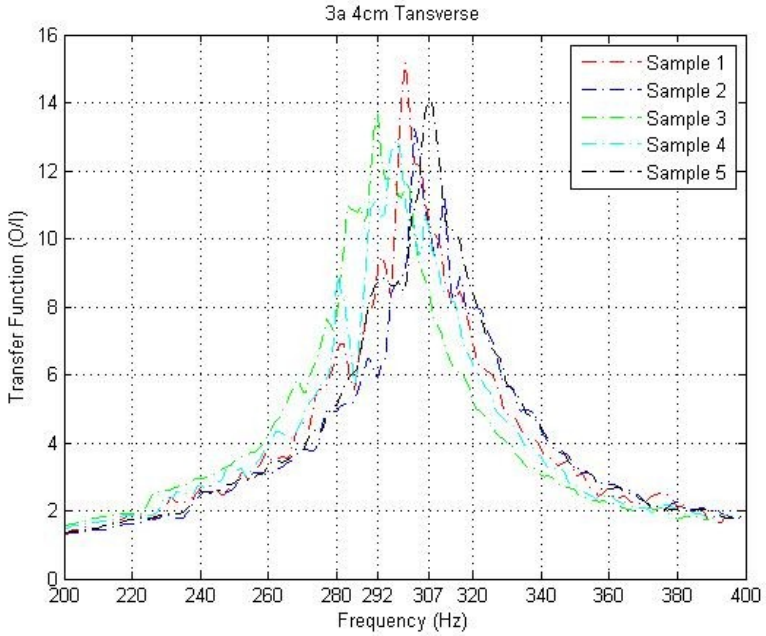

Figure App.D-12 Experimental results of 3A 4cm transverse transfer function

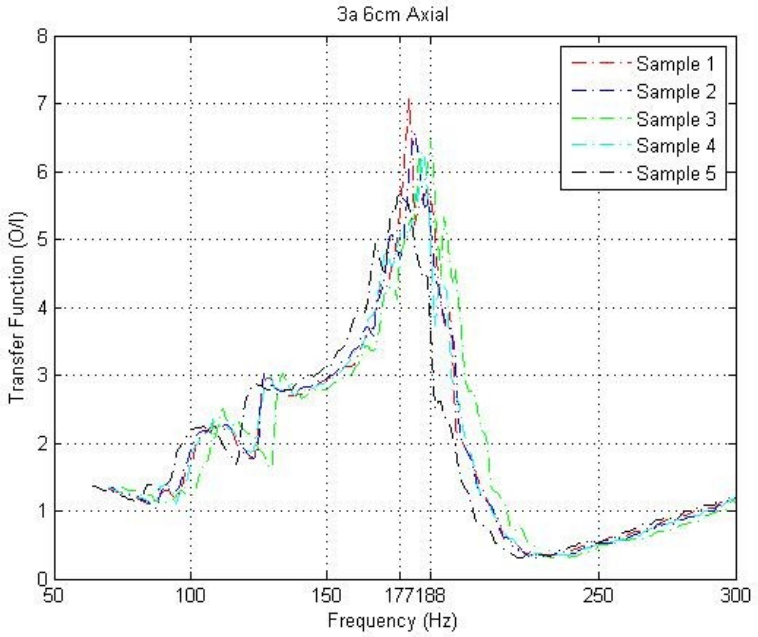

Figure App.D-13 Experimental results of 3A 6cm axial transfer function

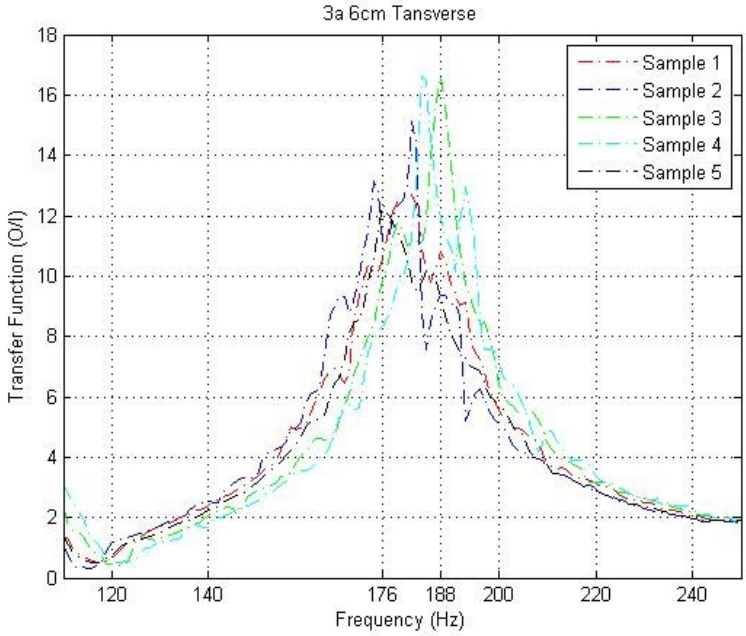

Figure App.D-14 Experimental results of 3A 6cm transverse transfer function

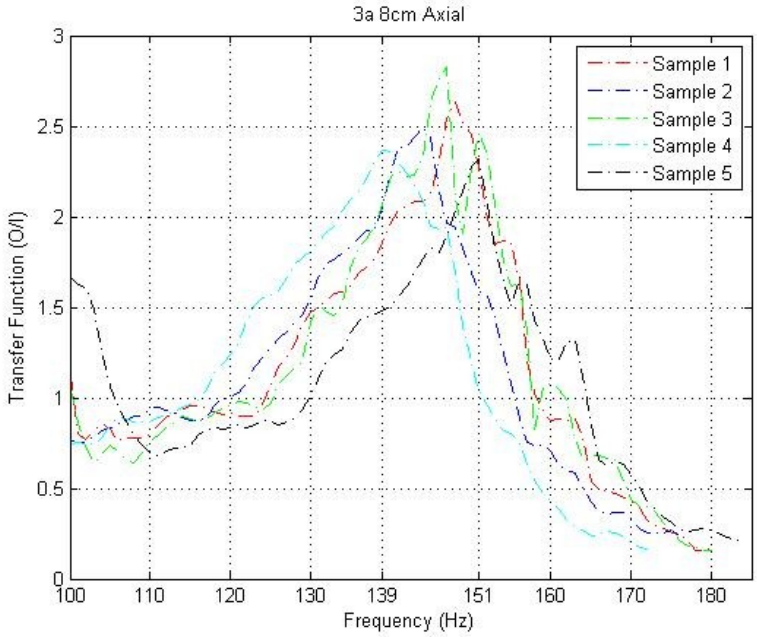

Figure App.D-15 Experimental results of 3A 8cm axial transfer function

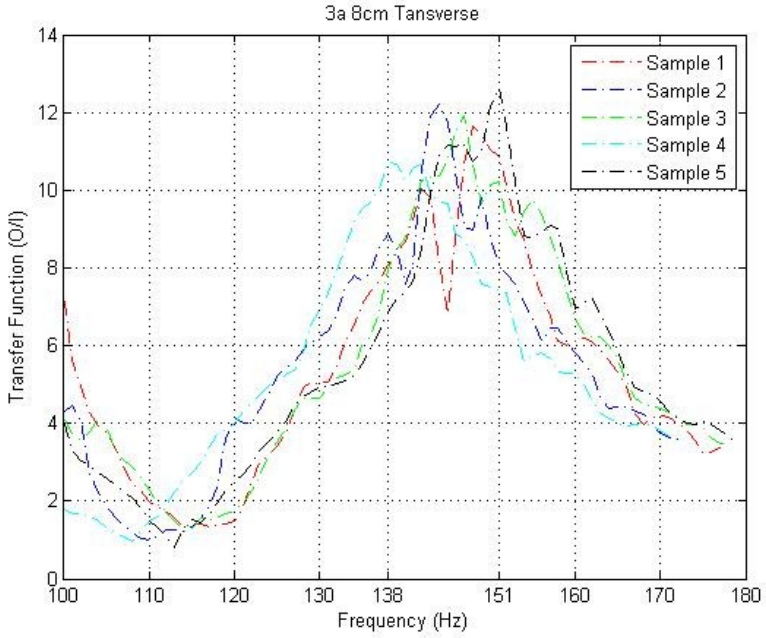

Figure App.D-16 Experimental results of 3A 8cm transverse transfer function

3.3.2.3 Results of Type 3B with Cable Lengths of 2cm, 4cm, 6cm and 8cm

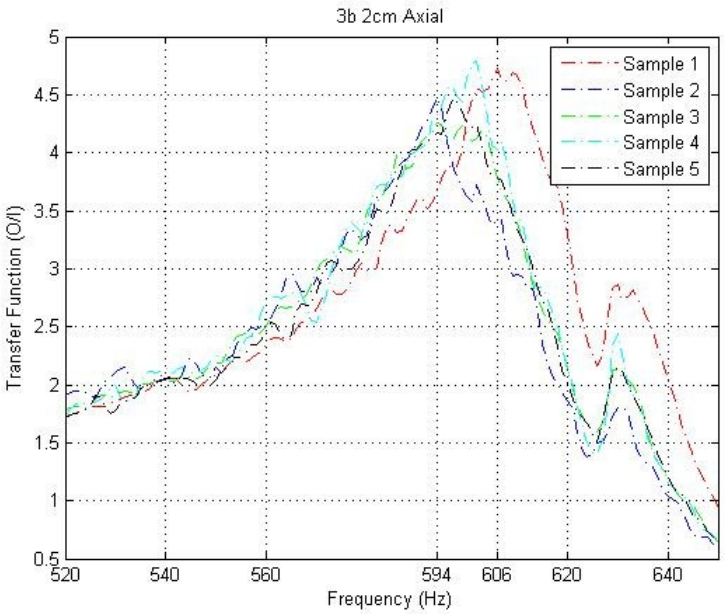

Figure App.D-17 Experimental results of 3B 2cm axial transfer function

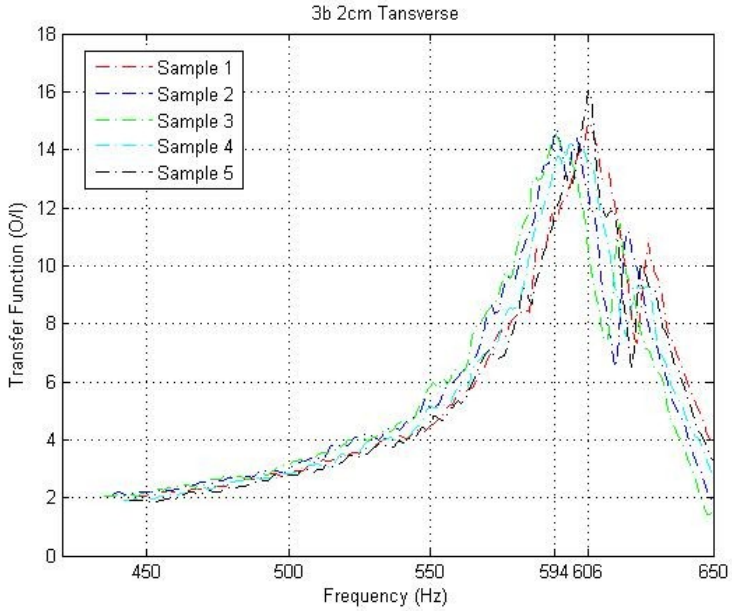

Figure App.D-18 Experimental results of 3B 2cm transverse transfer function

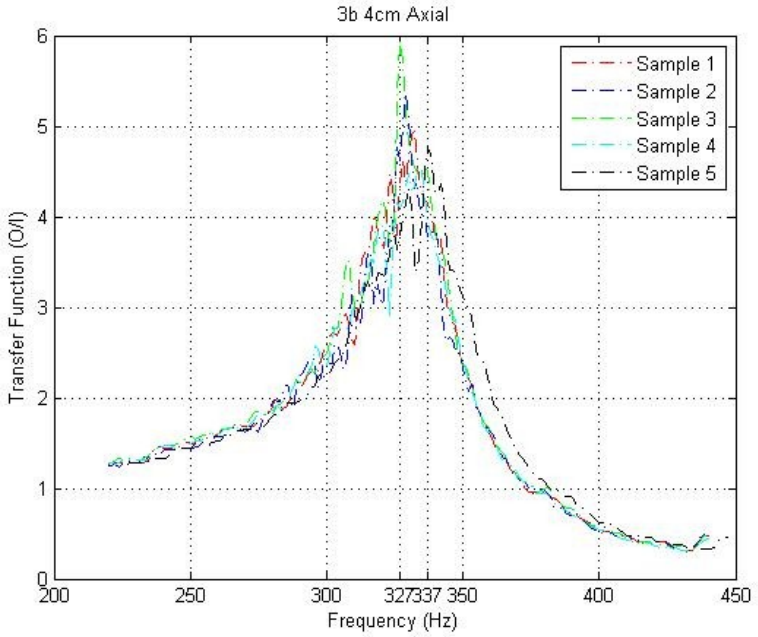

Figure App.D-19 Experimental results of 3B 4cm axial transfer function

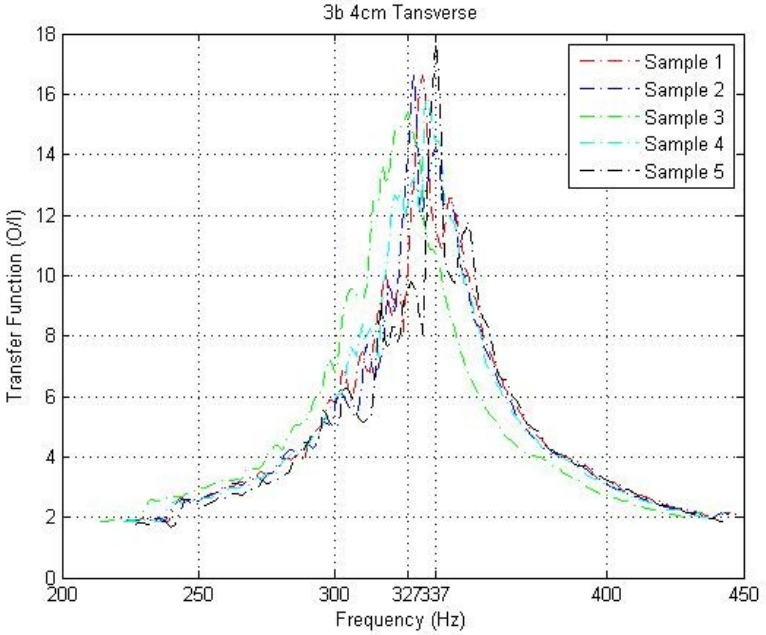

Figure App.D-20 Experimental results of 3B 4cm transverse transfer function

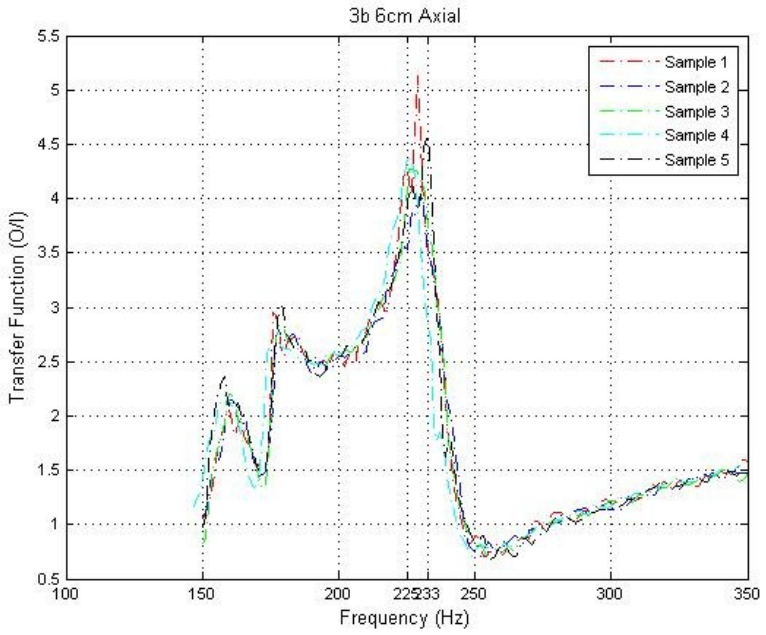

Figure App.D-21 Experimental results of 3B 6cm axial transfer function

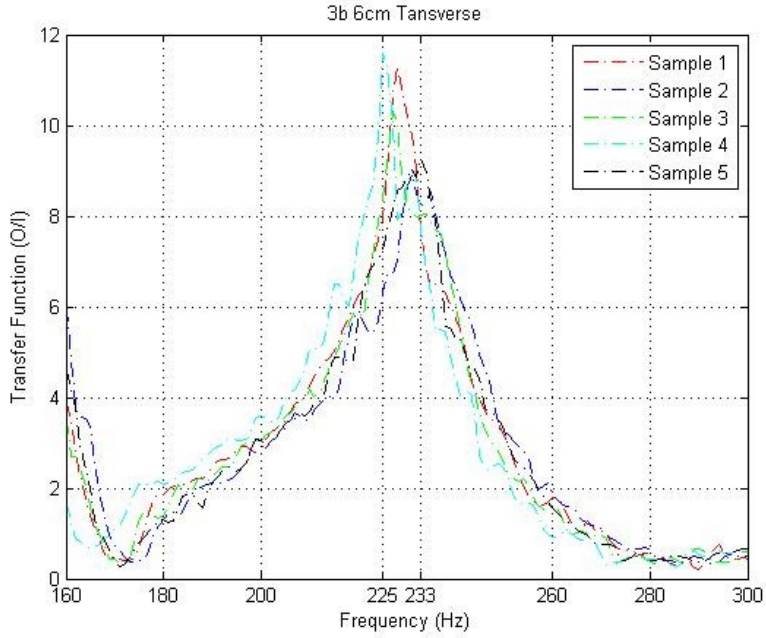

Figure App.D-22 Experimental results of 3B 6cm transverse transfer function

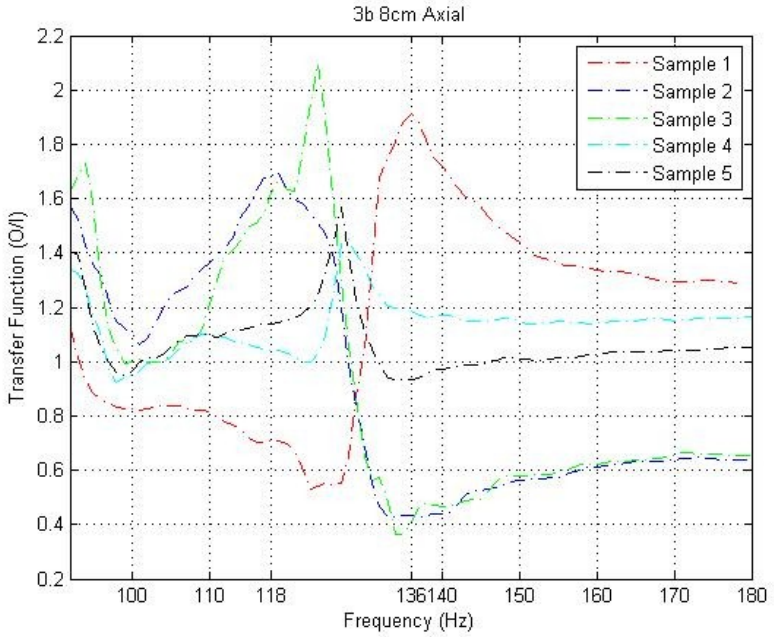

Figure App.D-23 Experimental results of 3B 8cm axial transfer function

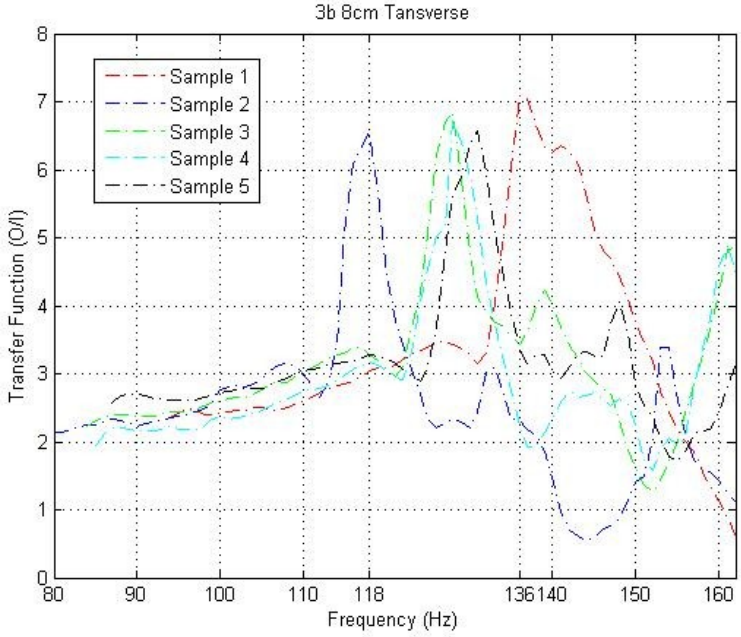

Figure App.D-24 Experimental results of 3B 8cm transverse transfer function

3.3.2.4 Results of Type 3C with Cable Lengths of 2cm, 4cm, 6cm and 8cm

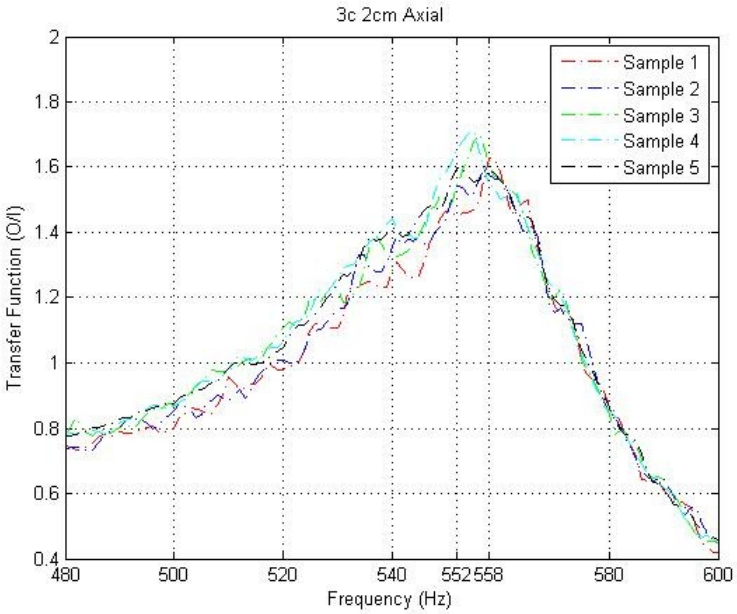

Figure App.D-25 Experimental results of 3C 2cm axial transfer function

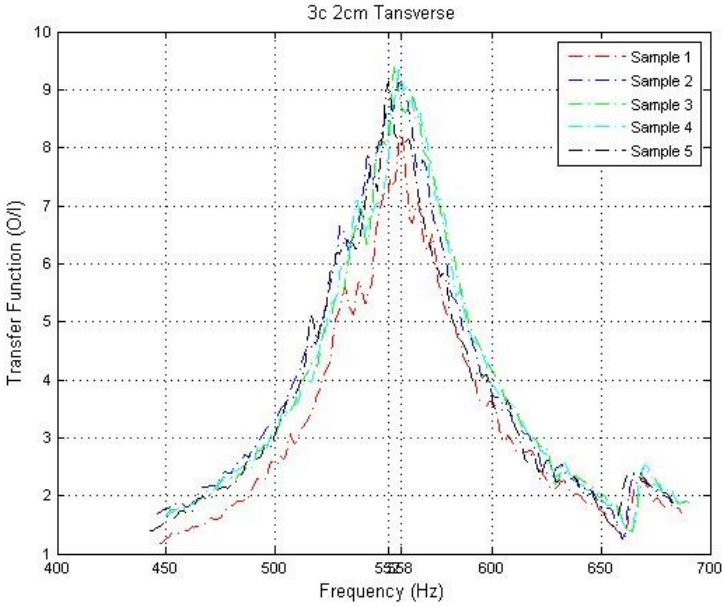

Figure App.D-26 Experimental results of 3C 2cm transverse transfer function

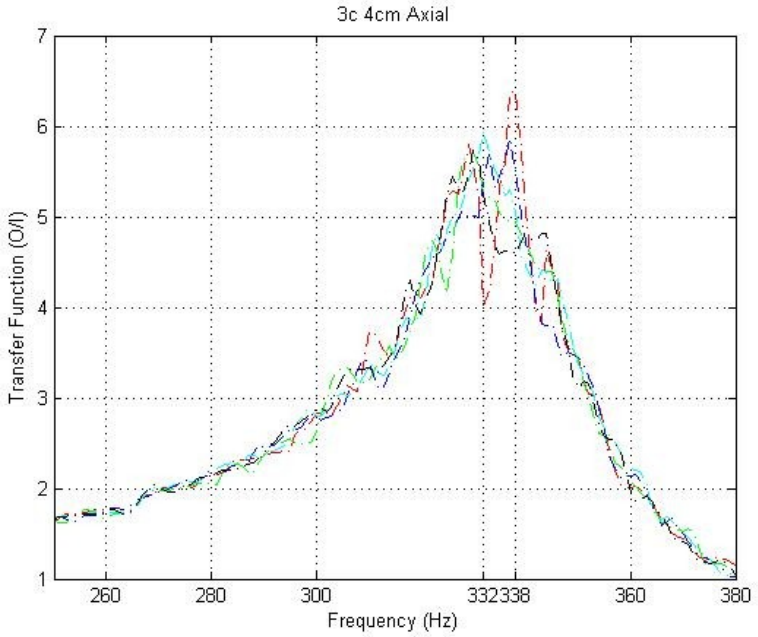

Figure App.D-27 Experimental results of 3C 4cm axial transfer function

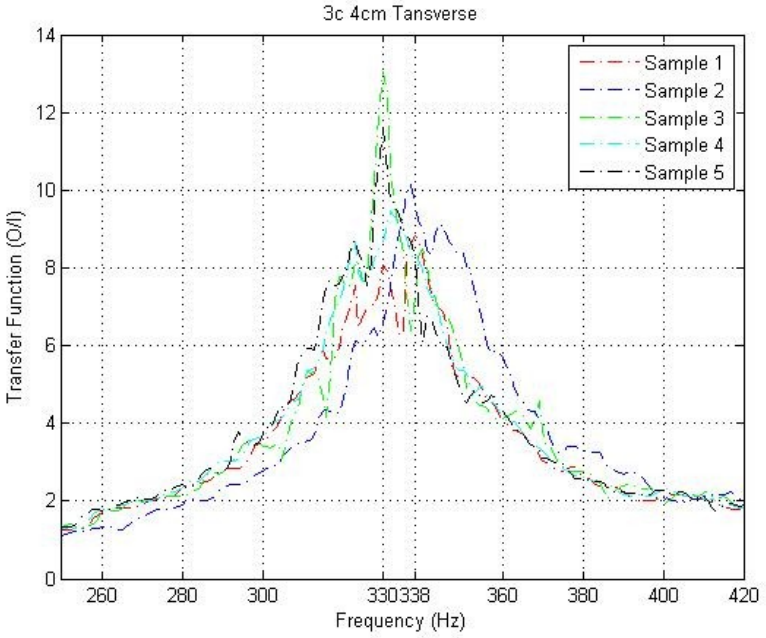

Figure App.D-28 Experimental results of 3C 4cm transverse transfer function

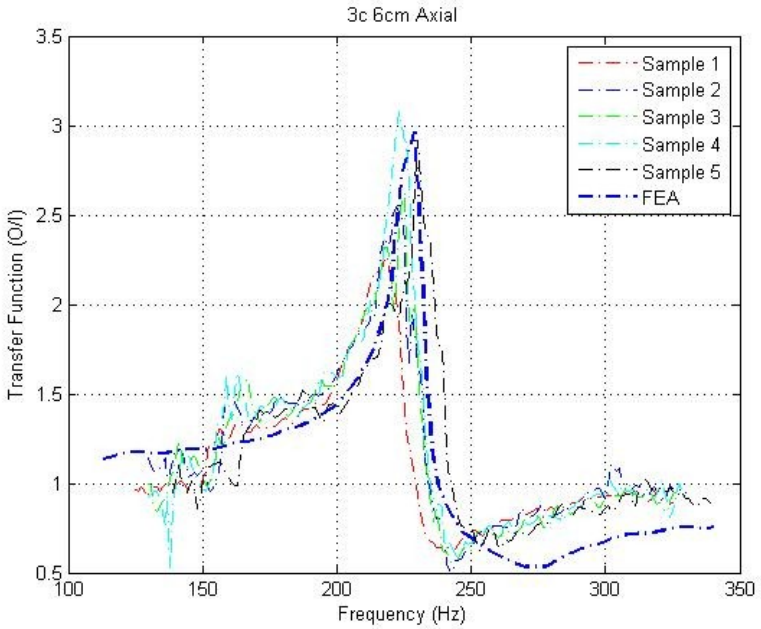

Figure App.D-29 Experimental results of 3C 6cm axial transfer function

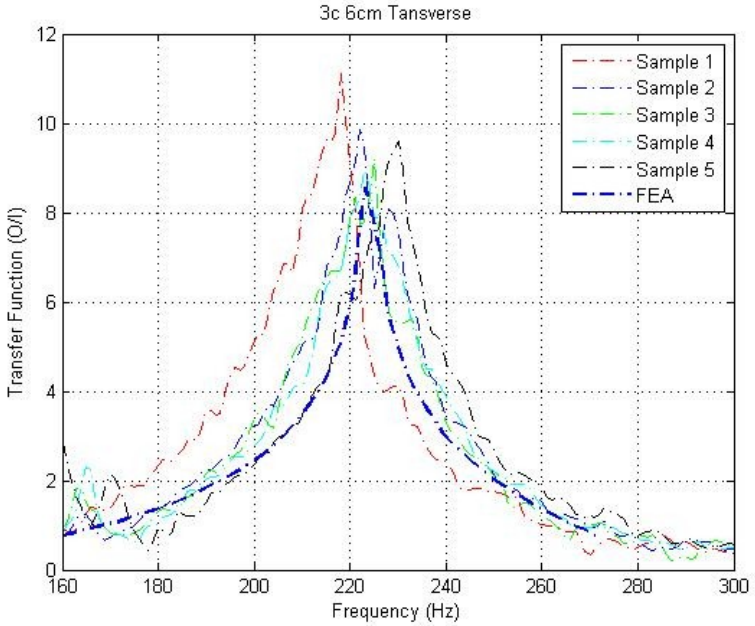

Figure App.D-30 Experimental results of 3C 6cm transverse transfer function

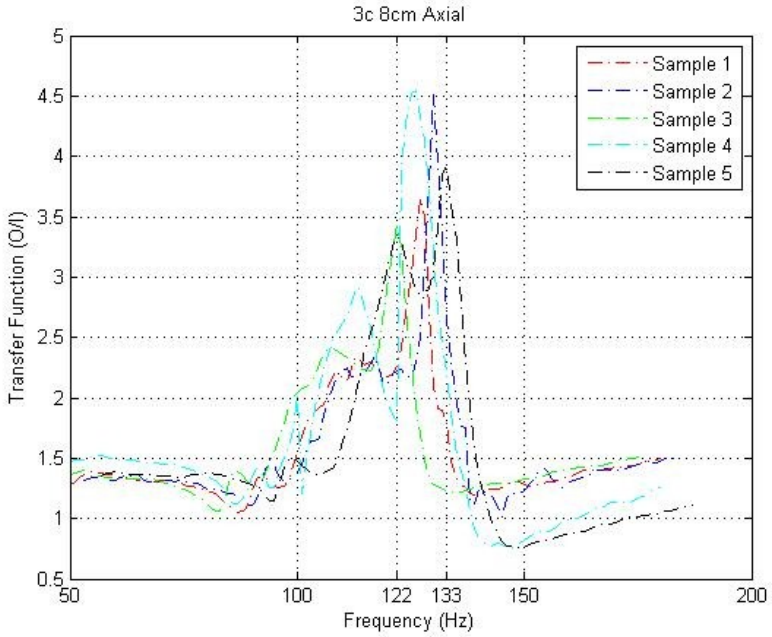

Figure App.D-31 Experimental results of 3C 8cm axial transfer function

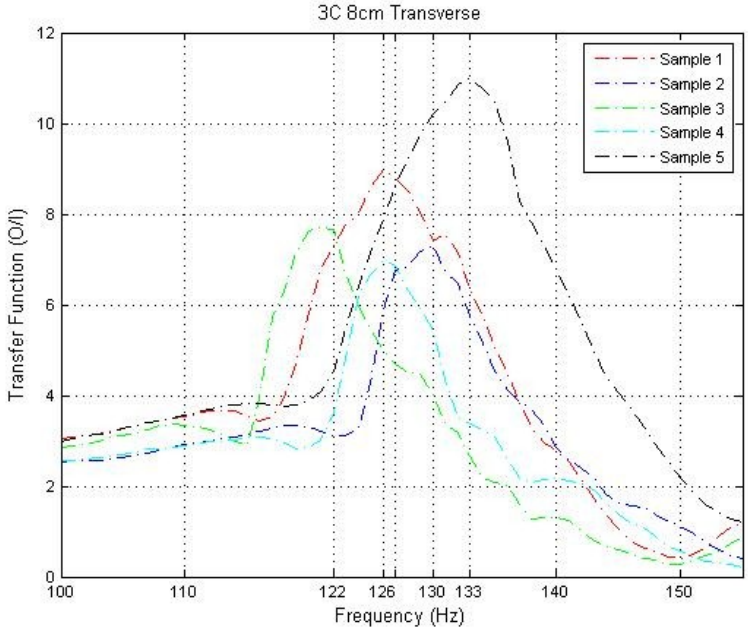

Figure App.D-32 Experimental results of 3C 8cm transverse transfer function

Appendix E Simulation Results of Frequency Response

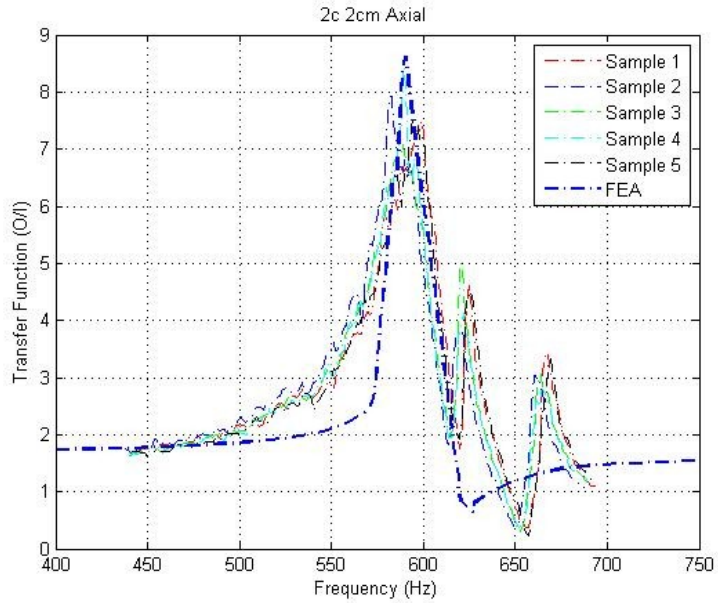

Figure App.E-1 Simulation results comparison of 2C 2cm axial transfer function

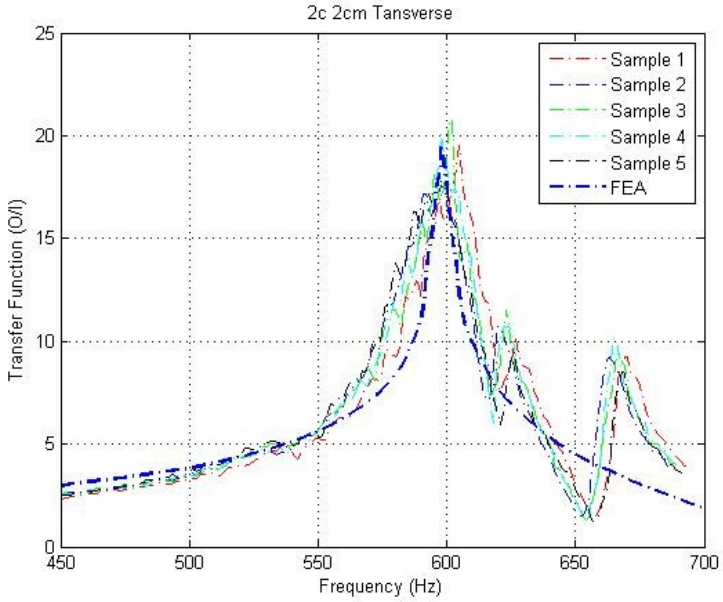

Figure App.E-2 Simulation results comparison of 2C 2cm transverse transfer function

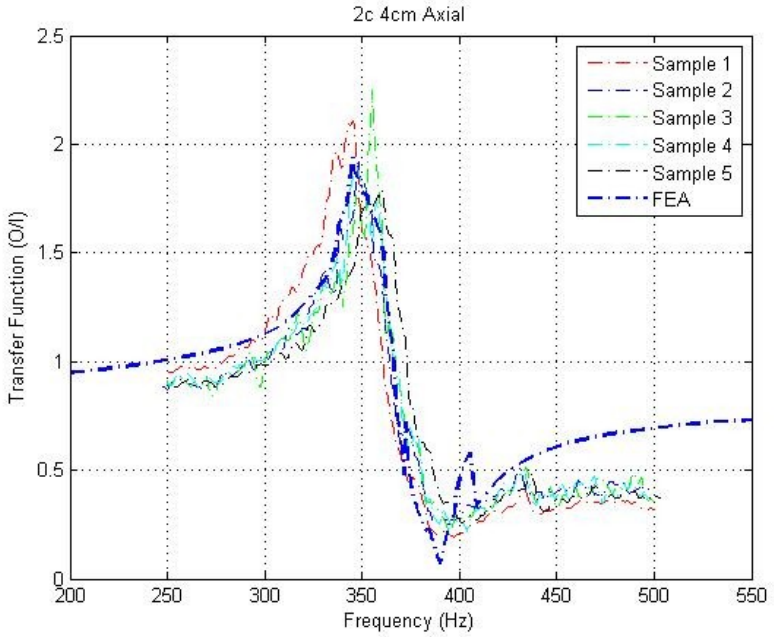

Figure App.E-3 Simulation results comparison of 2C 4cm axial transfer function

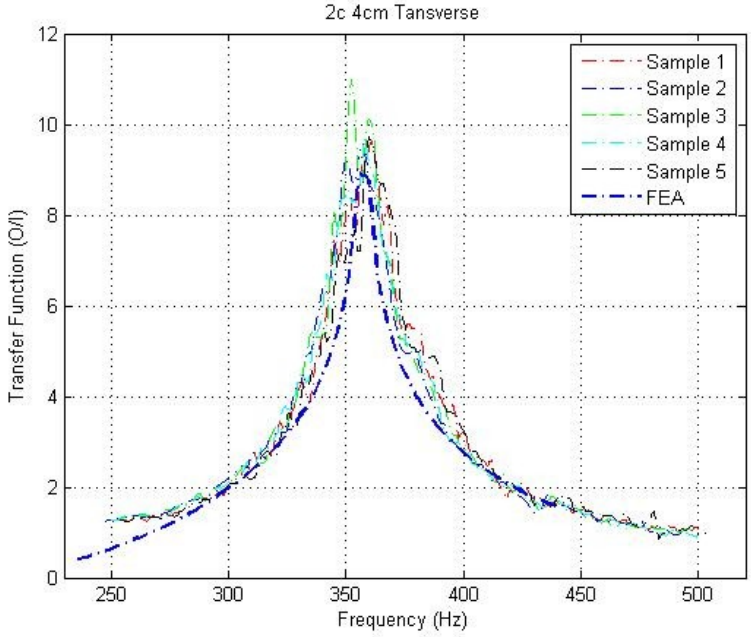

Figure App.E-4 Simulation results comparison of 2C 4cm transverse transfer function

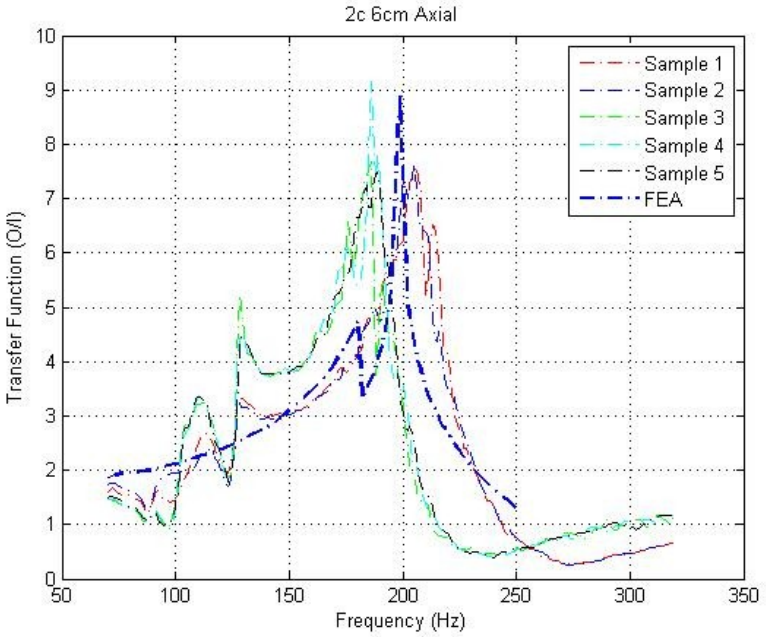

Figure App.E-5 Simulation results comparison of 2C 6cm axial transfer function

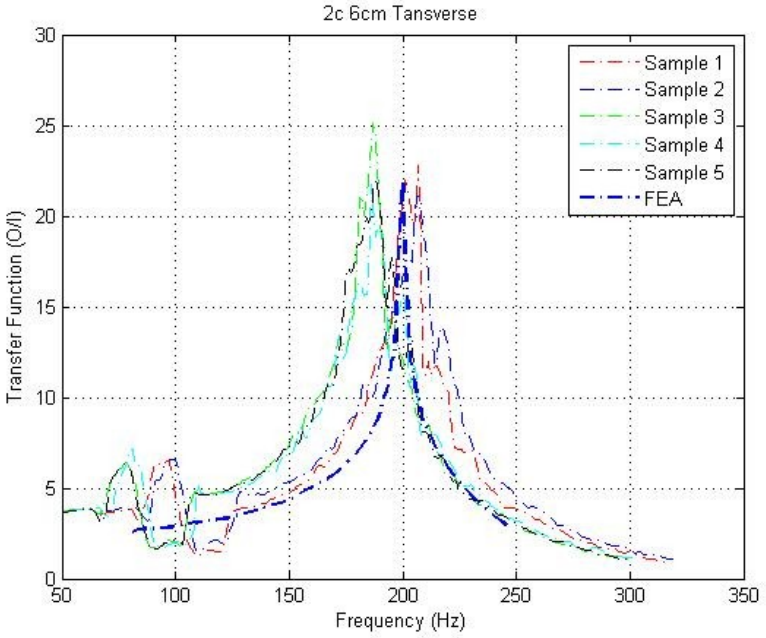

Figure App.E-6 Simulation results comparison of 2C 6cm transverse transfer function

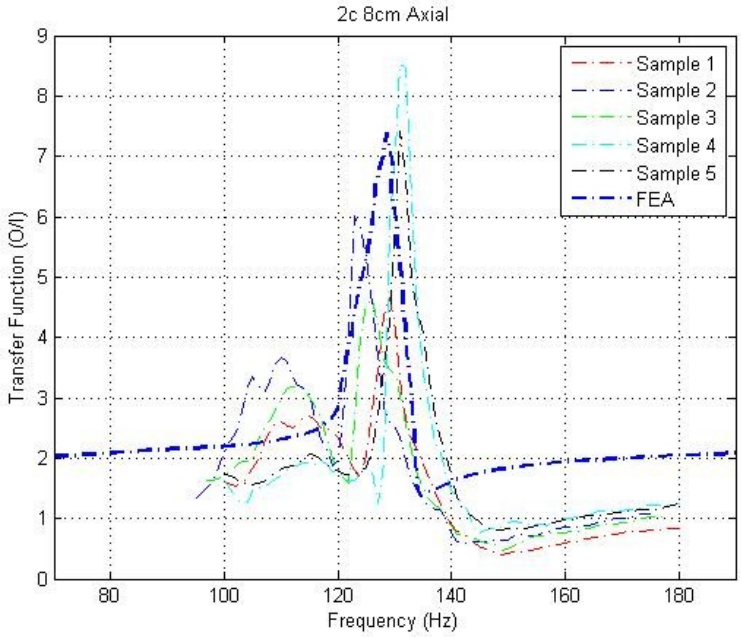

Figure App.E-7 Simulation results comparison of 2C 8cm axial transfer function

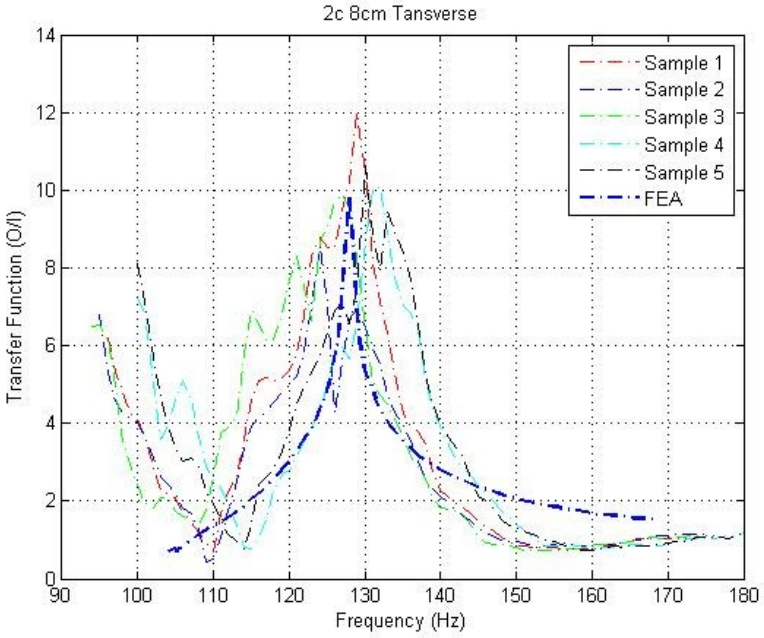

Figure App.E-8 Simulation results comparison of 2C 8cm transverse transfer function

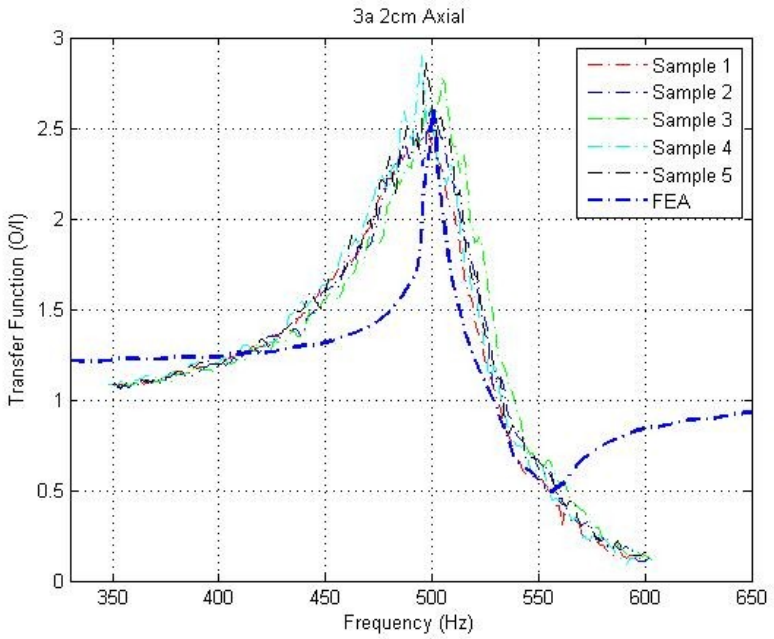

Figure App.E-9 Simulation results comparison of 3A 2cm axial transfer function

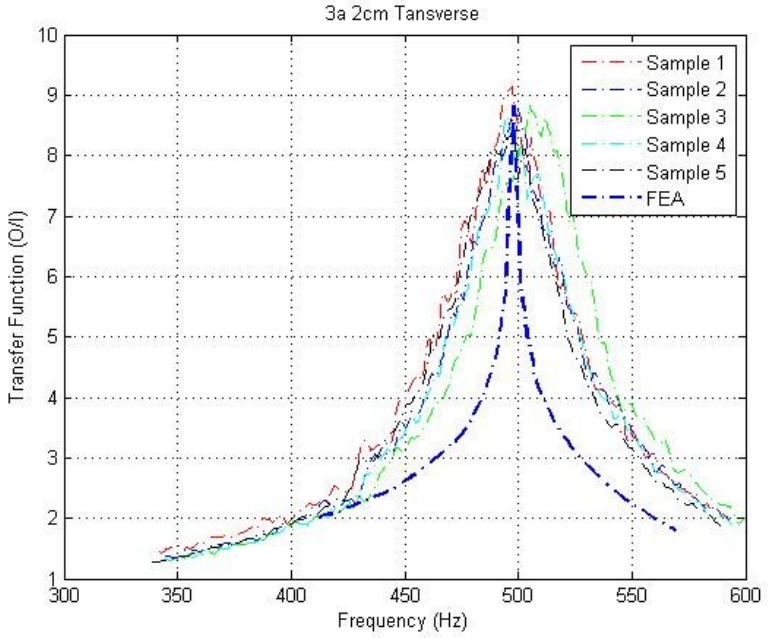

Figure App.E-10 Simulation results comparison of 3A 2cm transverse transfer function

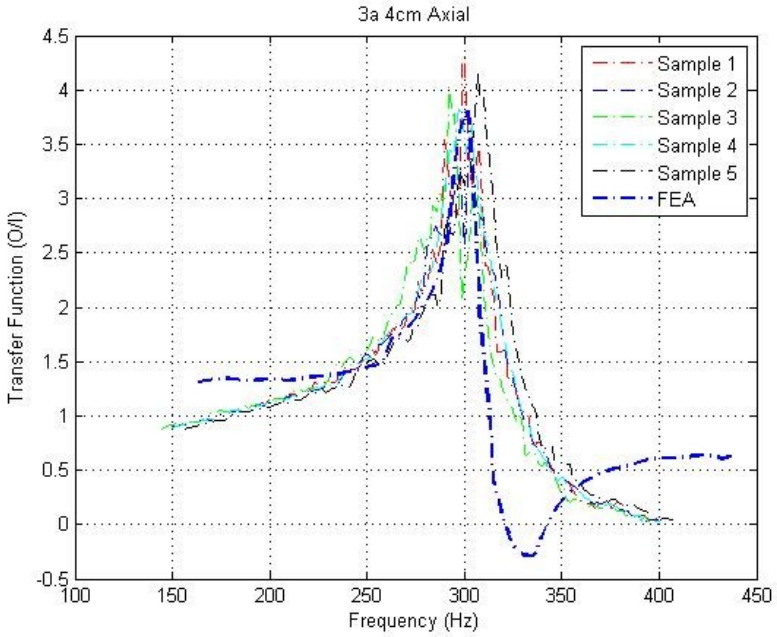

Figure App.E-11 Simulation results comparison of 3A 4cm axial transfer function

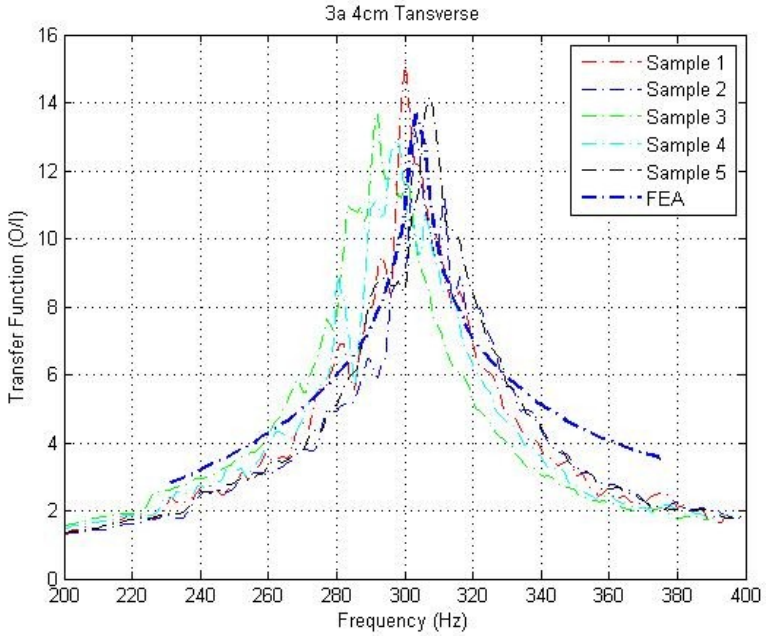

Figure App.E-12 Simulation results comparison of 3A 4cm transverse transfer function

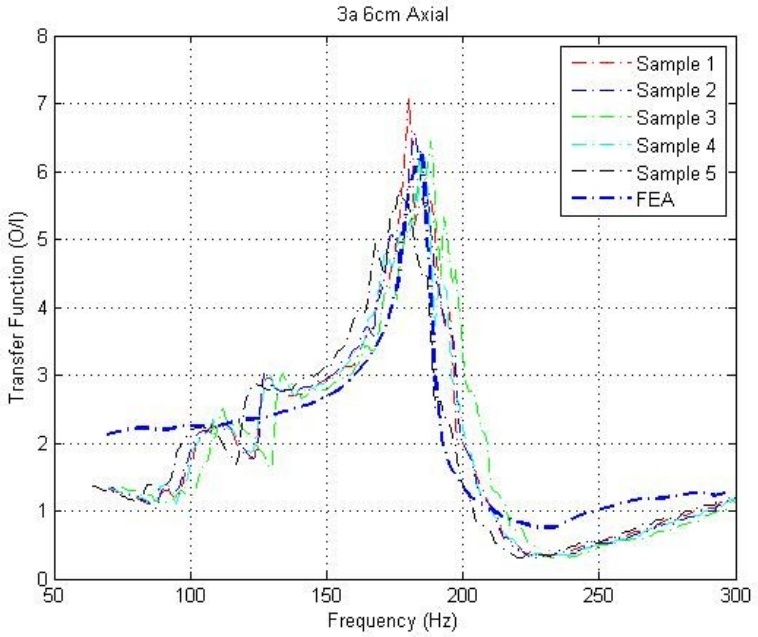

Figure App.E-13 Simulation results comparison of 3A 6cm axial transfer function

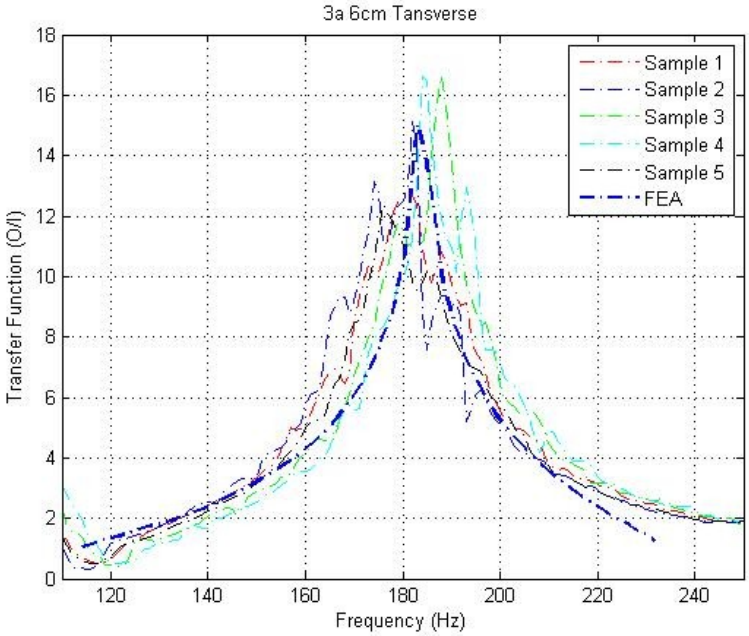

Figure App.E-14 Simulation results comparison of 3A 6cm transverse transfer function

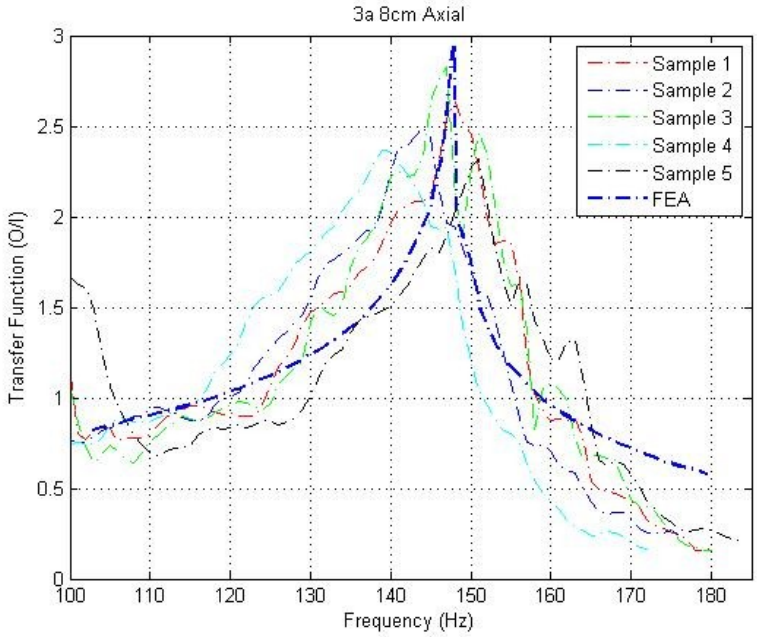

Figure App.E-15 Simulation results comparison of 3A 8cm axial transfer function

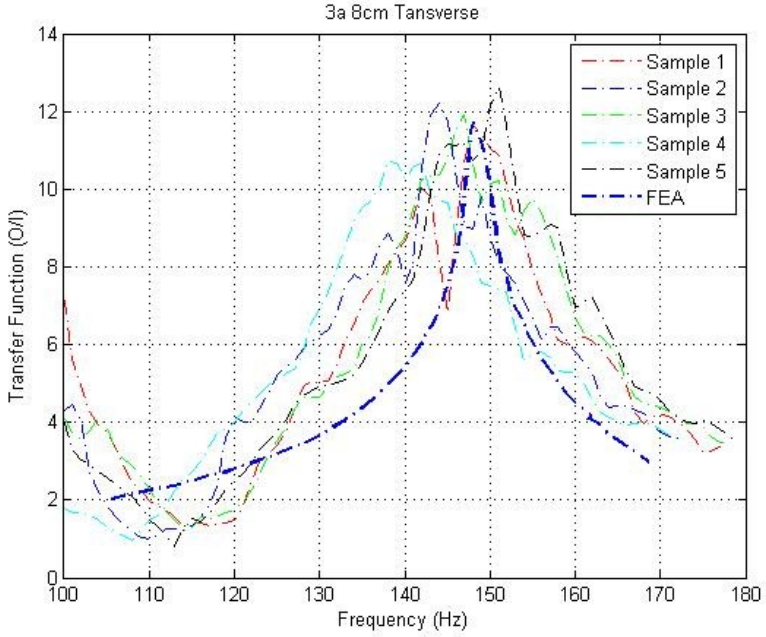

Figure App.E-16 Simulation results comparison of 3A 8cm transverse transfer function

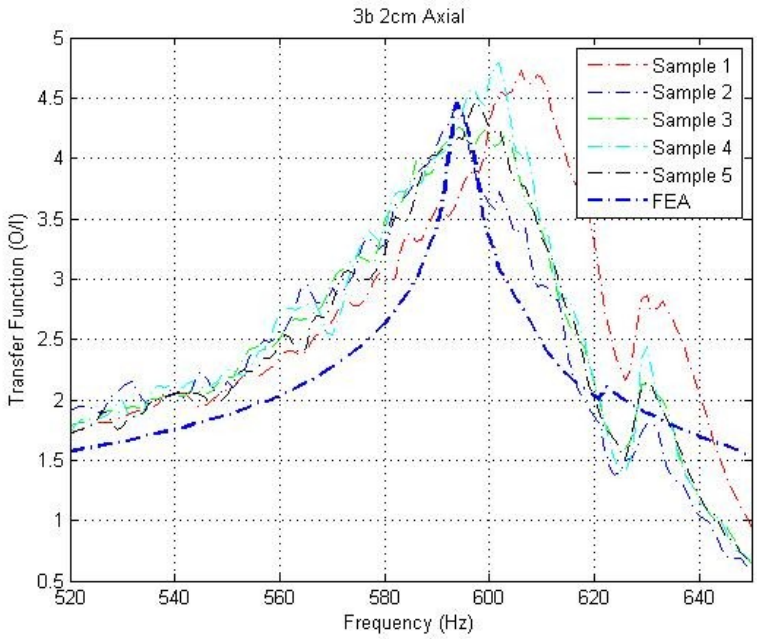

Figure App.E-17 Simulation results comparison of 3B 2cm axial transfer function

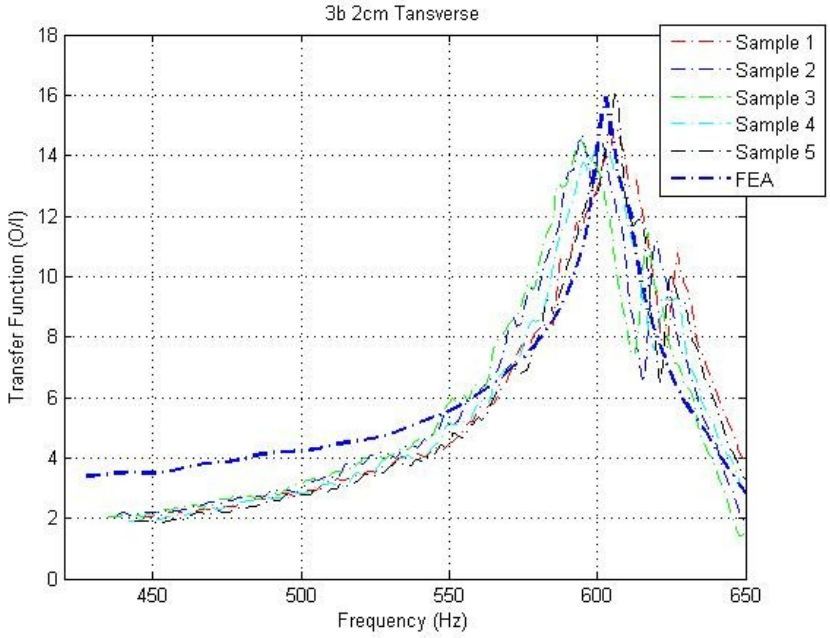

Figure App.E-18 Simulation results comparison of 3B 2cm transverse transfer function

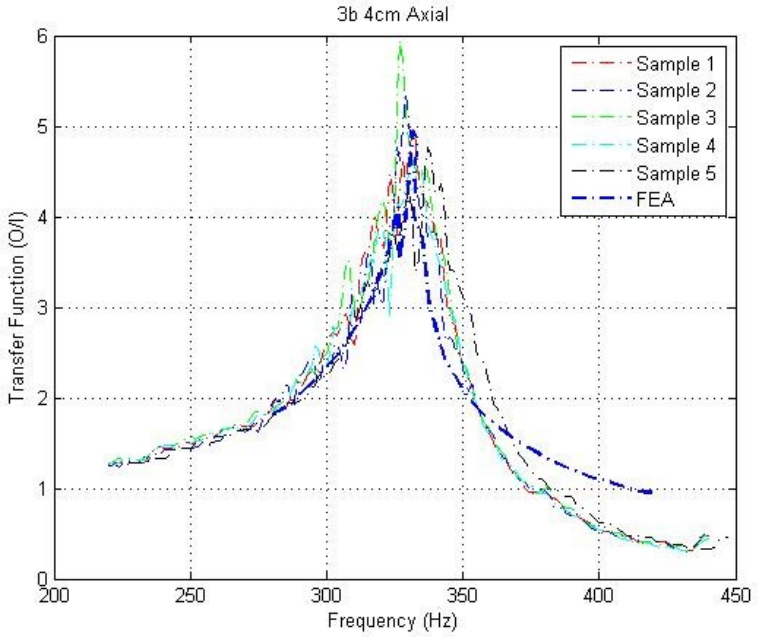

Figure App.E-19 Simulation results comparison of 3B 4cm axial transfer function

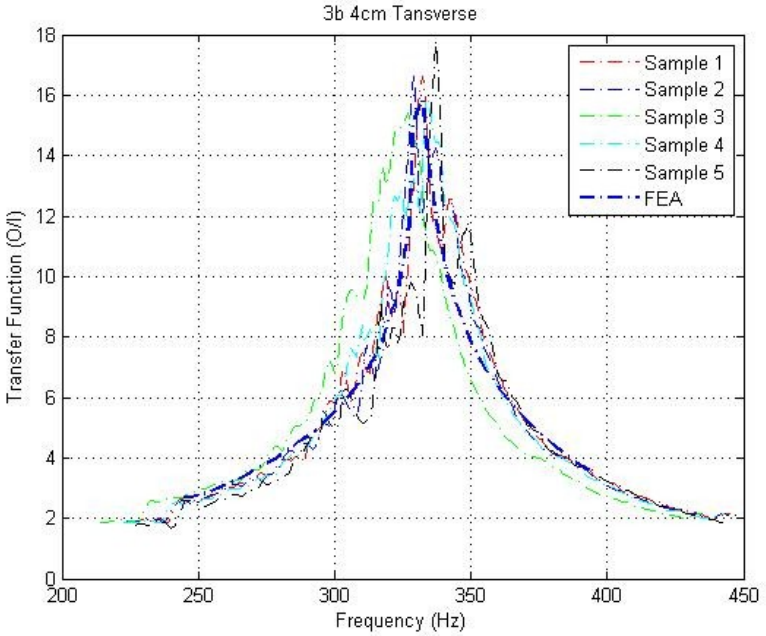

Figure App.E-20 Simulation results comparison of 3B 4cm transverse transfer function

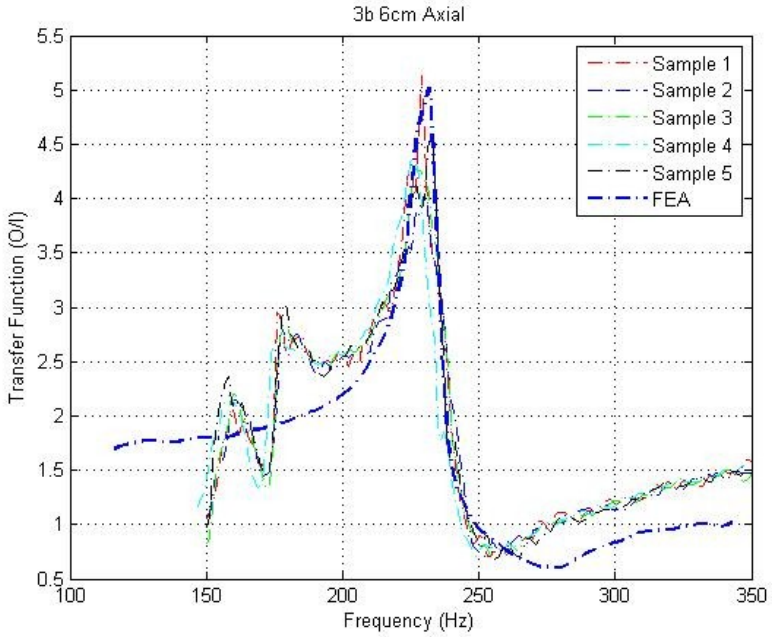

Figure App.E-21 Simulation results comparison of 3B 6cm axial transfer function

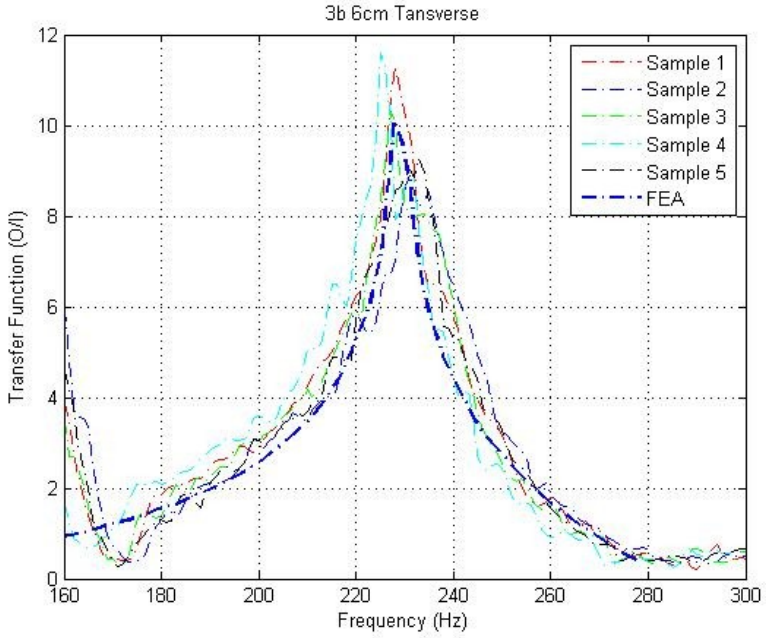

Figure App.E-22 Simulation results comparison of 3B 6cm transverse transfer function

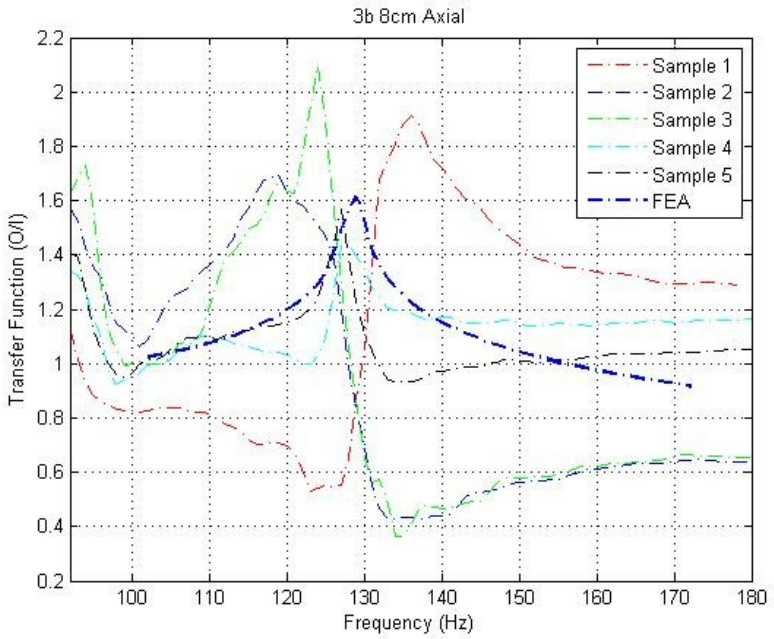

Figure App.E-23 Simulation results comparison of 3B 8cm axial transfer function

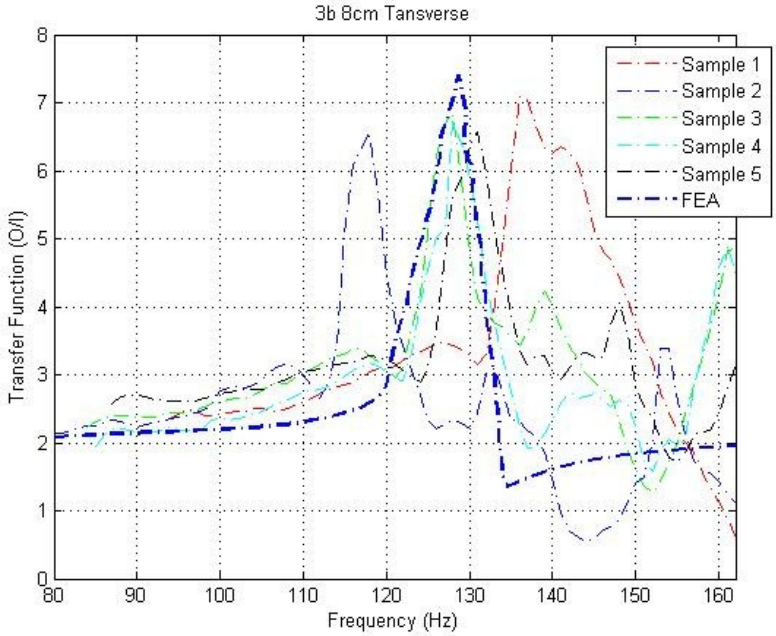

Figure App.E-24 Simulation results comparison of 3B 8cm transverse transfer function

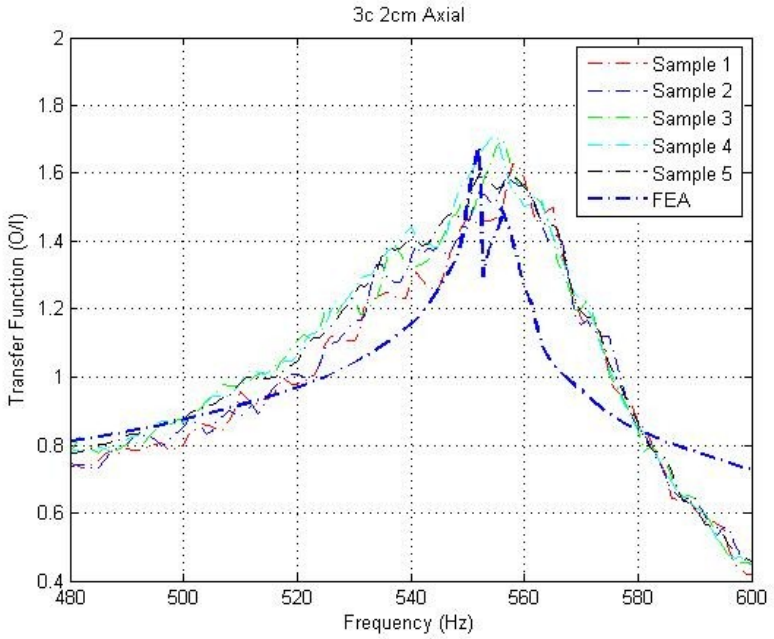

Figure App.E-25 Simulation results comparison of 3C 2cm axial transfer function

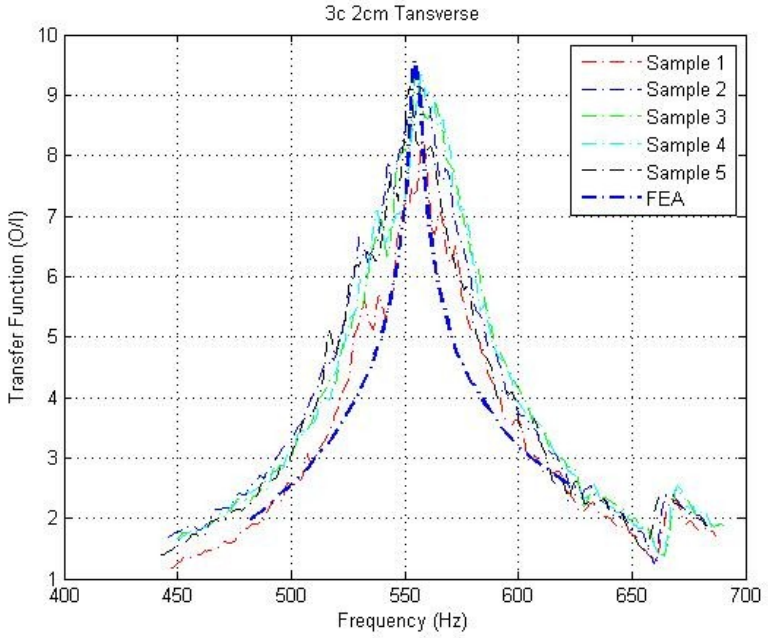

Figure App.E-26 Simulation results comparison of 3C 2cm transverse transfer function

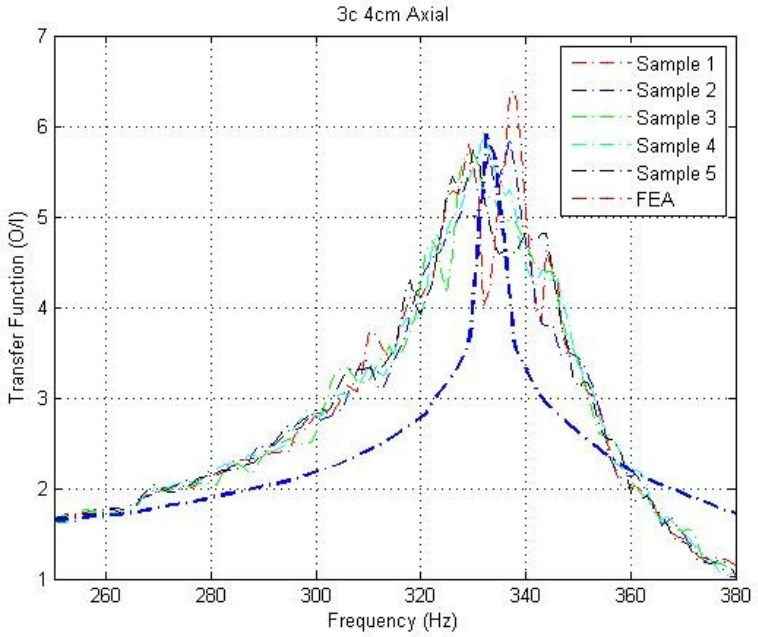

Figure App.E-27 Simulation results comparison of 3C 4cm axial transfer function

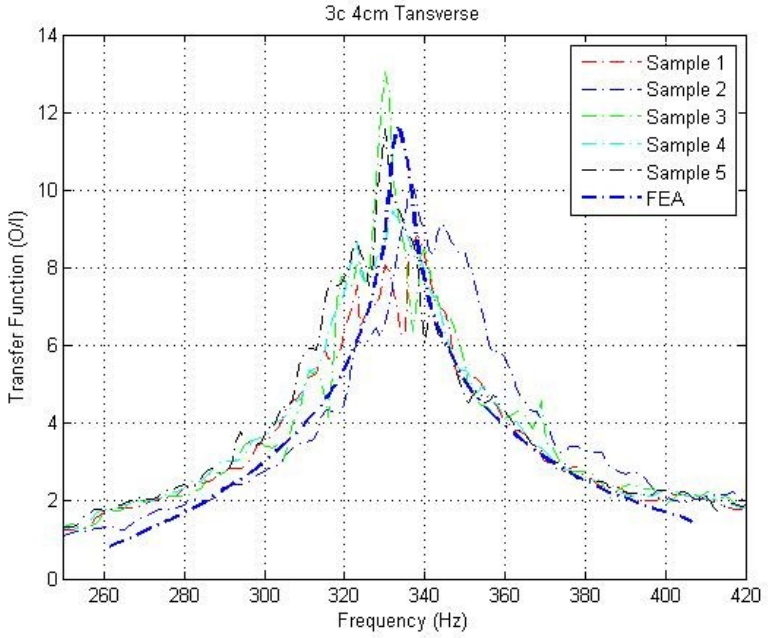

Figure App.E-28 Simulation results comparison of 3C 4cm transverse transfer function

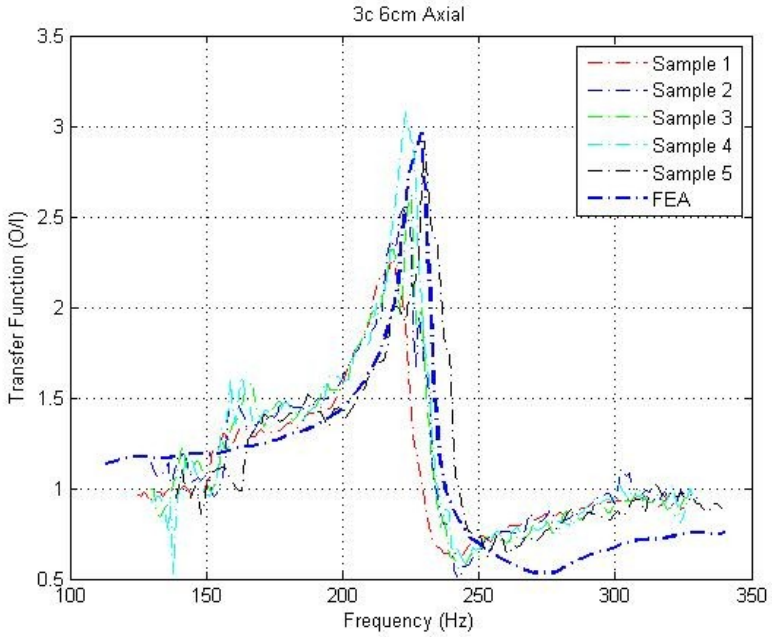

Figure App.E-29 Simulation results comparison of 3C 6cm axial transfer function

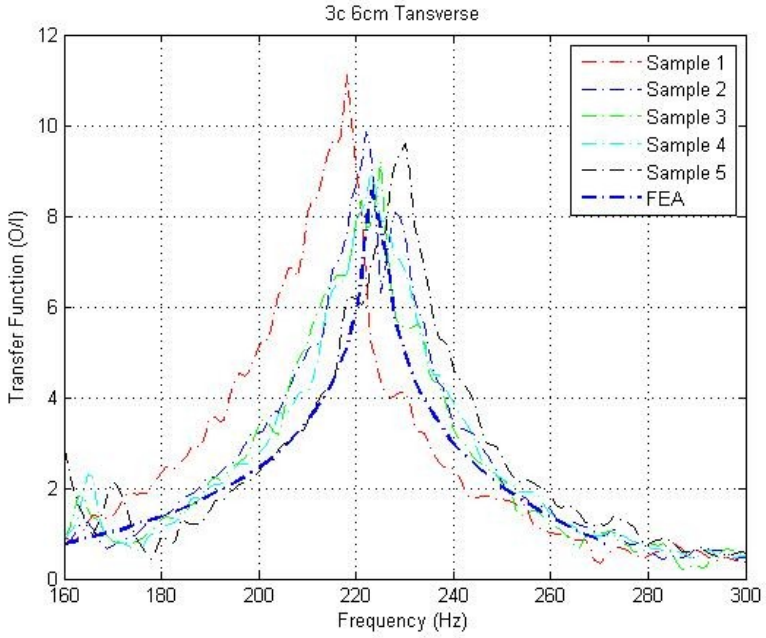

Figure App.E-30 Simulation results comparison of 3C 6cm transverse transfer function

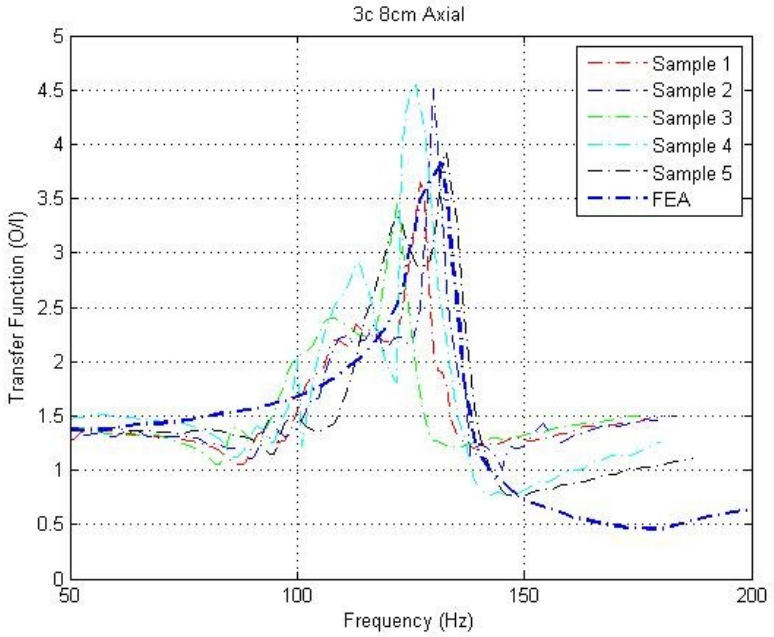

Figure App.E-31 Simulation results comparison of 3C 8cm axial transfer function

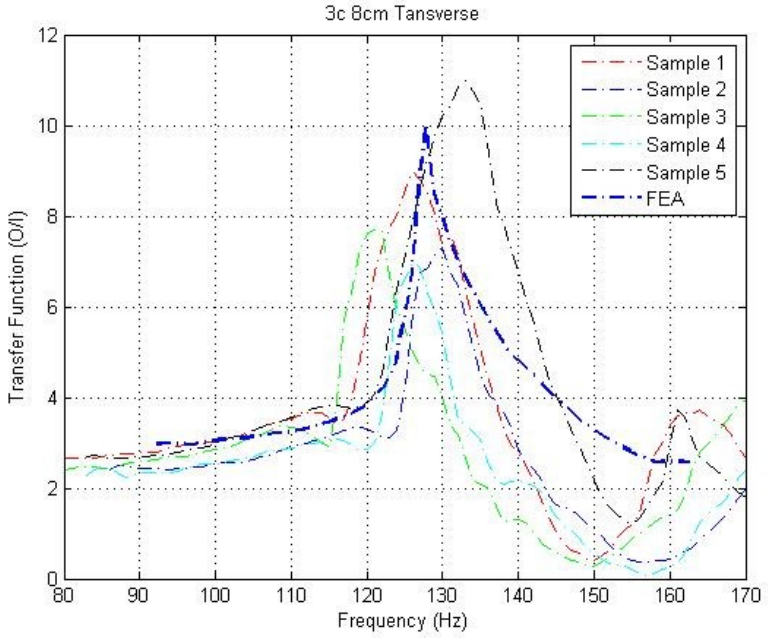

Figure App.E-32 Simulation results comparison of 3C 8cm transverse transfer function

Appendix F Simulation Results of Relative Motion

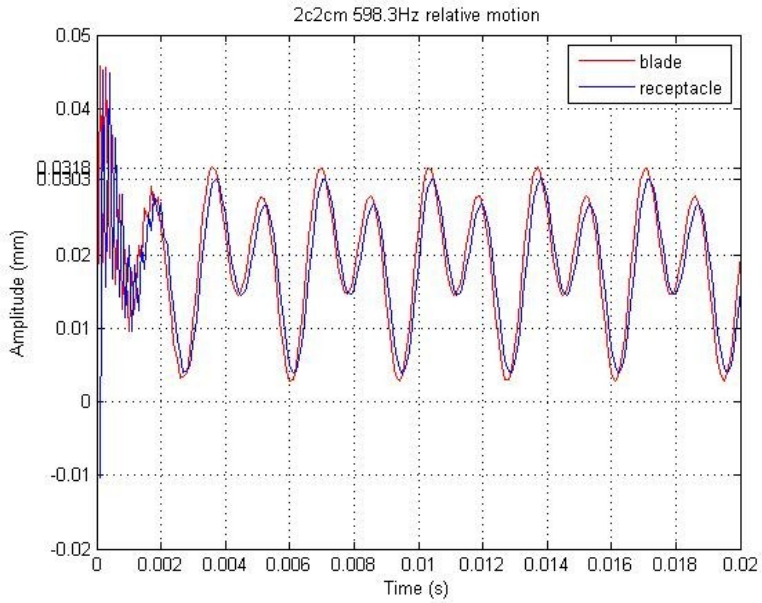

Figure App.F-1 Six cycles of the blade and receptacle of 2C 2cm under 598.3Hz

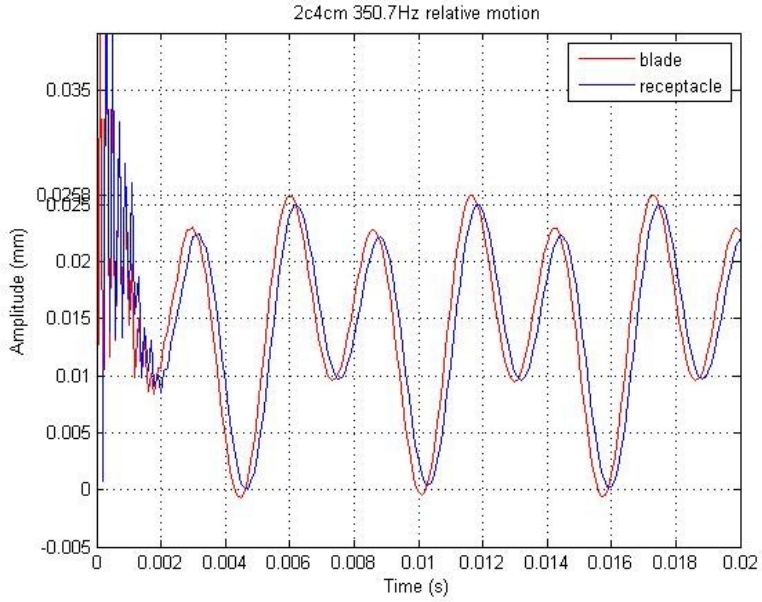

Figure App.F-2 Three cycles of the blade and receptacle of 2C 4cm under 350.7Hz

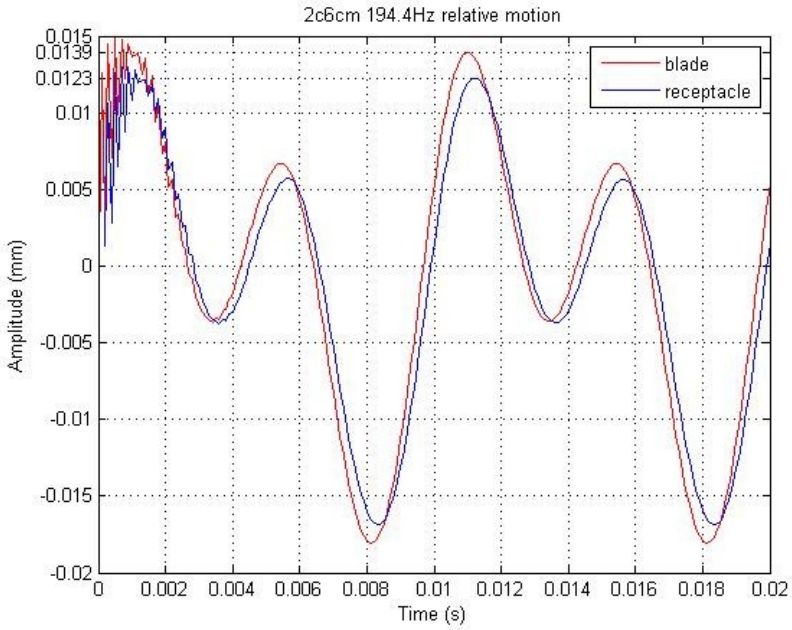

Figure App.F-3 Two cycles of the blade and receptacle of 2C 6cm under 194.4Hz

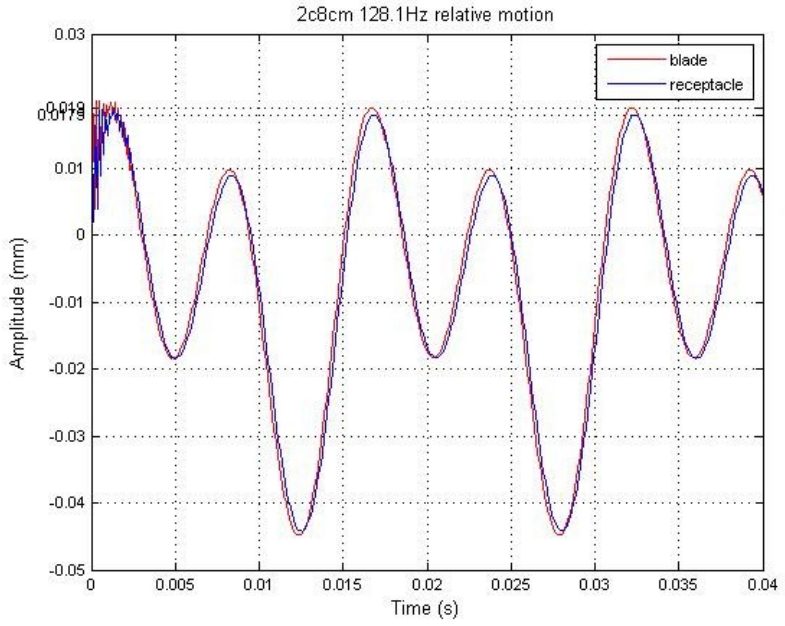

Figure App.F-4 Two cycles of the blade and receptacle of 2C 8cm under 128.1Hz

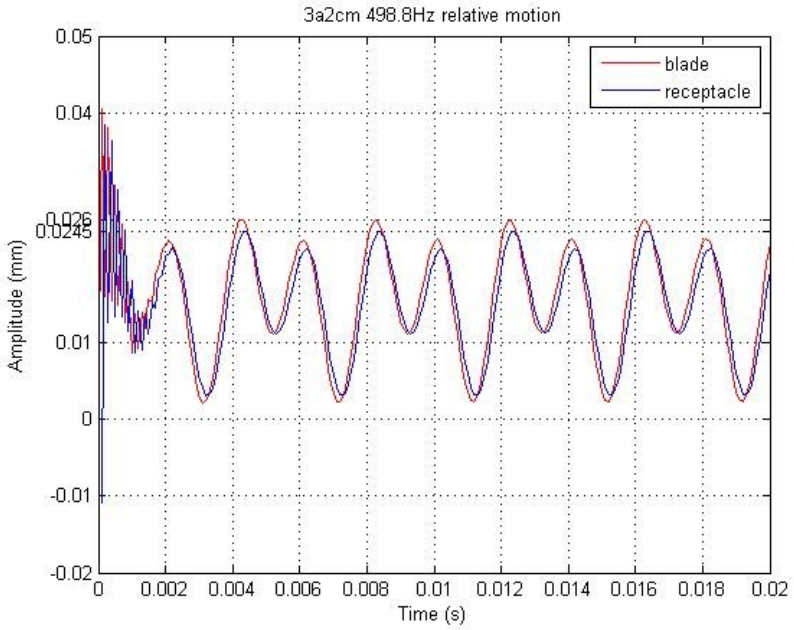

Figure App.F-5 Five cycles of the blade and receptacle of 3A 2cm under 498.8Hz

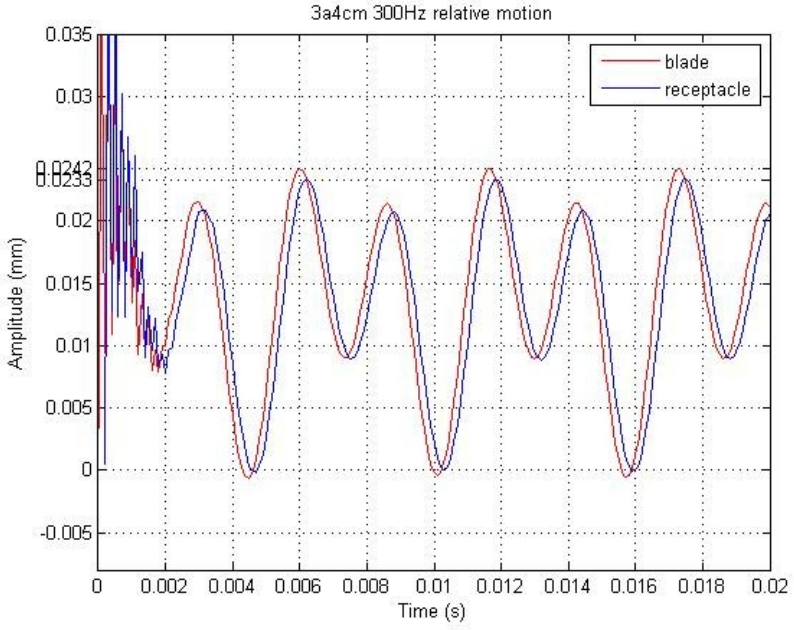

Figure App.F-6 Three cycles of the blade and receptacle of 3A 4cm under 300Hz

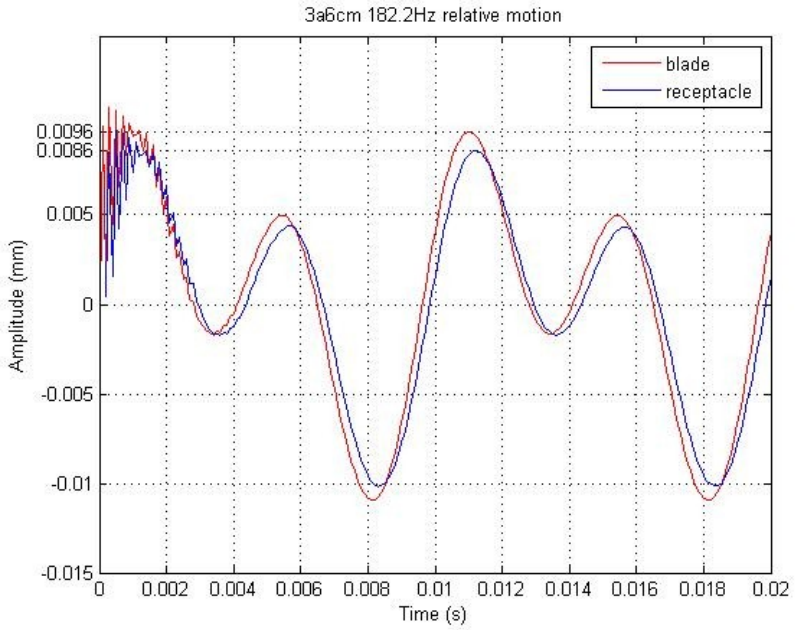

Figure App.F-7 Two cycles of the blade and receptacle of 3A 6cm under 182Hz

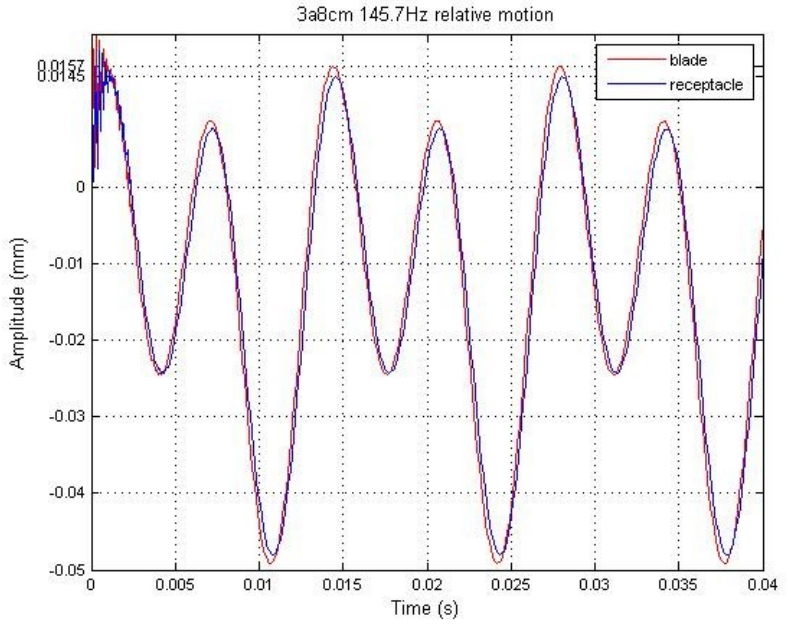

Figure App.F-8 Three cycles of the blade and receptacle of 3A 8cm under 145.7Hz

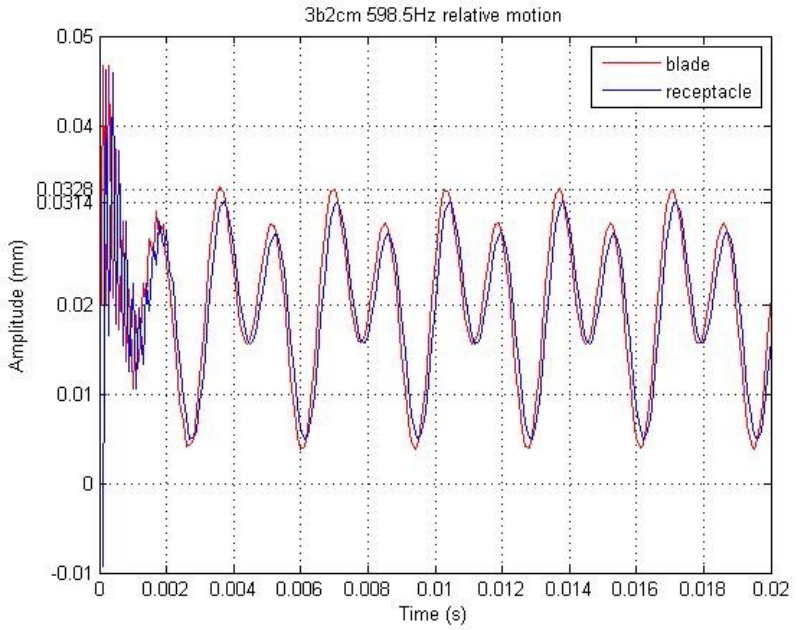

Figure App.F-9 Six cycles of the blade and receptacle of 3B 2cm under 598.5Hz

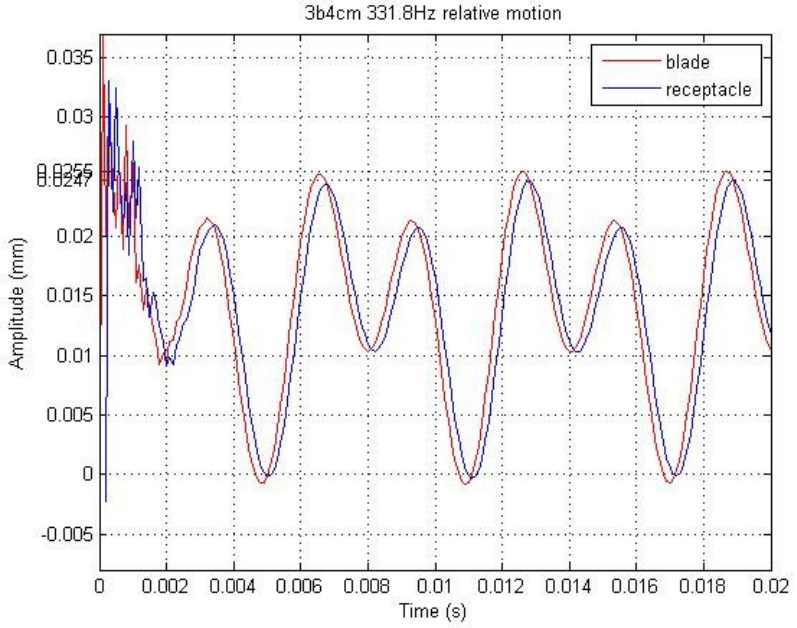

Figure App.F-10 Three cycles of the blade and receptacle of 3B 4cm under 331.8Hz

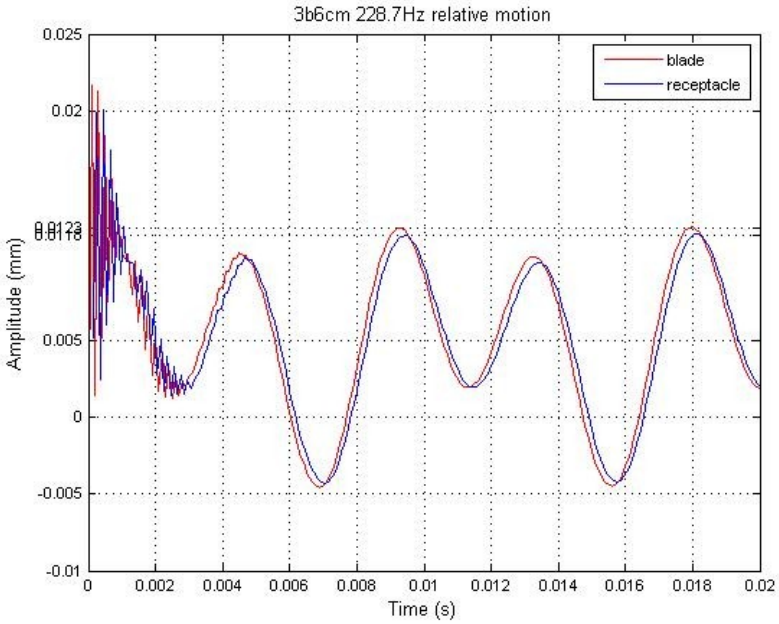

Figure App.F-11 Two cycles of the blade and receptacle of 3B 6cm under 228.7Hz

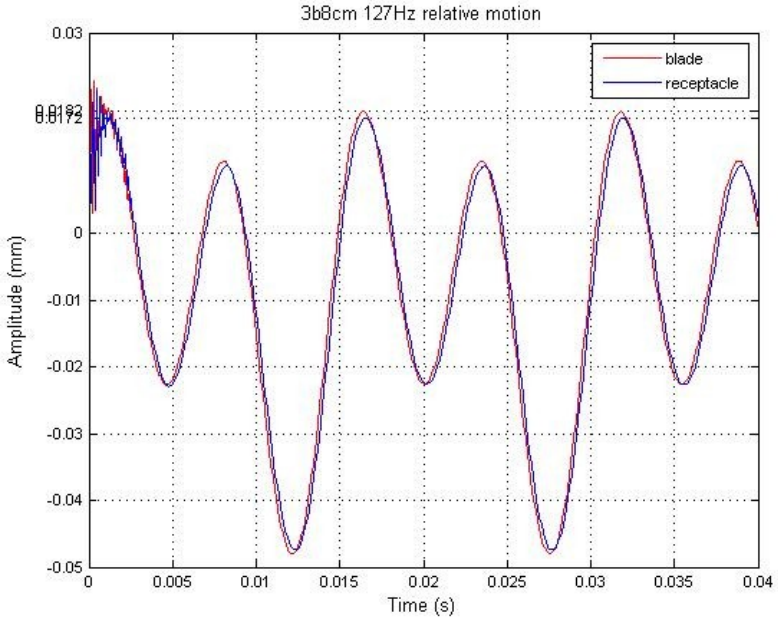

Figure App.F-12 Two cycles of the blade and receptacle of 3B 8cm under 127Hz

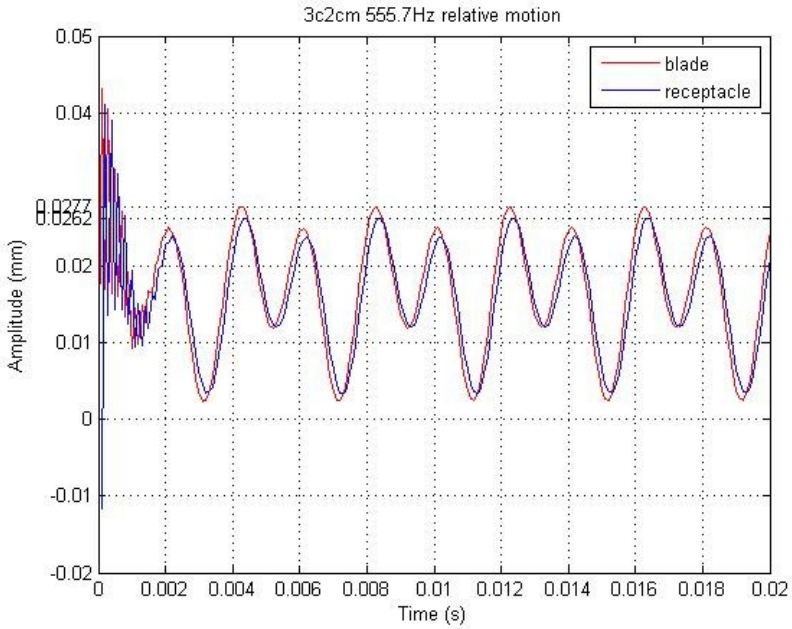

Figure App.F-13 Five cycles of the blade and receptacle of 3C 2cm under 555.7Hz

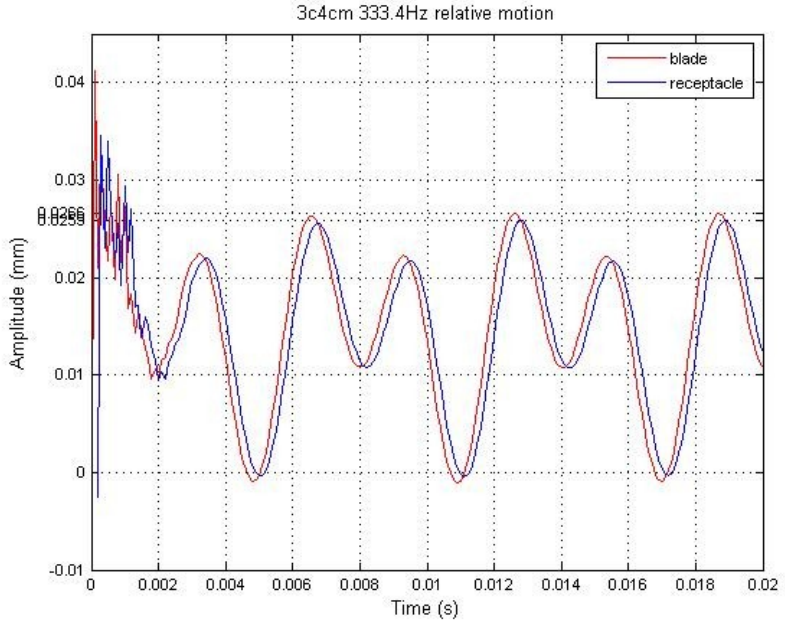

Figure App.F-14 Three cycles of the blade and receptacle of 3C 4cm under 333.4Hz

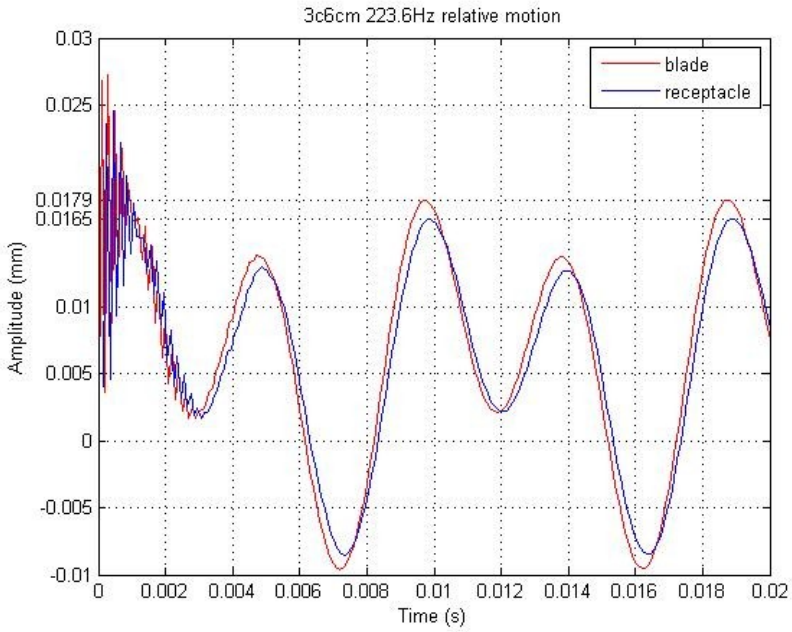

Figure App.F-15 Two cycles of the blade and receptacle of 3C 6cm under 223.6Hz

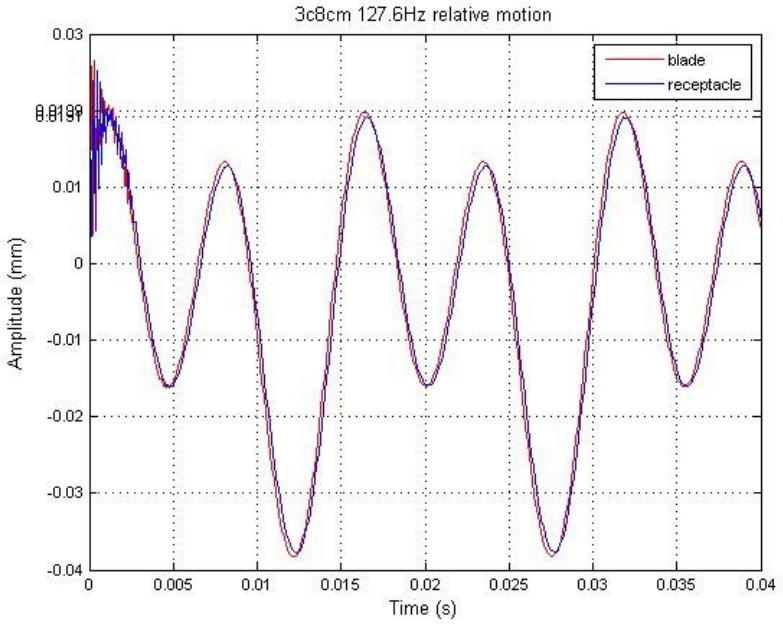

Figure App.F-16 Two cycles of the blade and receptacle of 3C 8cm under 127.6Hz